



National Library
of Canada

Bibliothèque nationale
du Canada

Canadian Theses Service Service des thèses canadiennes

Ottawa, Canada
K1A 0N4

NOTICE

The quality of this microform is heavily dependent upon the quality of the original thesis submitted for microfilming. Every effort has been made to ensure the highest quality of reproduction possible.

If pages are missing, contact the university which granted the degree.

Some pages may have indistinct print especially if the original pages were typed with a poor typewriter ribbon or if the university sent us an inferior photocopy.

Reproduction in full or in part of this microform is governed by the Canadian Copyright Act, R.S.C. 1970, c. C-30, and subsequent amendments.

AVIS

La qualité de cette microforme dépend grandement de la qualité de la thèse soumise au microfilmage. Nous avons tout fait pour assurer une qualité supérieure de reproduction.

S'il manque des pages, veuillez communiquer avec l'université qui a conféré le grade.

La qualité d'impression de certaines pages peut laisser à désirer, surtout si les pages originales ont été dactylographiées à l'aide d'un ruban usé ou si l'université nous a fait parvenir une photocopie de qualité inférieure.

La reproduction, même partielle, de cette microforme est soumise à la Loi canadienne sur le droit d'auteur, SRC 1970, c. C-30, et ses amendements subséquents.

THE UNIVERSITY OF ALBERTA

SINGLE PHOTON RESPONSES AND THEIR SUMMATION

IN LOCUST PHOTORECEPTORS

BY

ARTURO ERNESTO CARLO PECE

A THESIS

SUBMITTED TO THE FACULTY OF GRADUATE STUDIES AND
RESEARCH IN PARTIAL FULFILLMENT OF THE REQUIREMENTS FOR
THE DEGREE OF DOCTOR OF PHILOSOPHY

DEPARTMENT OF PHYSIOLOGY

EDMONTON, ALBERTA

FALL 1990



**National Library
of Canada**

**Bibliothèque nationale
du Canada**

Canadian Theses Service Service des thèses canadiennes

**Ottawa, Canada
K1A 0N4**

The author has granted an irrevocable non-exclusive licence allowing the National Library of Canada to reproduce, loan, distribute or sell copies of his/her thesis by any means and in any form or format, making this thesis available to interested persons.

The author retains ownership of the copyright in his/her thesis. Neither the thesis nor substantial extracts from it may be printed or otherwise reproduced without his/her permission.

L'auteur a accordé une licence irrévocable et non exclusive permettant à la Bibliothèque nationale du Canada de reproduire, prêter, distribuer ou vendre des copies de sa thèse de quelque manière et sous quelque forme que ce soit pour mettre des exemplaires de cette thèse à la disposition des personnes intéressées.

L'auteur conserve la propriété du droit d'auteur qui protège sa thèse. Ni la thèse ni des extraits substantiels de celle-ci ne doivent être imprimés ou autrement reproduits sans son autorisation.

ISBN 0-315-64798-1



DEPARTMENT OF
ELECTRICAL ENGINEERING

Queen's University
Kingston, Canada
K7L 3N6

September 17, 1990

842101.

Faculty of Graduate Studies and Research
University of Alberta
Edmonton, Alberta
T6G 2E1

Dear Sirs,

This letter will authorize Mr. A.E.C. Pece to include in his doctoral dissertation any material from the article "Nonlinear mechanisms for gain adaptation in locust photoreceptors", published in the Biophysical Journal 57:733-743 (1990), of which I was a co-author.

Sincerely,

Michael Kornberg

Dr. M.J. Kornberg
Associate Professor of Electrical Engineering

[Handwritten initials]



University of Alberta
Edmonton

Canada T6G 2H7

Department of Physiology
Faculty of Medicine

7-55 Medical Sciences Building
Telephone: (403) 492-3359
Facsimile: (403) 492-8915

12 September 1990

Faculty of Graduate Studies
University of Alberta
Edmonton, Alberta
T6G 2E1

A.E.C. Pece - 842101

Dear Sir:

The above student is currently completing a Ph.D. degree under my supervision. He has my permission to use, in his Ph.D. Thesis, material from manuscripts published jointly with me. Specifically, the joint manuscripts concerned are:

1. Single photon responses in locust photoreceptors: the effects of stimulus location and time course, *Journal of Comparative Physiology* **164**: 365-375 (1989).
2. Nonlinear mechanisms for gain adaptation in locust photoreceptors, *Biophysical Journal* **57**: 733-743 (1990).
3. Sublinear summation of responses in locust photoreceptors (Submitted for publication).

Manuscript #2 was also co-authored by Drs. M.J. Korenberg and J.E. Kuster. However, the thesis does not contain any results or concepts contributed by Dr. Kuster. Therefore, it will only be necessary to obtain similar permission from Dr. Korenberg.

Yours sincerely,

Dr. A.S. French
Professor of Physiology
☎ 403-492-3326
FAX: 403-492-8915

UNIVERSITY OF ALBERTA

RELEASE FORM

NAME OF AUTHOR: ARTURO ERNESTO CARLO PECE
TITLE OF THESIS: SINGLE PHOTON RESPONSES AND THEIR
SUMMATION IN LOCUST PHOTORECEPTORS
DEGREE: DOCTOR OF PHILOSOPHY
YEAR THIS DEGREE GRANTED: FALL 1990

Permission is hereby granted to the University of Alberta library to reproduce single copies of this thesis and to lend or sell such copies for private, scholarly or scientific research purposes only.

The author reserves other publication rights, and neither the thesis nor extensive extracts from it may be printed or otherwise reproduced without the author's permission.

Pece

via S. Domenico 3

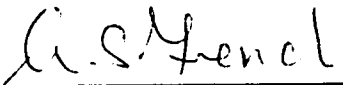
71100 Foggia, Italy

Date: 12 October 1990

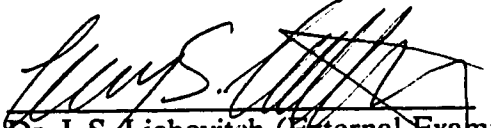
UNIVERSITY OF ALBERTA

FACULTY OF GRADUATE STUDIES AND RESEARCH

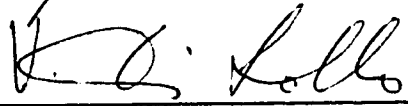
THE UNDERSIGNED CERTIFY THAT THEY HAVE READ, AND RECOMMEND TO THE FACULTY OF GRADUATE STUDIES AND RESEARCH FOR ACCEPTANCE, A THESIS ENTITLED "SINGLE PHOTON RESPONSES AND THEIR SUMMATION IN LOCUST PHOTORECEPTORS" SUBMITTED BY ARTURO E.C. PECE IN PARTIAL FULFILLMENT OF THE REQUIREMENTS FOR THE DEGREE OF DOCTOR OF PHILOSOPHY.



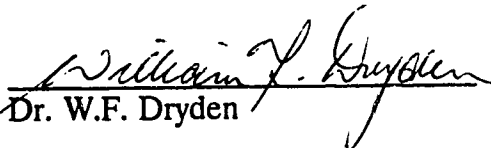
Dr. A.S. French (Supervisor)




Dr. L.S. Liebovitch (External Examiner)




Dr. V. DiLollo



Dr. W.F. Dryden



Dr. K.G. Pearson



Dr. R.B. Stein

Date: 28 September 1990

**This thesis is dedicated
to my Mother Cristina
to my dear Aunts
and to Joyce Spicer**

ABSTRACT

Several approaches were used to investigate the mechanisms by which photoreceptor responses to transient stimuli are modulated in amplitude. The results indicate that the most important mechanism is a shunting voltage-activated conductance which is sensitive to a depolarization of only a few millivolts from resting potential. The main implication of this finding is that insect photoreceptors are not only transducing light into membrane current, but process the resulting electrical signal by mechanisms similar to those operating in other neurons. One important practical implication is that the dynamics of the voltage response to light cannot be taken to reflect the dynamics of the phototransduction process, if this latter process is meant as terminating with the opening of light-sensitive membrane channels.

A preliminary investigation was aimed at determining whether the transduction properties of the photoreceptor are independent of the site of photon absorption. This was necessary because localized stimulation was employed in some later experiments. The results of this study indicated that single photon responses are statistically very similar, regardless of the site of stimulation. Single photon responses show a large variability even when stimulation is localized. This variability is likely to be intrinsic to the transduction process.

Another investigation demonstrated that the gain control mechanism operating in dark-adapted photoreceptors stimulated with flashes, also operates in light-adapted photoreceptors stimulated with a pseudorandom light signal. Since the resulting gain control process is much more significant under the former conditions, further

experiments were performed on dark-adapted photoreceptors. These experiments demonstrated (1) that the interaction between two stimuli is not affected by the distance between the stimuli, and therefore that the gain control mechanism is probably not mediated by a diffusible transmitter; (2) that the interaction between a flash stimulus and a current stimulus is similar to that between flash stimuli, and therefore that a membrane process, probably a voltage-activated conductance, mediates the gain control mechanism. These results, taken together, imply that membrane phenomena taking place after the activation of the light-sensitive conductance are important in shaping the responses of photoreceptors.

ACKNOWLEDGEMENTS

Andrew French is to be thanked for encouraging me to expand my experience in vision research and for listening to my occasionally unreasonable requests, which has resulted in a fairly stress-free supervision. The people in Andrew's laboratory have all been helpful in one way or another. Particular mention should be made of Marek Duszyk, Rod Gramlich, and Lisa Stockbridge, who have shared the lab with me for the longest time, and of Margaret French, who has been a friend to all of us and can be considered an honorary member of the laboratory.

Richard Payne gave useful suggestions on the methods and control experiment of Chapter II. Mike Korenberg collaborated in the research described in Chapter III and Stan Klein gave helpful comments on that research. Roger Hardie provided a preprint of a manuscript and insightful comments on the research described in Chapter IV.

Although not directly connected with this thesis, I would like to acknowledge my intellectual debt to the "Logic of Scientific Discovery" by Karl Popper, a book that shaped my conception of scientific research, and to the people I met at the Department of Biophysics, University of Groningen, Netherlands, who introduced me to biological cybernetics and to vision research.

I am grateful to the Department of Physiology and the Alberta Heritage Foundation for Medical Research for financial support during my graduate studies.

INDEX

I. A GENERAL INTRODUCTION TO INSECT PHOTORECEPTORS	1
I.1. The insect eye	5
I.2. Mechanisms of phototransduction	9
I.3. Summation of elementary responses	16
I.4. System analysis	20
I.5. Organization of the following chapters	23
I.6. References	25
II. SINGLE PHOTON RESPONSES: EFFECTS OF STIMULUS LOCATION ON AMPLITUDE AND TIME COURSE	31
II.1. Introduction	31
II.2. Methods	33
II.3. Results	41
II.4. Discussion	61
II.5. References	71
III. PHENOMENOLOGY OF GAIN CONTROL: A COMPARISON OF WHITE- NOISE AND IMPULSE RESPONSES	74
III.1. Introduction	74
III.2. Methods	78
III.3. Experimental results	84

III.4. Model simulations	94
III.5. Discussion	103
III.6. References	110
IV. PHYSIOLOGICAL DISSECTION OF THE GAIN CONTROL MECHANISM	113
IV.1. Introduction	113
IV.2. Methods	117
IV.3. Results	122
IV.4. Discussion	140
IV.5. References	145
V. GENERAL DISCUSSION: GAIN CONTROL AT THE MEMBRANE LEVEL	148
V.1. Modelling of the gain control process	148
V.2. Voltage-activated conductances in photoreceptors	159
V.3. Conclusions	166
V.4. References	170

LIST OF TABLES

Table II.1	Numbers of predicted, observed, analyzed responses.	43
Table II.2	Statistics of bump amplitude.	48
Table II.3	Statistics of time to peak of bumps.	51
Table II.4	Statistics of relative width of bumps.	54
Table II.5	Statistics of cell effects on bump parameters.	57
Table II.6	Intrinsic correlation coefficients of bump parameters.	58

LIST OF FIGURES

Figure I.1.	Diagram of the locust ommatidium.	6
Figure II.1	Preparation for localized stimulation.	35
Figure II.2	Bump parameters as functions of location.	44
Figure II.3	Distributions of bump amplitudes in cell #1.	47
Figure II.4	Distributions of times to peak of bumps in cell #1.	50
Figure II.5	Distributions of relative widths of bumps in cell #1.	53
Figure II.6	Scattergram of bump time course parameters.	60
Figure III.1	Linear kernels from double-flash experiment.	86
Figure III.2	Second-order kernel from flash experiment.	87
Figure III.3	Linear kernels from white-noise experiments.	90
Figure III.4	Second-order kernels from white-noise experiments.	92
Figure III.5	Minimum separable models of gain control.	95
Figure III.6	Comparison of simulated and experimental responses.	102
Figure IV.1	Preparation for two-slit experiments.	123
Figure IV.2	Normalized depressions with two different slit distances.	125
Figure IV.3	Differences between times to peak of depression and of response.	126
Figure IV.4	Different levels of adaptation at two sites.	129
Figure IV.5	Sub-linear summation of flash and current responses.	132
Figure IV.6	Results of flash plus current experiments.	135
Figure IV.7	Normalized depressions after TEA injection.	137

Figure IV.8	Effect of TEA on step response to light.	139
Figure V.1	Model of light-to-voltage transduction mechanism.	152

LIST OF SYMBOLS

Units

ep	stimulus energy: effective photon (photon effectively transduced)
ep/s	stimulus power: effective photon per second
mM	concentration: millimolar
ms	time: millisecond
mV	voltage: millivolt
mW/cm ²	irradiance: milliwatt per square centimeter
MΩ	resistance: megaohm
nA	current: nanoampere
nS	conductance: nanosiemens
μm	length: micrometer

Acronyms

AC	alternating current (fluctuations around background level)
cGMP	cyclic guanine monophosphate
DC	direct-current (background level)
EGTA	ethyleneglycol-bis-(β-aminoethyl ether)N,N,N'N'-tetraacetic acid

ERG	electroretinogram
LED	light-emitting diode
RMS	root-mean square (standard deviation)
TEA	tetraethylammonium chloride
TTX	tetrodotoxin

Other symbols

<i>a</i>	conductance activated per unit light intensity (nS/ep)
<i>A(d)</i>	attenuation factor due to cable conduction from site <i>d</i> (dimensionless)
<i>b</i>	conductance activated per unit depolarization (nS/mV)
<i>c</i>	concentration of active element of phototransduction cascade (mM)
<i>d</i>	distance from the closer end of the photoreceptor (μm)
<i>E</i>	reversal potential relative to resting potential (mV)
<i>f(\delta)</i>	linear component of separable second-order kernel $p_2(\tau, \delta)$ (ep^{-1})
F	linear system element with impulse response <i>f</i>
<i>G(v)</i>	total light-insensitive membrane conductance (nS)
<i>G_r</i>	membrane conductance at rest (nS)
<i>G₀</i>	effective membrane conductance $G_r - bE_b$ (nS)
<i>H</i>	membrane current per unit light intensity (nA/ep)
<i>h_i</i>	Volterra or Wiener kernel of order <i>i</i> (mV/ep ^{<i>i</i>})
<i>I</i>	membrane current injected through the microelectrode (nA)

$k(\tau)$	linear component of separable second-order kernel $p_2(\tau, \delta)$ (mV/ep)
$k_p(\tau)$	estimate of k_p obtained from the experimental p_2 (mV/ep)
K	linear system element with impulse response k
L	total length of photoreceptive structure (μm)
n	parameter of the modified Naka-Rushton curve (Eq. I.4) (dimensionless)
N	static nonlinear system element
p	probability
p_2	second-order kernel transposed according to Eq. III.2 (mV/ep ²)
r	correlation coefficient
$R(d)$	membrane input resistance at distance d from the proximal end of the cell (M Ω)
t	time (ms)
t_p	time to peak (ms)
v	membrane depolarization above resting potential (mV)
v_p	peak depolarization (mV), a parameter of the log-normal model (Eq. II.1)
w	relative width (dimensionless), a parameter of the log-normal model (Eq. II.1)
x	light intensity (ep or, for white-noise stimuli, ep/s)
\bar{x}	average light intensity (units as above)
y	gain control signal (Fig. III.5)
z	gain-regulated input signal (Fig. III.5)
α, β	any pair of parameters of a single photon response
δ or $\Delta\tau$	time variable of transposed kernel $p_2(\tau, \delta)$ (ms)

Δt	inter-flash interval (ms)
Δv	response depression (mV)
λ	cell length constant (μm)
μ	average
σ	standard deviation
σ_x	RMS power level of the input signal (ep/s)
ρ	axial intracellular resistance per unit length ($\text{M}\Omega/\mu\text{m}$)
τ	time variable of Volterra or Wiener kernel (ms)
χ^2	Chi-square statistical test

I. A GENERAL INTRODUCTION TO INSECT PHOTORECEPTORS

Insects are one of the most successful animal groups. In number of species, they outnumber all other living forms combined, and in number of individuals they are probably the largest group of animals which live freely above the ground. Part of this success must be due to their visual system. Like other classes of arthropods and two unrelated groups (vertebrates and cephalopods), insects have a visual system which actually allows them to see (*i.e.* to form images of the visual world), which we take for granted, but is not the purpose for which photoreceptors evolved originally.

There are two basic types of eyes capable of forming images. Compound eyes, one of these two types, are only found in arthropods, including insects. The three ocelli which are located between the two compound eyes of insects should not be confused with the subject of the present study. Compound eyes form an image which is like a time-varying mosaic, each element of this mosaic being the light intensity exciting one photoreceptor. This mosaic is transformed into another mosaic, whose elements are not light intensities but the membrane potentials of the photoreceptors. All of this is also true of camera eyes, but compound eyes differ in the optical means by which the optical mosaic is generated. As a consequence of the different optics, the functional mosaic of neural activities has a striking parallel in the anatomical mosaic of the compound eye.

Other "mosaic" transformations take place at further stages in the visual system.

Of course, mosaics located in visual ganglia do not have a one-to-one relationship with the photoreceptors, since the information from several photoreceptors must interact to allow the brain to make sense of the visual world. How the brain does that is one of the main problems in neuroscience, part of the larger problem of how the brain processes information. A large portion of the information that the brain handles is visual information: large areas of the cerebral cortex are concerned with vision more or less directly, and, in the fly brain (supra- and sub-oesophageal ganglions), about 260,000 out of 340,000 neurons are located in the optic lobes (Strausfeld, 1976, pages 53-54). This imbalance with respect to the other senses is likely to be due to the amount of visual information that has to be processed as well as to the fact that this processing is not a trivial task. Animal groups which have not evolved image-forming eyes do not have very well developed brains.

The concentration of research effort on the visual system, relative to other sensory systems, parallels the extent of neural resources devoted to vision. Apart from the biological relevance of sight, this interest is also due to the ease with which the visual system can be experimentally stimulated in a controlled, quantitative way.

The compound eyes and optic lobes of insects offer an opportunity to investigate visual information processing in a relatively simple system, including only a few hundred thousand neurons for each side of the brain. Even this figure is deceptively large: the cellular structure of most optic ganglia is very repetitive. For instance, the second optic ganglia, or *medullae*, include almost half of the neurons in the fly brain (about 150,000 - Strausfeld, 1976), but these neurons are actually arranged in

repetitive columns, each retinotopically-ordered column containing only about 26 neurons. In this respect, insects offer to vision research some of the advantages that some blind invertebrates offer to other areas of neuroscience. However, insect neurones are very small, unlike those found in the slugs and leeches which have proved useful subjects for studies of motor pattern generation and of learning (Kandel, 1976; Koester and Byrne, 1980; Muller *et al.*, 1981).

Insects are also very suitable for quantitative behavioral investigations. Their advantages over vertebrates include a relatively stereotyped behavior and being available in large supply. Compared to molluscs or worms, their advantages include the smaller number of degrees of freedom of their body and the speed with which they behave. Since vision plays an important role in an insect life, insects are a good preparation for the study of the visual control of behavior (von Frisch, 1971; Wehner, 1981; Borst and Egelhaaf, 1989).

The horseshoe crab, *Limulus*, is an arthropod like insects, and more closely related to spiders and scorpions than to crabs, in spite of its common name. It has a visual system which is phylogenetically related to that of insects, with the advantage of having larger nerve cells. *Limulus* has been the focus of much experimental research. This research led to the development of the concept of lateral inhibition (Hartline and Ratliff, 1972). However, vision plays a relatively small role in the life of *Limulus* (Barlow, 1990). *Limulus* lacks the strong, fast reactions to visual stimuli which have caused interest in insect vision. We shall often refer to research on *Limulus* photoreceptors, since its visual physiology has a relatively close relationship to that

of insects.

Although photoreceptors process information coming from a single source, the light intensity in a small visual angle, they are not simple linear transducers with the sole task of changing the physical nature of the mosaic elements. Photoreceptors are equipped with the physiology required to perform the first steps in the processing of visual information. These steps involve intensity coding and adaptation, which together optimize the gain of the photoreceptor to improve its signal-to-noise ratio and provide an image of the world which the brain can work with. Much progress has been made in understanding the function of these transformations (*e.g.* Attwell, 1986; Laughlin, 1987). The present study is mainly concerned with the mechanisms involved in these transformations and therefore follows a top-down, rather than bottom-up approach.

The rest of this chapter is organized into five sections. In section I.1, the structure of the compound eye of the locust will be outlined. In section I.2, current models of the phototransduction mechanisms in vertebrates and invertebrates will be reviewed, with particular reference to the elementary responses of photoreceptors, *i.e.* responses to single photons. Section I.3 will discuss how these elementary responses summate when more than one photon is transduced. Section I.4 will briefly introduce the system analysis methods employed in chapter III. Section I.5 will briefly review the research described in this dissertation and put it in perspective.

I.1. The insect eye

Ommatidia

The mosaic elements of the compound eye are called ommatidia. Each ommatidium includes several photoreceptors, as well as glial and pigment cells. Insect ommatidia typically include eight photoreceptors. Fig. I.1 is a schematic representation of a locust ommatidium. More detailed descriptions can be found in Trujillo-Cenoz (1972) and, for locust ommatidia, in Wilson *et al.* (1978). The hexagonal facet which is the part of the ommatidium seen from the outside is the lenslet, the distal layer of the cornea. Beneath the cornea lies another optical structure, the cone, and beneath the cone we find the photoreceptors, also known as reticular cells. The whole ommatidium, except for the cornea, is enveloped by pigment cells which isolate it from other ommatidia. Additional pigment cells surround the cone. The photoreceptors also contain some pigment granules of their own. The entire ommatidium is about 400 μm long, of which 100 are taken mostly by the optical apparatus and 300 by the photoreceptors. Proximally, the ommatidium is delimited by the basilar membrane, which is the same kind of connective sheath which envelops all insect ganglia. The optic lobes lie immediately beneath the basilar membrane. The photoreceptor axons cross the basilar membrane to make synapses on neurons in the optic lobe. There are no centrifugal axons from the optic lobes to the ommatidium.

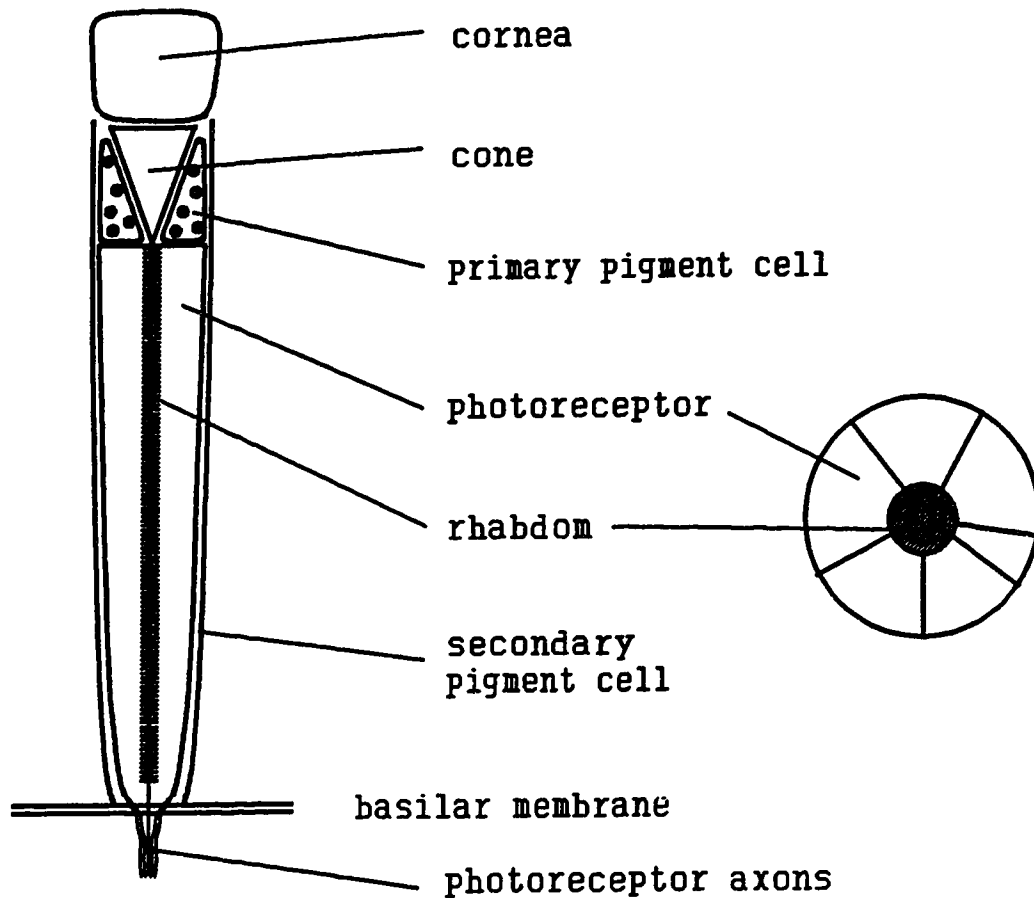


Fig. I.1. Schematic diagram of the locust ommatidium. Left, a section parallel to the long axis. Pigment granules of secondary pigment cells and of photoreceptors and cell nuclei are not represented. Right, a transversal section at the middle of the rhabdom (about $250 \mu\text{m}$ from the outer surface of the cornea and $150 \mu\text{m}$ from the basilar membrane). Note that cells have different cross-sectional areas and make variable contributions to the rhabdom depending on the level of the transversal section. Two thinner photoreceptors which do not make a contribution to the rhabdom at this level are not represented. Adapted from Wilson *et al.* (1980).

There are several different ways in which a compound eye can form an optical image (Nilsson, 1990). Locusts have simple apposition eyes, in which only light entering through the cornea along the ommatidium main axis or at a close angle to it reaches the photoreceptors. Optically, this is perhaps the simplest kind of compound eye.

Locust photoreceptors

Insect photoreceptors have a specialized membrane structure containing the rhodopsin, like vertebrates. This structure is called the rhabdomere and is a system of microvilli protruding from the cell membrane towards the central axis of the ommatidium. The rhabdomere runs along most or all of the photoreceptor, except of course for the photoreceptor axon. In most insects, including locusts, the rhabdomeres from all the cells of the ommatidium are so close together that they appear as a single structure under the microscope. This structure is called rhabdom. Light photons can only excite the photoreceptors if they reach the rhodopsin molecules contained in the rhabdom.

The eight photoreceptors within an ommatidium differ from each other in structure as well as in absolute sensitivity, spectral sensitivity, and polarization sensitivity. The different morphological types have been characterized in several insect species (review: Menzel, 1979), but not in locusts. There have been two reports (Bennett *et al.*, 1967; Vishnevskaya *et al.*, 1986) in which three types of locust photoreceptors could be distinguished by their spectral sensitivity, but the

corresponding anatomical types were not identified.

The invertebrate visual pigments are evolutionarily related to vertebrate rhodopsin and are usually referred to as rhodopsin by analogy. One important physiological difference is that invertebrate rhodopsin, when converted to metarhodopsin, does not bleach, *i.e.* the all-*trans* retinal does not detach from the opsin. Another important difference is that the metarhodopsin is usually converted back to rhodopsin by absorption of light, in the same way as in the forward conversion rhodopsin → metarhodopsin. However, the two processes generally have different absorption spectra (Hamdorf, 1979).

Most invertebrate photoreceptors, unlike their vertebrate counterparts, respond to light with a depolarization. This makes their response much easier to understand for the neuroscientist who is used to depolarizing responses to stimuli. Like vertebrate photoreceptors, those of insects do not generate action potentials: the light-induced depolarization is propagated mostly by passive cable conduction to the synaptic terminals. However, action potentials can be observed in bee photoreceptors subjected to very strong stimuli (Baumann, 1974).

I.2. Mechanisms of phototransduction

The ventral eye of the horseshoe crab

Limulus has two compound eyes on the sides of the head, like insects. These are called lateral eyes. However, it also has several other eyes, having different functions (Barlow, 1990). Research on phototransduction has concentrated on the ventral eye, since its photoreceptors are large and easy to penetrate with microelectrodes.

While compound eye photoreceptors are very regular in morphology, because of the requirements of their packing, ventral eye photoreceptors have irregularly shaped cell bodies with an axon attached. The rhabdomere itself is irregular in shape and sometimes divided.

The lateral eye photoreceptor was the first photoreceptor from which intracellular recordings were made. Early experiments led to the development of a model of phototransduction in which a cascade of first-order enzymatic reactions leads to an increase of membrane conductance to cations and therefore to depolarization (Fuortes and Hodgkin, 1964). A first-order enzymatic reaction is one in which a single molecule of substance c_1 catalyzes a reaction in which one molecule of substrate s_2 is converted to another, different active substance c_2 , according to the reaction:



in which c_2 is transformed into the inactive form u_2 at a constant rate k_2 , while s_2 is

converted into c_2 at the rate $k_1 \cdot c_1$. In general, u_2 either is identical to s_2 or is recycled into s_2 . Such a reaction leads to the differential equation:

$$\frac{\partial c_2}{\partial t} = k_1^* c_1 - k_2 c_2 \quad (\text{I.2})$$

Where we substituted $k_1^* = k_1 \cdot s_2$, assuming that the substrate is not depleted and its concentration can be taken as a constant. As can be seen from Eq. I.2, $c_2(t)$ is a low-pass filtered version of $c_1(t)$. The transfer function of this low-pass filter has a single first-order pole, with time constant $1/k_2$. A saturation effect would occur if the substrate were depleted, so that Eq. I.2 would no longer be valid. If c_2 in turn catalyzes another reaction of the kind of Eq. I.1, then the resulting product is a low-pass filtered version of c_1 , with a transfer function including two first-order poles. Substances c_1 and c_2 do not need to be enzymes, but can be any chemical substance capable of activating another substance. In the first stage, c_1 is actually a photon, s_2 a rhodopsin molecule, and c_2 a metarhodopsin molecule. In the last stage, s_2 and c_2 are membrane channels in a closed and open state, respectively. Fuortes and Hodgkin (1964) found that a model with between 9 and 11 poles with equal time constants could provide a good fit to the photoreceptor response. While these early studies were based on recordings of voltage responses from the lateral eye photoreceptor, subsequent studies concentrated on recording current responses under voltage clamp from the ventral eye photoreceptor. Note that in this chapter "current response" will indicate a variation of membrane current after stimulation with light,

while in Chapter IV it will indicate a variation of membrane voltage after stimulation with current. The meaning should be evident from the context.

Research on the biochemical mechanism of phototransduction has concentrated on vertebrate rods. However, recent reports suggest that a G-protein, calcium, and inositol-trisphosphate are intermediates in the transduction cascade of *Limulus* (Fein, 1986). An alternative model, not necessarily incompatible with the first, includes cyclic nucleotides (Johnson *et al.*, 1986). The terminal molecular component of the cascade, the light-activated channel (a somewhat ambiguous term, since the channel is not directly activated by light) has been identified by patch-clamp recordings (Bacigalupo and Lisman, 1984).

Vertebrate photoreceptors

Vertebrate photoreceptors are characterized by a hyperpolarizing response to illumination. The hyperpolarization is caused by the decrease of a membrane conductance with a reversal potential close to zero. In both these respects, vertebrate photoreceptors behave in an opposite way from most invertebrate photoreceptors. A modified cascade model with an inverted polarity was found to account for the response time course (Baylor *et al.*, 1974).

Early physiological research indicated that calcium might be one of the elements of the transduction cascade, since calcium ions reduce the light-inactivated conductance (Hagins, 1972). Subsequently, patch-clamp methods made it possible to expose the intracellular side of the cell membrane to various agents, demonstrating

that cGMP also has a fast and specific effect on the light-inactivated conductance. At the same time, it became clear that intracellular calcium is actually reduced during illumination. The new picture includes a fall in cGMP, leading to a fall in light-inactivated conductance, which in turn hyperpolarizes the cell membrane (Lamb, 1986; Pugh and Miller, 1987). Therefore, the polarity of the response is inverted not only at the membrane level, but also at the level of the intracellular transmitter which opens the channel.

In the following, we shall refer to photoreceptors of insects or *Limulus*, unless otherwise specified. Therefore, we shall assume that a photoreceptor is always depolarized by light, *etc.*

Insect photoreceptors

The cascade model of phototransduction did not prove to be very effective in describing the voltage responses of insect photoreceptors. French (1980) analyzed the frequency response of fly photoreceptors and found that two second-order poles are required to fit the response. However, a second-order pole does not have a single obvious biochemical analog, as a first-order pole does. Payne and Howard (1981) proposed an alternative model, in which the photoreceptor impulse response is a Gaussian function of the logarithm of time, centered at a certain time after the impulse (flash). This model includes only three parameters but requires an even more complex physiological justification.

The biochemistry of insect phototransduction has been investigated in normal and

mutant flies (Selinger and Minke, 1988). Inositol trisphosphate seems to be involved in the same way as in *Limulus*.

Responses to single photons

At very low levels of illumination, the responses of several photoreceptors consist of discrete waves of depolarization, called (quantum) bumps (review: Stieve, 1984). It is believed that each of these bumps is the result of the transduction of a single photon. The evidence for this hypothesis is: (1) the intervals between bumps have an exponential distribution under steady illumination, and when the stimulus is a dim flash, the numbers of bumps generated for each flash have a Poisson distribution; these are the distributions expected for single photon absorptions; (2) the frequency of bumps is linearly proportional to light intensity (Yeandle, 1985).

Bumps are the elementary component of phototransduction in the same way as channel opening is the elementary component of conductance increase or miniature synaptic potentials are the elementary components of synaptic transmission. Like miniature potentials, and unlike channel opening, bumps do not involve the operation of a single biochemical entity. However, a single rhodopsin molecule is at the origin of each bump. The first step in bump generation can be described by Eq. I.1, in which c_1 is a single photon and s_2 is a single rhodopsin molecule, which is turned into metarhodopsin c_2 . Subsequent stages include some amplification, so that the average number of activated molecules increases at each stage. In the last stage, c_1 is a transmitter which binds to the membrane channel s_2 and increases its probability of

turning into the open state c_2 . As we pointed out, Eq. I.1 is a very general scheme without any implications for the chemical nature of the reactions involved.

All of these reactions are stochastic at the molecular level. Therefore, the resulting voltage response should be variable in amplitude and time course, as was indeed observed. Borsellino and Fuortes (1968) formulated a stochastic model of bump generation in *Limulus* ventral photoreceptors. This model takes into account the random processes occurring at each stage in the cascade. More recently, Schnackenberg (1989) demonstrated that average bump durations and latencies in the ventral photoreceptor are not compatible with a simple cascade model, as the macroscopic response seems to be.

Spontaneous bumps are also observed. These could result from spontaneous transitions between rhodopsin and metarhodopsin, although their shape and amplitude seem to differ from those observed in light-induced bumps (Stieve, 1984) and the temperature dependence of their frequency seems to indicate that a different process is operating (Fein and Szuts, 1982).

Bumps were first observed in *Limulus* lateral eye photoreceptors, with amplitudes as large as 10 mV on average if the cell was dark-adapted (Yeandle, 1958). Next to *Limulus*, the largest bumps can be observed in locust photoreceptors. If the recording conditions are good, bumps of 4 mV on average can be observed in this preparation (Howard, 1983). Unlike *Limulus* photoreceptors, those of locusts do not seem to generate any bumps in the dark (Lillywhite, 1977). One of the first investigations on locust bumps (Lillywhite, 1978) distinguished two classes of bumps on the basis of a

double peak in the bump amplitude distribution. The smaller bumps were thought to arise from neighbouring photoreceptors electrically coupled to the cell being recorded from. Subsequently, Howard (1983) found amplitude distributions with a single peak and suggested that smaller bumps do indeed arise from neighbouring cells which are electrically coupled, but only when this coupling has been artefactually created by the electrode penetration.

In vertebrate photoreceptors, bumps can be observed only as membrane current fluctuations (Yau *et al.*, 1977). In physiological conditions, a single photon absorption leads to a hyperpolarization which is below the noise level of the recording, because the underlying current spreads over several cells which are electrically coupled (not artefactually). Bumps in vertebrate rods show little variability in amplitude and time course, presumably because a fairly large number of molecules is involved in the process at all stages (Baylor *et al.*, 1979).

As mentioned above, the variability observed in *Limulus* and insect bumps has been attributed to fluctuations at the molecular level. Such variability would then be intrinsic to the transduction mechanism. Responses to stimuli containing many effective photons would become approximately deterministic because of the law of large numbers. However, the molecular origin of the variability has not been conclusively demonstrated. Chapter II confirms the findings of previous investigations which provided direct evidence in *Limulus* (Spiegler and Yeandle, 1974) and indirect evidence in locusts (Lillywhite, 1978) that bump variability is not due to the variability of the site of photon absorption. These findings have implications for models of

phototransduction based on the observed variability of bumps (Borsellino and Fuortes, 1968; Schnakenberg, 1989).

I.3. Summation of elementary responses

Saturation

If responses to single photons were to summate linearly, as Eq. I.1 implies, then the summation of 100 bumps would lead to several hundred mV of depolarization in *Limulus* and locust photoreceptors. Obviously, this is not physiologically possible: the voltage response will saturate according to the relationship:

$$v = \frac{Eax}{G_r + ax} \quad (\text{I.3})$$

where v is the membrane depolarization, x is the light intensity, a is the increase of light-activated conductance per unit light intensity, E is the reversal potential of the light-activated conductance, and G_r is the membrane conductance at rest (in the dark). Eq. I.3 is known in vision research as the Naka-Rushton curve (Naka and Rushton, 1966), while most biologists know it by the name of Michaelis-Menten curve for enzyme kinetics. Note that in this dissertation v will always refer to the value of the membrane voltage relative to the resting potential, *i.e.* to the membrane depolarization. Similarly, reversal potentials will be indicated relative to the resting

potential.

Equation I.3 ignores the dynamics of phototransduction, but would be sufficient to describe the peak response to a flash or the steady-state response to steady illumination, according to the simple models of phototransduction described above. However, a photoreceptor working according to Eq. I.3 would have a serious drawback: if the average light intensity is sufficient to saturate the photoresponse, then the animal would be functionally blind, since its photoreceptors would be completely and constantly depolarized. If the sensitivity a is reduced to prevent saturation, then the responses to dim light would become indistinguishable from background noise.

Adaptation

At any moment, a natural scene contains a range of light intensities of about 2 log-units on average, but the contrast between adjacent objects is rarely more than one log-unit (Laughlin, 1981, page 212). Therefore, the useful operating range of a photoreceptor following Eq. I.3 would be sufficient to encode normally encountered contrast assuming that the reversal potential E is more than 1 log-unit larger than the standard deviation of the noise. The problem mentioned in the previous paragraph arises from the large variations of illuminance during the day, as well as those due to weather conditions, forest shade, *etc.* Photoreceptors can, and do, solve the problem by adaptation, *i.e.* by changing the gain factor a according to the average light intensity to which they are exposed. Adaptation is actually a general term

including several different mechanisms (Autrum, 1981). Circadian variations independent of illumination are also known: in this case, the visual system has prior, genetic knowledge of the changes of illuminance which are to be expected in a 24 h period.

Adaptation mechanisms affect the gain so that the steady-state response to illumination no longer follows Eq. I.3 . However, a flash response should still follow that equation, although the factor a would be affected by the adaptation level of the photoreceptor.

Intensity coding

In insect photoreceptors, the intensity-response relationship obtained with flashes increases more slowly than Eq. I.3 predicts. The mechanism underlying this discrepancy is one of the main topics of this dissertation. The intensity-response curve determined experimentally can be fitted with a modification of Eq. I.3:

$$v = \frac{Eax^n}{G_r + ax^n} \quad (\text{I.4})$$

where $0 < n \leq 1$. The values of n providing the best fit to the experimental data depend on the species (Laughlin, 1981). For instance, n is equal to 0.5 for locusts (Laughlin and Lillywhite, 1982), to 0.66 for the fly *Calliphora* (Laughlin and Hardie, 1978), and to 0.6 for the fruitfly *Drosophila* (Wu and Pak, 1978). The fit provided by Eq. I.4 is accurate only for moderately low stimulus intensities, producing responses

less than half of E (Matic and Laughlin, 1981).

The relationship between light stimulation and voltage response is known as **intensity coding**, since the voltage response can be considered as a code for a certain value of the light intensity. A photoreceptor which codes intensity according to Eq. I.4 operates a **sublinear summation** of responses, because the response to m photons is less than m times the response to a single photon. The difference between the linear prediction and the actual response will be referred to as **response depression** in the following chapters. A positive value of this depression will be taken to indicate that the linear prediction is larger than the actual response. There is reason to believe that sublinear summation is of functional relevance to the operation of the visual system and that the response depression is generated by a specific physiological mechanism. This mechanism will be defined as **gain control mechanism**.

Sublinear summation is known to occur only in insects. Vertebrate photoreceptor responses follow Eq. I.3 (turtle cones: Baylor and Fuortes, 1970; skate rods: Dowling and Ripps, 1972; gecko rods: Kleinschmidt and Dowling, 1975), except when the "flash" is actually more than one second in duration, long enough to be affected by the adaptation that it causes (salamander rods and cones: Normann and Werblin, 1974). Crayfish photoreceptors also follow Eq. I.3 (Glantz, 1972). To our knowledge, no such measurements have been reported for *Limulus*, but at low flash intensities the response has been shown to be linear both in lateral eye photoreceptors (Borsellino and Fuortes, 1968) and under voltage clamp in ventral eye photoreceptors (Lisman and Brown, 1975; Fein and Charlton, 1977), although an earlier publication

reported different results (Srebro and Behbehani, 1974). Linearity at low flash intensities is compatible with Eq. I.3 but not with Eq. I.4. Squid photoreceptors (Hagins, 1965) and rat rods (Penn and Hagins, 1972) also respond linearly to small intensities.

I.4. System analysis

This section will provide a brief and not very rigorous overview of the mathematical techniques employed in Chapter III. A more extensive treatment can be found in Marmarelis and Marmarelis (1978), Schetzen (1980), or Bendat and Piersol (1986).

A system is said to be linear if the sum of two inputs $x_0(t)$ and $x_1(t)$ produces a response $v_{0+1}(t)$ equal to the sum of the responses $v_0(t)$ and $v_1(t)$ to the individual inputs. A linear system is completely characterized by its impulse response, which in the case of a photoreceptor is the response to a flash. Any input to the system can be decomposed into a train of closely spaced impulses, which generate additive impulse responses.

Since the responses that will be discussed show a sublinear summation, we must employ nonlinear system analysis. By analogy to the linear impulse response, a "second-order impulse response" can be defined as the extra response which is generated by the interaction between 2 impulses, as compared to the sum of

responses to the individual flashes. In the case of sublinear summation, the extra response has a reversed polarity compared to the linear response.

The linear impulse response is a function of time after the impulse. Similarly, the "second-order impulse response", or second-order Volterra kernel, is a function of 2 time variables, the time after the first impulse and the time after the second impulse. A kernel of order i is generally represented as:

$$h_i(\tau_1, \tau_2, \dots, \tau_i) \quad (I.5)$$

and is a function of i time variables (given in milliseconds in this dissertation). Volterra and Wiener kernels differ in the methods by which they are calculated (see section III.2) as well as in the methods in which they must be used for calculating the system output. In the case of Volterra kernels, the system output is given by:

$$\begin{aligned} v(t) = & h_0 + \int_0^{\infty} h_1(\tau_1) x(t-\tau_1) d\tau_1 + \\ & + \int_0^{\infty} \int_0^{\infty} h_2(\tau_1, \tau_2) x(t-\tau_1) x(t-\tau_2) d\tau_1 d\tau_2 + \dots \end{aligned} \quad (I.6)$$

Where $v(t)$ is the system output and $x(t)$ is the system input, as functions of time.

If the system is not linear, its response to an impulse is not equal to its linear (first-order) Volterra kernel, since even a single impulse interacts with itself to generate second- and higher- order responses. Because of this limitation, Wiener kernels are favoured over Volterra kernels for system analysis. Wiener kernels are calculated by cross-correlation between the input and the output of the system. If the

input signal $x(t)$ is random (more specifically, if it is a Gaussian white noise signal), the first-order Wiener kernel can be defined as:

$$h_1(\tau_1) = \frac{1}{\sigma_x^2} \int_{-\infty}^{+\infty} v(t) x(t-\tau_1) dt \quad (I.7)$$

Where σ_x^2 is the power level of the input signal (the square of the RMS power level). Similar, but more complex, formulas apply for Wiener kernels of second or higher order.

In the case of linear or second-order systems, the Wiener and Volterra kernels are identical. However, if nonlinearities of higher order are present, first- and second-order Wiener kernels can be computed from responses to white noise without prior knowledge of these nonlinearities, while Volterra kernels cannot be computed from responses to single and paired impulses in such a case. On the other hand, Wiener kernels do not have the intuitive physical interpretation that Volterra kernels have.

Volterra and Wiener kernels are synthetic representations of the input-output relationship of a system. This relationship can be explained by various underlying mechanisms. However, a mechanism that predicts a relationship different from that determined by system analysis techniques can be ruled out by comparison between the predicted and experimental kernels.

I.5. Organization of the following chapters

The question that will be addressed in chapter II is related to the origin of variability of single photon responses. The experiments described in that chapter provide support for the hypothesis that this variability is intrinsic to the mechanism of phototransduction. Apart from the implications of these findings for models of the mechanism itself, the study was a preliminary investigation employing localized stimuli in a superfused eye preparation. This technique was later used for some of the experiments described in Chapter IV. Knowledge of the characteristics of elementary responses at different sites in the photoreceptor was helpful in investigating nonlinear interactions between localized stimuli.

The main problem investigated in this dissertation is the biophysical mechanism of the sublinear summation described in section I.3. Chapter III presents results obtained by system analysis techniques. The kernels obtained by two different techniques proved to be similar, suggesting that common mechanisms of transduction and gain control were operating in the two different stimulus conditions. However, the kernels did not provide conclusive evidence as to what these mechanisms could be.

Chapter IV describes results indicating that the gain control mechanism is a voltage-activated conductance. The experiments described in that chapter were aimed at identifying the nature of the mechanism, rather than providing a complete characterization of the hypothetical membrane conductance. Further work along

these lines would seem indicated.

Finally, Chapter V provides a quantitative, although preliminary, model of the gain control mechanism, based on the results of the previous chapters. This model makes some specific predictions about voltage-activated channels in the photoreceptor membrane, as well as about the input-output relationship of the photoreceptor. These predictions should be tested by further research. Chapter V also contains a brief review of voltage-activated conductances in photoreceptors and a summary of the main conclusions of this dissertation.

I.6. References

- Attwell D (1986) Ion channels and signal processing in the outer retina. *Quart J Exp Physiol* 71:497-536.
- Autrum H (1981) Light and dark adaptation in invertebrates. In: Handbook of Sensory Physiology VII/6c (H. Autrum, ed.) 1-91. Springer-Verlag, Berlin.
- Bacigalupo J, Lisman JE (1984) Light activated channels in *limulus* ventral photoreceptors. *Biophys J* 45:3-5.
- Barlow R (1990) What the brain tells the eye. *Sci Am* 262 (April 1990), 90-95.
- Baumann F (1974) Electrophysiological properties of the honeybee retina. In: The compound eye and vision of insects (G.A. Horridge, ed.) 53-74. Clarendon Press, Oxford.
- Baylor DA, Fuortes MGF (1970) Electrical responses of single cones in the retina of the turtle. *J Physiol* 207:77-92.
- Baylor DA, Hodgkin AL, Lamb TD (1974) Reconstruction of the electrical responses of turtle cones to flashes and steps of light. *J Physiol* 242:759-791.
- Baylor DA, Lamb TD, Yau KW (1979) Responses of retinal rods to single photons. *J Physiol* 288:613-634.
- Bendat JS, Piersol AG (1986) Random data: analysis and measurement procedures. Wiley, New York.
- Bennett RB, Tunstall J, Horridge GA (1967) Spectral sensitivity of single retinula cells of the locust. *Z Vergl Physiol* 55:195-206.

- Borsellino A, Fuortes MGF (1968) Responses to single photons in visual cells of *Limulus*. *J Physiol* 196:507-539.
- Borst A, Egelhaaf M (1989) Principles of visual motion detection. *Trends Neurosci* 13:55-64.
- Dowling JE, Ripps H (1972) Adaptation in skate photoreceptors. *J Gen Physiol* 60:698-719.
- Fein A (1986) Excitation and adaptation of *Limulus* photoreceptors by light and inositol 1,4,5-trisphosphate. *Trends Neurosci* 9:110-114.
- Fein A, Charlton JS (1977) Enhancement and phototransduction in the ventral eye of *Limulus*. *J Gen Physiol* 69:553-569.
- Fein A, Szuts EZ (1982) Photoreceptors: their role in vision. Cambridge University Press, Cambridge.
- French A (1980) The linear dynamic properties of phototransduction in the fly compound eye. *J Physiol* 308:385-401.
- Fulpius B, Baumann F (1969) Effects of sodium, potassium and calcium ions on slow and spike potentials in single photoreceptor cells. *J Gen Physiol* 53:541-561.
- Fuortes MGF, Hodgkin AL (1964) Changes in time scale and sensitivity in the ommatidia of *Limulus*. *J Physiol* 172:239-263.
- Glantz RM (1972) Visual adaptation: a case of non-linear summation. *Vision Res* 12:103-109.
- Hagins WA (1972) The visual process: excitatory mechanisms in the primary receptor cells. *Ann Rev Biophys Bioeng* 1:131-158.

- Hagins WA (1965) Electrical signs of information flow in photoreceptors. *Cold Spring Harbor Symp Quant Biol* 30:403-418.
- Hamdorf K (1979) The physiology of invertebrate visual pigments. In: Handbook of Sensory Physiology, VII/6A (H. Autrum, ed.) 145-224. Springer-Verlag, Berlin.
- Hartline HK, Ratliff F (1972) Inhibitory interactions in the retina of *Limulus*. In: Handbook of Sensory Physiology, VII/2 (M.G.F. Fuortes, ed.), 381-448. Springer-Verlag, Berlin.
- Howard J (1983) Variations in the voltage response to single quanta of light in the photoreceptors of *Locusta migratoria*. *Biophys Struct Mech* 9:341-348.
- Johnson EC, Robinson PR, Lisman JE (1986) Cyclic GMP is involved in the excitation of invertebrate photoreceptors. *Nature* 324:468-470.
- Kandel E (1976) Cellular basis of behavior: an introduction to behavioral neurobiology. Freeman, San Francisco.
- Kleinschmidt J, Dowling JE (1975) Intracellular recordings from gecko photoreceptors during light and dark adaptation. *J Gen Physiol* 65:617-648.
- Koester J, Byrne JH (1980) Molluscan nerve cells: from biophysics to behavior. Cold Spring Harbor Laboratory, Cold Spring Harbor, NY.
- Lamb TD (1986) Transduction in vertebrate photoreceptors: the roles of cyclic GMP and calcium. *Trends Neurosci* 9:224-228.
- Laughlin SB (1981) Neural principles in the visual system. In: Handbook of Sensory Physiology, VII/6B (H. Autrum, ed.) 133-280. Springer-Verlag, Berlin.
- Laughlin SB (1987) Form and function in retinal processing. *Trends Neurosci*

10:478-483.

Laughlin SB, Hardie RC (1978) Common strategies for light adaptation in the peripheral visual systems of fly and dragonfly. *J Comp Physiol A* 128:319-340.

Laughlin SB, Lillywhite PG (1982) Intrinsic noise in locust photoreceptors. *J Physiol* 332:25-45.

Lillywhite PG (1977) Single photon signals and transduction in an insect eye. *J Comp Physiol A* 122:189-200.

Lillywhite PG (1978) Coupling between locust photoreceptors revealed by a study of quantum bumps. *J Comp Physiol A* 125:13-27.

Lisman JE, Brown JE (1975) Light-induced changes of sensitivity in *Limulus* ventral photoreceptors. *J Gen Physiol* 66:473-488.

Marmarelis PZ, Marmarelis VZ (1978) Analysis of Physiological systems. The white-noise approach. Plenum Press, New York.

Matic T, Laughlin SB (1981) Changes in the intensity-response function of an insect's photoreceptors due to light adaptation. *J Comp Physiol* 145:169-177.

Menzel R (1979) Spectral sensitivity and colour vision in invertebrates. In: Handbook of Sensory Physiology VII/6A (H. Autrum, ed.) 503-580. Springer-Verlag, Berlin.

Muller KJ, Nicholls JG, Stent GS (1981) Neurobiology of the leech. Cold Spring Harbor Laboratory, Cold Spring Harbor, NY.

Naka KI, Rushton WAH (1966) S-potentials from colour units in the retina of fish (Cyprinidae). *J Physiol* 185:536-555.

Nilsson DE (1990) From cornea to retinal image in invertebrate eyes. *Trends Neurosci*

13:55-64.

Normann RA, Werblin FS (1974) Control of retinal sensitivity. I: Light and dark-adaptation of vertebrate rods and cones. *J Gen Physiol* 63:37-61.

Payne R, Howard J (1981) Response of an insect photoreceptor: a simple log-normal model. *Nature* 290:415-416.

Penn RD, Hagins WA (1972) Kinetics of the photocurrent of retinal rods. *Biophys J* 12:1073-1094.

Pugh Jr EN, Miller WE - section editors (1987) Special topic: phototransduction in vertebrates. *Ann Rev Physiol* 49:711-812.

Schetzen M (1980) The Volterra and Wiener theories of nonlinear systems. Wiley, New York.

Schnakenberg J (1989) amplification and latency in photoreceptors: integrated or separated phenomena?. *Biol Cybern* 60:421-437.

Selinger Z, Minke B (1988) Inositol lipid cascade of vision studied in mutant flies. *Cold Spring Harbor Symp Quant Biol* 53:333-341.

Spiegler JB, Yeandle S (1974) Independence of location of light absorption and discrete wave latency distribution in *Limulus* ventral nerve photoreceptors. *J Gen Physiol* 64:494-502.

Srebro R, Behbehani M (1974) Light adaptation in the ventral photoreceptor of *Limulus*. *J Gen Physiol* 64:166-185.

Stieve H (1984) Bumps, the elementary excitatory responses of invertebrates. In: The molecular mechanism of photoreception (H. Stieve, ed.) 199-230. Springer-Verlag,

Berlin.

Strausfeld NJ (1976) Atlas of an insect brain. Springer-Verlag, Berlin.

Trujillo-Cenoz O (1972) The structural organization of the compound eye in insects.

In: Handbook of Sensory physiology, VII/2 (M.G.F. Fuortes, ed.), 5-62. Springer-Verlag, Berlin.

Vishnevskaya TM, Cherkasov AD, Shura-Bura TM (1986) Spectral sensitivity of photoreceptors in the compound eye of the locust. *Neurophysiology* 18:54-60.

von Frisch K (1971) Bees: their vision, chemical senses, and language. Cornell University Press, Ithaca, NY.

Wehner R (1981) Spatial vision in arthropods. In: Handbook of Sensory Physiology, VII/6C (H. Autrum, ed.) 287-616. Springer-Verlag, Berlin.

Wilson M, Garrard P, McGinness S (1978) The unit structure of the locust compound eye. *Cell Tiss Res* 195:205-226.

Wu C-F, Pak WL (1978) Light-induced voltage noise in the photoreceptor of *Drosophila melanogaster*. *J Gen Physiol* 71:249-268.

Yau KW, Lamb TD, Baylor DA (1977) Light-induced fluctuations in membrane current of single toad rod outer segments. *Nature* 269:78-81.

Yeandle S (1958) Evidence of quantized slow potentials in the eye of *Limulus*. *Am J Ophthalmol* 46(3,part 2):82-87.

Yeandle S (1985) Statistics and quantum bumps in arthropod photoreceptors. *Federation Proc* 44:2947-2949.

II. SINGLE PHOTON RESPONSES:

EFFECTS OF STIMULUS LOCATION ON AMPLITUDE AND TIME COURSE¹

II.1. Introduction

Dark-adapted photoreceptors of several invertebrates have been found to generate discrete membrane potential responses, called quantum bumps, when exposed to low levels of illumination. There is strong evidence that each bump is triggered by a single photon absorption, although in some species bumps are also generated at a constant rate independently of illumination. Quantum bumps may be viewed as products of the elementary processes of phototransduction (for reviews, see Fein and Szuts, 1982; Stieve, 1986) and a model for the generation of bumps is therefore an essential component to understanding the phototransduction mechanism. Quantum bumps are very variable in latency, amplitude, and time course. It is generally assumed that this variability arises from statistical fluctuations in the chemical reactions involved (Borsellino and Fuortes, 1968), but an alternative possibility is that the variability arises at least in part from differences in the sensitivity and speed of response at different locations in the photoreceptor. In *Limulus* ventral photoreceptors, a single bump originates from a conductance change which is limited to a small region of the

¹ A version of this chapter has been published: Pece AEC, French AS (1989) *Journal of Comparative Physiology A* 164:365-375.

photoreceptor with a radius of about 2 μm (Brown and Coles, 1979). This mechanism would allow regional dishomogeneity to contribute to the variability of bumps.

Brown *et al.* (1979) found that *Limulus* ventral photoreceptors are nearly isopotential, even when subjected to saturating illumination, and Payne (1982) estimated the length constant of locust photoreceptors to be greater than the length of the cell. These results demonstrate that variable attenuation due to passive cable conduction of bumps originating at random sites within the photoreceptor cannot account for the variability of the bumps. However, if the average amplitudes and/or time courses of bumps originating at different locations were different because of regional variations in the transduction mechanism, then randomness in the photon absorption site would contribute to bump variability.

During natural stimulation of photoreceptors, photons are absorbed at random positions within the cell, so that bump variability could result from both intrinsic factors, such as chemical fluctuations, and regional factors. One way to reduce or eliminate the variability due to regional factors would be to restrict the light stimulus to a small region of the photoreceptive structure (rhabdomere). Using this technique in *Limulus* ventral photoreceptors, Spiegler and Yeandle (1974) found no significant differences in bump latency distributions, but significant differences in bump amplitude distributions with stimulation at 2 different positions in the cell. However, intrinsic amplitude variability was still present at each site of stimulation.

This chapter describes the results of a similar investigation of quantum bumps in locust photoreceptors. This preparation allowed localized optical stimulation, at

locations which were reproducible in different animals. This is because the locust photoreceptor is a thin, elongated structure, in which a light stimulus only needs to be restricted along the long axis, and the position of the stimulus along this axis can easily be measured (see Wilson *et al.*, 1978, for a description of the photoreceptor structure). By contrast, in *Limulus* the photoreceptor is more spherical and the rhabdomere varies in shape and location between cells. Other advantages of the locust are that spontaneous bumps do not affect the statistics (Lillywhite, 1977) and that the spread of bump latencies is smaller than it is in *Limulus* (Howard, 1983).

The statistical analysis was based on the parameters of the log-normal model for the time-course of phototransduction (Payne and Howard, 1981; see Methods). This model had the advantage of using only 3 parameters, each of which, after suitable transformation, had similarly-shaped distributions for all cells and locations of stimulation. We investigated whether the parameters of the log-normal model were statistically affected by the position within the photoreceptor where quantum bumps are generated.

II.2. Methods

Preparation

Adult locusts (*Locusta migratoria*) from a laboratory colony were maintained under a 12 h light, 12 h dark photocycle. In order to allow optical stimulation of different

regions of the photoreceptor, we used a modification of the preparation developed by Payne (1980). The head of the locust was first divided into 2 parts by a horizontal cut, separating the mandibles from the upper part of the head. The upper part was then divided again by a transverse cut going across both compound eyes (see Fig. II.1). The anterior part was pinned to a layer of Sylgard on the bottom of the perfusion chamber, with the cut surface of the eyes facing upwards. The perfusion saline was the same as that used by Payne (1980) and contained 200 mM NaCl, 3.4 mM KCl, 0.5 mM CaCl₂, 10 mM HEPES and 90 mM glucose. The pH was between 7.0 and 7.4. The saline was saturated with O₂ and pumped into and out of the perfusion chamber by a peristaltic pump. The perfusion rate was 4 ml/min. and the volume of saline in the chamber was about 1.5 ml. The photoreceptors were dark-adapted for at least one hour before the experiment.

Stimulation

The optical stimulus was generated by a Xenon flash tube and transmitted to the preparation through a fiber-optic light guide to a slit 25 μm wide in the focal plane of the phototube of a Wild M5A microscope. The flash tube was controlled by a PDP-11 digital computer using a digital-to-analog converter. The image of the slit was focused on the preparation and oriented perpendicularly to the long axis of the photoreceptors. The width of the image of the slit was 15 μm or in some experiments 30 μm , depending on the setting of the magnification in the microscope. A micromanipulator screw holding the end of the light guide in the phototube was used

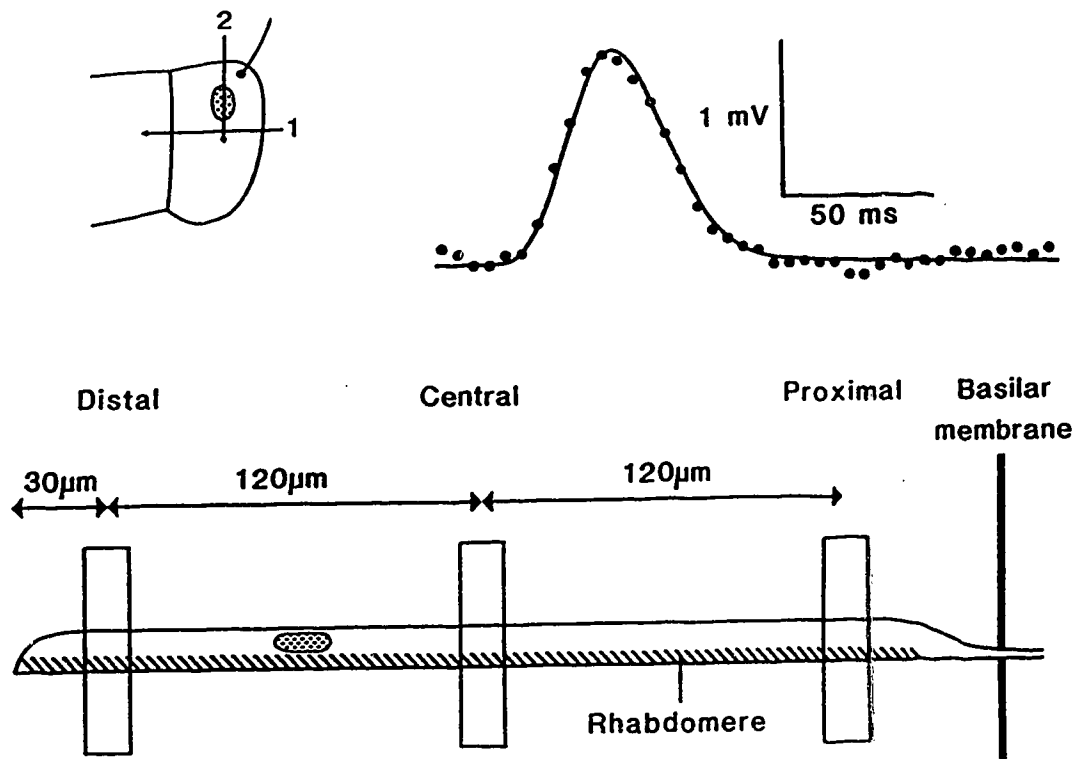


Fig. II.1. Upper left: Diagram of the cuts made through the locust head to expose a section of the eye for recordings.

Upper right: Voltage recording of a single bump in cell #1 versus time after the flash (dots) together with the computer fit to the log-normal model of Eq. II.1 (continuous line). The best fit was obtained with parameters $v_p = 1.33$ mV, $t_p = 75$ ms, $w = 0.19$.

Lower: Diagram of a photoreceptor with superimposed bars representing the 3 positions of the light stimuli that were used. The recording electrode was inserted immediately distal to the central stimulus position.

to move the image of the slit on the preparation. The time course and the intensity of the flash were measured with a phototransistor (Motorola MRD 3050) and were found to be very consistent. The duration of the flash was less than 0.15 ms. Each flash delivered a maximum of about 700 photons/ μm^2 on the preparation. The flash intensity was adjusted by an iris diaphragm on the phototube, and with neutral density filters, for each position within each cell so that less than half of the flashes gave rise to bumps.

Recordings

Intracellular recordings from reticular cells were performed with standard glass intracellular microelectrodes filled with 3 M potassium acetate and having resistances ranging between 60 and 100 M Ω . Electrodes were lowered onto the preparation while trying to keep the electrode tip immediately distal to the central stimulus site (see Fig. II.1). The reference Ag-AgCl electrode was kept in the superfusion bath. Resting potentials were in the range 40-80 mV.

Intracellular potentials were amplified by a Getting model 5 microelectrode amplifier and sampled at 2.5 ms intervals by a 12-bit analog-to-digital converter connected to the computer. Each flash response was stored separately on a magnetic disc as a set of data points representing intracellular voltage samples at 2.5 ms intervals for a total time of 250 ms after the flash. Individual responses were only stored if the intracellular voltage rose above a threshold criterion during this time interval. The threshold was 5.0 times the standard deviation of the recorded voltage

noise in the dark. Flashes were generated every 0.5 s until a response rising above threshold was recorded; this response was stored and flashes resumed after a 2.1 s interval, to avoid adaptation effects. In order to minimize the occurrence of multiple bumps, the stimulus intensity was adjusted to produce a response rising above threshold for not more than 50% of the flashes. The protocol was somewhat different for the first three cells in the tables: the total duration of the individual flash responses was 225 ms, the threshold criterion was 5.6 times the standard deviation of the noise in the dark, and flashes were regularly generated every 1.5 s but only the responses of amplitude above threshold were stored.

Records of bumps obtained in this way were recorded together in computer data files. Each data file contained bumps resulting from stimulation at a single location, and one or more data files were obtained for each location within each cell. This procedure probably introduced artefactual differences between positions within each cell, since the recording could not be expected to be perfectly stable. However, the order in which each location was stimulated was different in different cells.

Bump parameter calculation

Each individual flash response was fitted with the equation:

$$v = v_p \cdot \exp\{-[\ln(t/t_p)]^2 / 2w^2\} \quad (\text{II.1})$$

where v is the membrane voltage in mV, t is the time after an instantaneous flash of light, v_p is the peak response amplitude in mV, t_p is the time to peak (time between

flash and peak voltage response) in ms, and w is a dimensionless width parameter. We shall refer to w as 'relative width' since w is proportional within 1% to the ratio of half-amplitude width to time-to-peak, the proportionality factor being 2.35 (Howard *et al.*, 1984). Eq. II.1 represents the log-normal model of the time-course of photoreceptor potentials (Payne and Howard, 1981). An example of a bump, together with its computer-generated fitting curve, is shown in Fig. II.1 (upper right). The log-normal model has not been applied previously to the analysis of single bumps, but we found that it can describe bumps quite well and its parameters have advantages for the statistical analyses that were carried out, as will be evident below.

All responses which could not be approximated by the log-normal fit were discarded. About one quarter of the responses above threshold had to be discarded, usually because more than one peak (and hence more than one bump) was present, or because of a drift in the baseline, or an excess of external noise. The selection was carried out in two phases: The first phase by the fitting program, which eliminated responses that were too wide to allow a measure of the baseline (presumably because more than one bump was present) and responses in which two separate peaks above threshold were present. In the first three cells, responses for which the final fit was significantly different from the experimental response, as measured by a square error criterion, were discarded as well. Since this last criterion resulted in very few responses being discarded, it was omitted for the other cells. The remaining responses were then displayed with the fit superimposed, inspected by eye, and discarded when distinct secondary peaks below threshold were present or when the record showed

clear trends away from the best fit in some particular period of the response. The selection was required only because estimates of any parameter would have been much more difficult in the discarded responses.

The correlations between the square error of the fit of each individual bump and several bump parameters were calculated for cells 1 and 2. The correlations between the error and the delay, time-to-peak, width parameter, or half-amplitude width were not significant, the largest being 0.03. Therefore, our selection criterion, for bumps which could be well fitted by the log-normal model, did not select bumps on the basis of their time-course parameters. There was a correlation equal to 0.26 ($p < 0.01$) between bump amplitude and square error of the fit. The reason for this correlation probably was that the systematic deviation of the response from the log-normal model was proportionally larger when the response itself was larger. In any case, even in the largest responses the log-normal model seemed to provide a good approximation of the amplitude, width, and time-to-peak of the bumps. As pointed out above, there was no need to select responses on the basis of the square error of the fit if the bumps were acceptable by all the other criteria, such as no multiple peaks *etc.*

Statistical analysis

Two of the three parameters of the log-normal model were transformed, the amplitude v_p to $\ln(v_p)$ and the time to peak t_p to $1/t_p$, as these transformed parameters had distributions with equal variance for all cells and all positions of the stimulus.

The significance of differences between the average parameters of bumps originating at different locations or from different cells was estimated by a two-way analysis of variance with interactions (Searle, 1971). The transformations of amplitude to log-amplitude and time to peak to inverse time to peak were required to ensure validity of the analysis of variance.

Within the context of our analysis, the set of all responses to stimulation at one position within one cell is called a 'subclass' of responses. When a two-way analysis of variance is performed on data with unequal, non-proportional subclass sample sizes, a problem of interpretation arises because part of the variance will be attributed to one or the other factor, cells or positions in our case, depending on which factor is analyzed first (Searle, 1971). We therefore performed both sequences of analysis, and the results from both will be presented.

Note that statistics of average, standard deviation, and correlation coefficients of cell effects (Table II.5) were performed after the least-square fits for the cell effects were transformed back to amplitudes and times to peak, as in the rightmost column of Tables II.2, II.3, and II.4. This procedure simplified the interpretation of the statistics for cell effects but might generate confusion with the corresponding statistics for individual bumps within a single subclass (Table II.6).

II.3. Results

The data presented here are based on recordings from 10 cells which were maintained long enough to store bumps due to stimulation at 3 sites in the photoreceptor: distal, central, and proximal. A total of 1617 bumps were analyzed, distributed approximately equally between the 3 locations. However, each of the 30 subclasses contained a different number of bumps. The central stimulus was placed approximately halfway between the distal and proximal ends of the photoreceptor. The other two stimuli were placed 120 μm proximally or distally to the central stimulus. The length of the rhabdomere in these cells is about 300 μm (Wilson *et al.*, 1978). The locations of the stimuli are shown in Fig. II.1.

Analysis of variance allowed the sum of squares of differences from the mean to be partitioned into components due to differences between cells, differences between locations, interactions between cells and locations (when the cells component and the positions component are not simply additive in producing the subclass means), and intrinsic variability or 'error'. As will be seen in the tables below, all values of F were significant at least at the $p < 0.01$ level and in this respect there were no differences between the results of the two different sequences of analyses (see Methods). We hypothesize that the significant interaction effects were caused by slow random fluctuations of cell parameters during each experiment. These fluctuations probably did not affect the least-squares fits to a great extent (see Discussion), except possibly for the width parameter.

Fig. II.2 shows the least-squares fits of position effects compared to the standard deviations of the intrinsic variability for the 3 parameters.

Note that log-amplitude and inverse time to peak have been transformed back to amplitude (normalized to the amplitude of an average bump originating at the center of the cell) and time to peak.

Frequency of responses

Light intensity had to be increased by a factor of between 1.0 and 1.5 log units in order to obtain a bump frequency, *i.e.* fraction of flashes eliciting a response, at the distal location comparable to that at the proximal and central locations. Moving the stimulus between the latter two locations required only minor adjustments of light intensity. The light intensities used for different cells were very similar within each location. Frequencies of responses interpreted as single bumps are listed in Table II.1. These frequencies can be compared with the frequencies predicted for Poisson distributions. The averages of the distributions were calculated from the number of flashes resulting in no response above threshold. The predicted frequencies of single bump responses are in Table II.1, second column. They are in close agreement with the actual frequencies for all subclasses, as would be expected if the responses interpreted as single bumps were indeed single-photon events. The χ^2 value was 10.53 ($p > 0.99$ for 30 degrees of freedom).

Table II.1. Numbers of responses expected to contain a single bump, of responses interpreted as single-bump events, and of presumed single-bump events which could be fitted by Eq. II.1.

Cell #	Position	Numbers of bumps		
		predicted	observed	analyzed
1	Distal	119.9	108	108
	Central	61.0	56	55
	Proximal	58.8	54	54
2	Distal	59.9	63	63
	Central	67.1	73	68
	Proximal	65.9	64	64
3	Distal	62.7	61	59
	Central	77.1	76	72
	Proximal	72.9	80	80
4	Distal	119.5	118	103
	Central	76.1	81	58
	Proximal	107.7	107	80
5	Distal	56.5	53	39
	Central	66.9	62	58
	Proximal	68.8	59	53
6	Distal	52.5	54	44
	Central	85.6	92	66
	Proximal	78.1	86	60
7	Distal	71.9	79	68
	Central	60.8	64	54
	Proximal	90.8	92	66
8	Distal	8.8	9	8
	Central	38.4	36	26
	Proximal	38.5	37	32
9	Distal	82.8	95	37
	Central	101.5	105	51
	Proximal	28.4	27	15
10	Distal	21.7	22	18
	Central	28.1	31	25
	Proximal	43.3	42	33
Total		1972.0	1986	1617
of which:	Distal			547
	Central			533
	Proximal			537

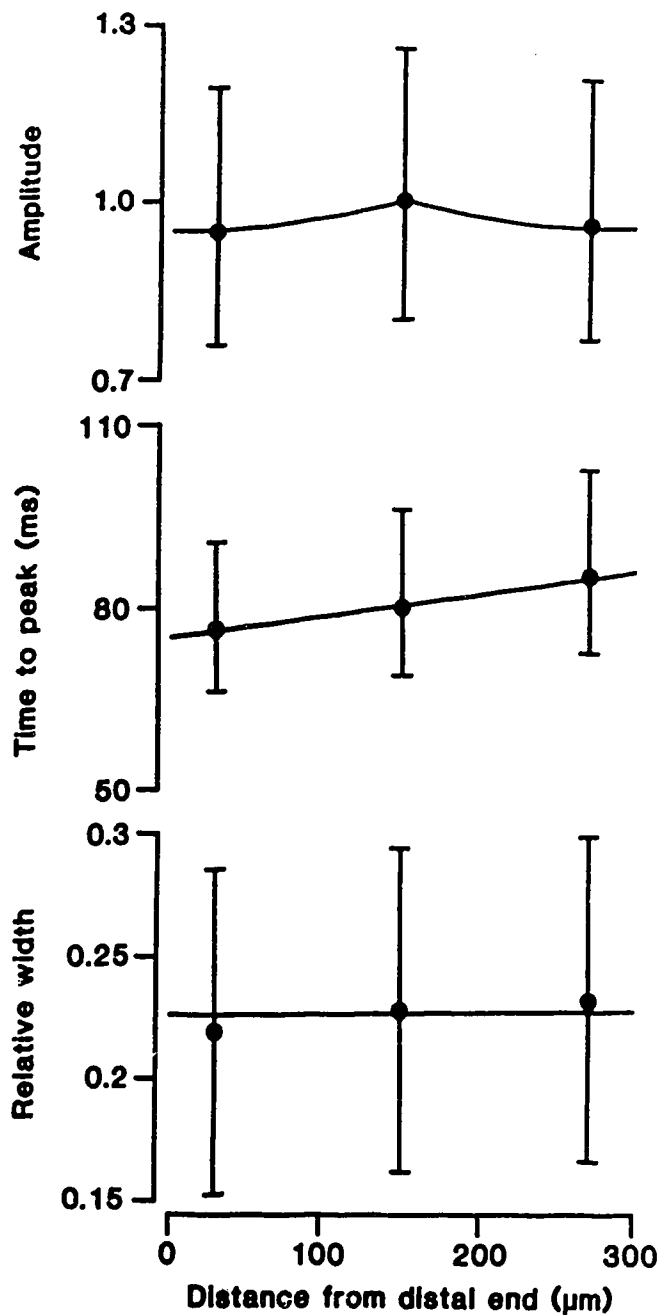


Fig. II.2. Bump parameters as functions of position along the photoreceptor. Filled circles were obtained from the least-squares fits of position effects from analysis of variance (Tables II.2, II.3, and II.4) and bars are intervals of one standard deviation of intrinsic variability on each side of the best fit. For the top 2 graphs, least-squares fits and intervals are transformed back from log-amplitude to amplitude (normalized to average amplitude of bumps generated centrally) and from inverse time-to-peak to time-to-peak. Continuous lines correspond to Eq. II.5 (amplitude), a linear regression fit (time to peak), and the hypothesis of invariance over position (relative width).

Light scatter

The light stimulus produced a sharply focused slit on the upper surface of the preparation, but since the cells we recorded from were generally not in the top layer of the slice, we tried to measure the extent by which the overlying layers of cells make the stimulus less sharply localized by light scattering. We oriented a slit (7 μm wide, 75 μm long) parallel to the long axes of the photoreceptor cells and shone a steady light through it. We moved the slit perpendicularly to its axis, so that the stimulus would fall on a series of different cells, and measured bump frequencies in a single cell during stimulation at different slit positions. We found that the sensitivity (as measured by bump frequency) decreased to half the maximum over about 20 μm . In a few cells, the sensitivity decreased at this rate only down to about 15% or 20% of the maximum, and then much more slowly, so that it was still above 10% at 120 μm from the peak. We have no explanation for this occasional finding. However, there was no evidence for significant scatter at similarly large distances in the longitudinal direction, since in all our experiments moving the slit by 120 μm from the central to the distal position resulted in a change of sensitivity of more than one order of magnitude, as mentioned above.

Bump amplitude

Distributions of bump amplitudes (parameter v_p in Eq. II.1) for the 3 locations are shown in Fig. II.3 for cell #1 from our tables. The distributions at different locations were similar, but if distributions from different cells were compared, it was found that

the variance and the mean amplitude increased together. However, we found that the natural logarithm of the amplitude in mV had a similar distribution for all cells and positions. Therefore, we used this transformed parameter, which we call log-amplitude, for all analyses.

Table II.2 contains subtotals means and least-squares fits of cell and position effects, together with the results of an analysis of variance for log-amplitude. The cell and position effects on log-amplitude were calculated with the constraint that the central position effect be null, in accordance with the hypothesis that position effects are caused by attenuation of the bumps arising distally and proximally, but not of the bumps originating centrally (see Discussion). Therefore, in Table II.2 the cell effects can be interpreted as the average bump amplitudes in mV and the position effects as the attenuation of this amplitude caused by the electrotonic distance between the stimulation and the recording sites.

As can be seen in the column of the sums of squares, the position effects gave a far smaller contribution to the total variability when compared to intrinsic or cell effects. Log-amplitude was approximately the same at proximal and distal locations, but was larger at the central location (Fig. II.2). However, the difference corresponded to only 5% of the average bump amplitude and was small when compared to the intrinsic variability, shown by error bars in the same figure. The fit in Fig. II.2 was based on estimates of cable attenuation of constant-current bumps originating at different locations within the photoreceptor and recorded at the center of the cell (see Discussion).

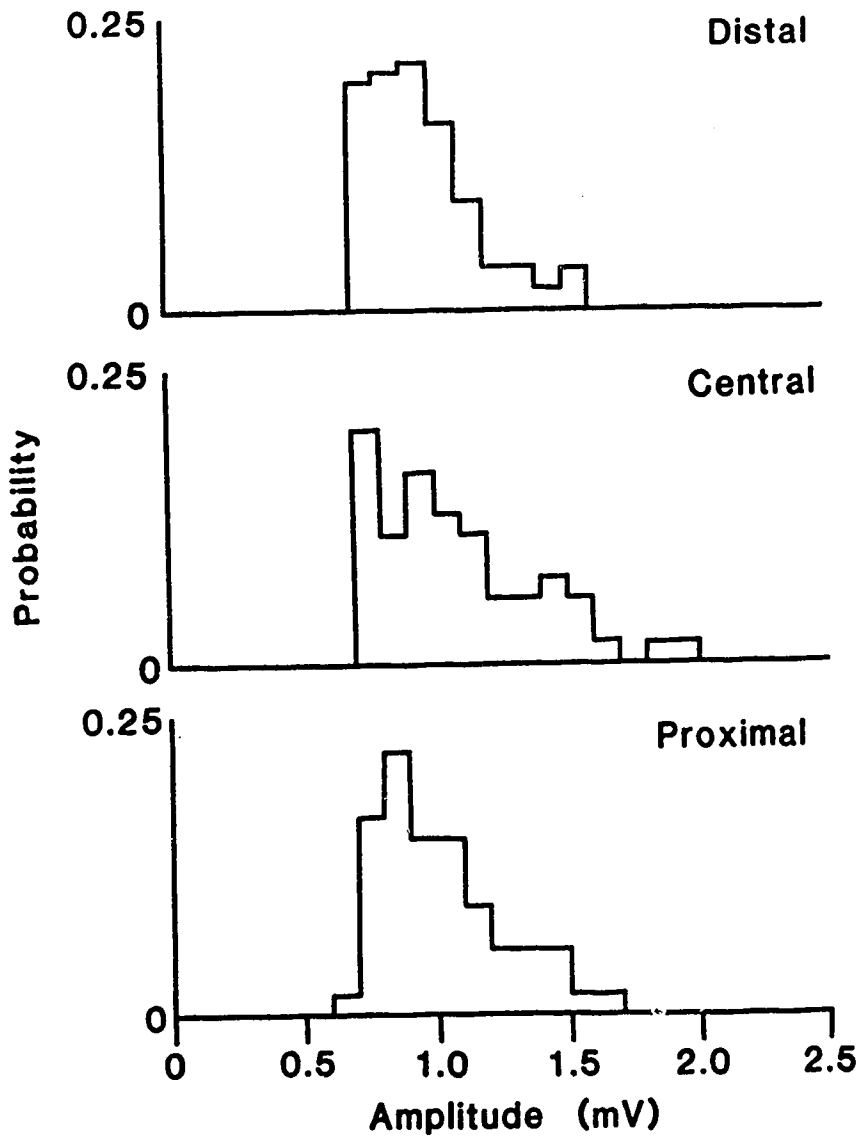


Fig. II.3. Distributions of bump amplitudes at the 3 locations in cell #1.

Table II.2.

A. Subclass averages and least-squares fits of cell and position effects on bump log-amplitude after transformation back to amplitude in mV. Position effect values were normalized relative to the central value, as in Fig. II.2.

Cell #	Distal	Central	Proximal	Cell effect
1	0.92	1.00	0.94	0.98
2	1.20	1.26	1.24	1.28
3	1.04	1.23	1.19	1.20
4	0.63	0.67	0.60	0.66
5	0.81	1.00	0.94	0.96
6	0.64	0.67	0.64	0.67
7	0.92	0.77	0.81	0.87
8	0.94	0.72	0.82	0.81
9	1.30	1.35	1.36	1.37
10	0.78	1.00	0.73	0.85
Position effect	0.94	1.00	0.95	

B. Analysis of variance table for log-amplitude.

Source	Sums of squares	d.f.	<i>F</i>
Intrinsic (error)	86.08	1587	
Cells	100.84	9	206.56
Cells after positions	99.16	9	203.11
Positions	2.66	2	24.48
Positions after cells	0.97	2	8.94
Interaction	5.00	18	5.13

All values of *F* were significant at the $p < 0.001$ level.

Between cells, amplitude was the most variable parameter, as measured by the coefficients of variation (ratios of standard deviations to averages) for least-square fits of cell means (Table II.5). The cell effects and the intrinsic variability gave comparable contributions to the total variability, as can be seen in the column of the sums of squares.

Bump time to peak

Fig. II.4 shows the distributions of times to peak for cell #1. Following a procedure similar to that used for the bump amplitude, we found that, although distributions of the time to peak (parameter t_p in Eq. II.1) were different in each cell and position, the inverse of the time to peak had a fairly regular distribution.

Subclass means, least-squares fits of cell and position effects, and results of the analysis of variance are given in Table II.3. The least-squares fits for cell effects shown on the table were calculated by setting the constraint that the sum of cell effects be null. Similarly, the fits for position effects on the table were calculated with the constraint that the sum of position effects be null.

Within the limitation that only three points were measured, average time to peak seemed to decrease almost linearly from proximal to distal position (Fig. II.2). For a typical cell, the average time to peak was 80 ms (see Table II.5) and the difference in time to peak measured at the two most distant sites in our experiments was about 8 ms, resulting in a slope of about 0.033 ms/ μ m.

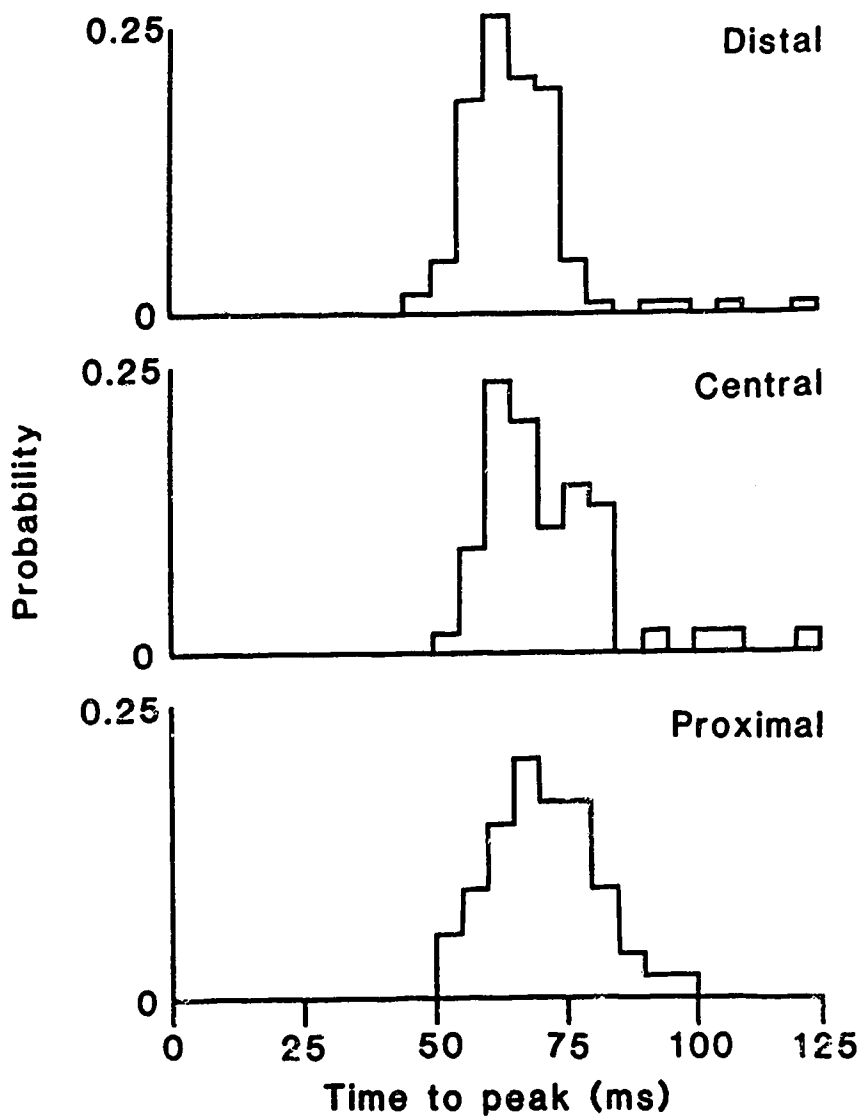


Fig. II.4. Distributions of times to peak of bumps at the 3 locations in cell #1.

Table II.3.

A. Subclass averages and least-squares fits of cell and position effects of inverse time to peak of bumps after transformation back to time to peak (in ms).

Cell #	Distal	Central	Proximal	Cell effect
1	62.54	67.28	66.42	65.28
2	71.72	72.74	77.52	73.88
3	62.52	74.56	81.11	72.54
4	78.23	87.45	91.03	84.71
5	92.70	94.80	101.08	95.83
6	82.51	75.94	79.49	78.46
7	74.74	68.00	76.95	73.42
8	79.84	83.52	74.60	77.17
9	97.71	93.84	108.73	98.48
10	79.47	104.11	102.07	95.08
Position effect	76.33	79.94	84.37	

B. Analysis of variance table for inverse time to peak (s^{-1})

Source	Sums of squares	d.f.	F
Intrinsic (error)	6779.78	1587	
Cells	4142.66	9	107.74
Cells after positions	3979.83	9	103.51
Positions	570.97	2	66.82
Positions after cells	408.14	2	47.77
Interactions	628.47	18	8.17

All values of F were significant at the $p < 0.001$ level.

Intrinsic variability was relatively lowest for time to peak, and this made the position effect more evident, but even for this parameter standard deviations within each position are clearly greater than the observed differences between positions (Fig. II.2).

Variability between cells was lower for time to peak than for amplitude, again as indicated by the coefficients of variations in Table II.5.

Relative width of bumps

Fig. II.5 shows the distributions of relative widths for cell #1. The relative width (w in Eq. II.1) was found to have a similar distribution for all cells and positions, so that no transformations were needed. Table II.4 contains the results of the analysis of variance, together with subclass means and least-squares fits of cell and position effects. As in Table II.3, we have calculated the cell effects with the constraint that the sum of position effects be null, and *vice versa*.

Relative width decreased from proximal to distal positions in a manner similar to time to peak, but to a smaller extent (Fig. II.2). Although, as shown in Table II.4, the differences between positions were significant, the ratio of the values of F for position effects and for interaction suggests that this difference was within the error due to slow fluctuations of cell parameters. This ratio can be interpreted as a new value of F with 2 and 18 degrees of freedom which compares the position effect to the error due to fluctuations, as discussed at the beginning of the Results section.

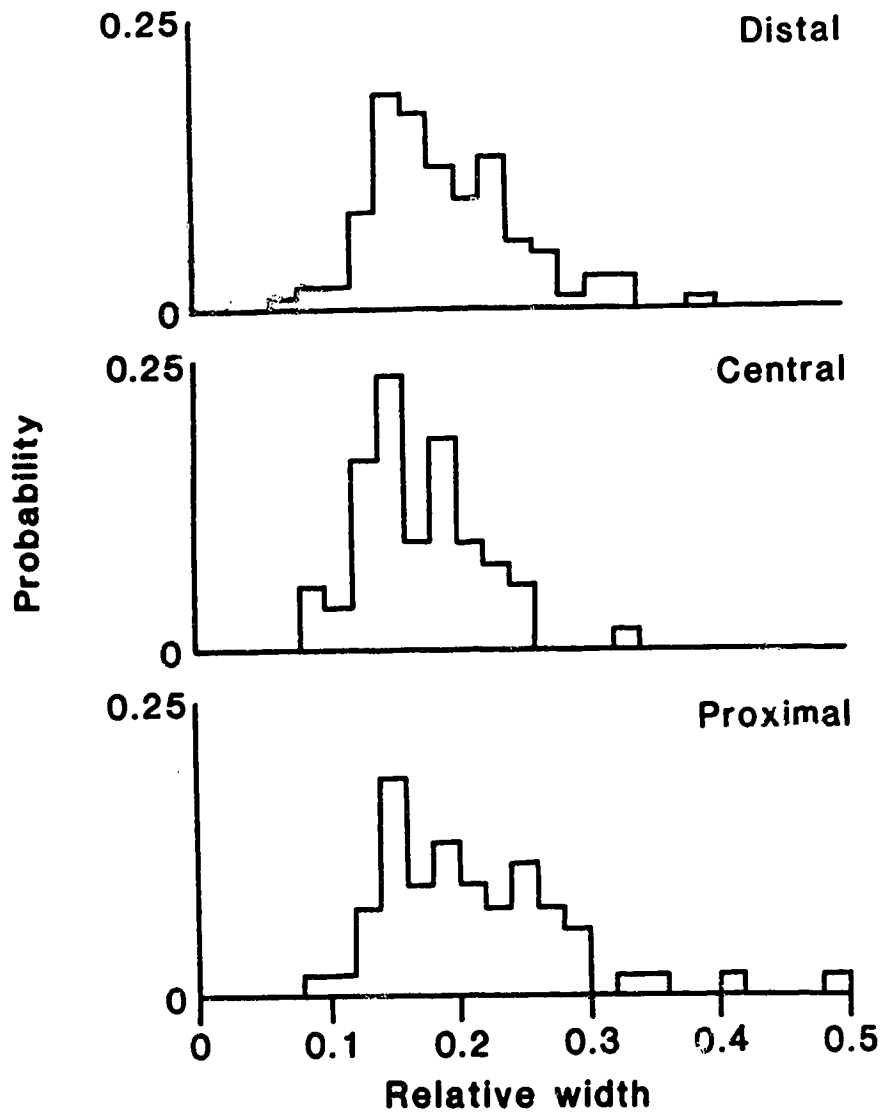


Fig. II.5. Distributions of relative widths of bumps at the 3 locations in cell #1.

Table II.4.**A. Subclass averages and least-squares fits of cell and position effects of relative width of bumps.**

Cell #	Distal	Central	Proximal	Cell effect
1	0.184	0.161	0.202	0.184
2	0.251	0.226	0.266	0.247
3	0.218	0.277	0.277	0.260
4	0.221	0.213	0.216	0.218
5	0.176	0.205	0.205	0.197
6	0.224	0.245	0.230	0.234
7	0.184	0.192	0.194	0.190
8	0.173	0.227	0.246	0.227
9	0.283	0.309	0.283	0.297
10	0.230	0.235	0.174	0.206
Position effect	0.218	0.228	0.232	

B. Analysis of variance table for relative width.

Source	Sums of squares	d.f.	F
Intrinsic (error)	6.887	1587	
Cells	1.671	9	42.78
Cells after positions	1.627	9	41.65
Positions	0.092	2	10.61
Positions after cells	0.048	2	5.55**
Interaction	0.362	18	4.63

All values of F were significant at the $p < 0.001$ level, except for *Positions after cells* (**), which was significant at the $p < 0.01$ level.

The values of F calculated in this way for the relative width are 2.29 if position effects are fitted before cell effects, and 1.20 for the opposite sequence of analysis. Since both values are associated with $p > 0.05$, the differences between position means for the relative width were probably within the error of the measurement.

Variability between cells was fairly low for relative width, comparable to that found for time to peak (Table II.5). On the other hand, intrinsic variability of relative width was rather large, so that intrinsic factors accounted for most of the sum of squares for this parameter.

Correlations between average cell parameters

The statistical significance of all correlation coefficients was estimated by means of a two-tailed Student's t test (Spiegel, 1975). The correlations between the average parameters for the cells are given in Table II.5; as pointed out at the end of the Methods section, correlations were computed using standard formulas on the average cell parameters, transformed back where necessary. Only the correlation between amplitude and relative width was significant. This means that cells with larger bumps on average tended to have wider bumps. However, it should be kept in mind that the probability of finding at least 1 correlation coefficient out of 3 with a nominal probability of 0.05 is actually close to 0.14. Therefore, the measured correlation might very well be accidental and will not be discussed further.

Correlations of parameters within each cell and position

Since most of the variability of cell parameters within each cell was intrinsic, it seemed worthwhile to determine whether parameter variations were correlated as reported by Howard (1983) for bumps recorded in intact animals. Such correlations would arise if common factors influenced more than one of the parameters. In our preparation, the small contributions due to position effects could be eliminated from the correlations. The correlation coefficients within subclasses, given in Table II.6, were calculated for the intrinsic variability of the transformed parameters. We used the usual formula:

$$r(\alpha, \beta) = \frac{\Sigma \alpha \beta}{\sqrt{\Sigma \alpha^2 \Sigma \beta^2}} \quad (\text{II.2})$$

(see *e.g.* Spiegel, 1975) where α and β are two transformed parameters of an individual bump after subtraction of their subclass average and $r(\alpha, \beta)$ is their correlation coefficient. Subtraction of the subclass average allowed a single correlation coefficient to be calculated for each pair of parameters, instead of calculating one such coefficient for each of the 30 subclasses. The strongest correlations were found between inverse time to peak and relative width, in all cells and locations, and were always positive. Correlations between log-amplitude and either of the other two parameters were positive and significant, but less strong. This pattern means that, within a given cell and position, wider bumps tended to occur earlier and have larger amplitude.

Table II.5.

Statistics of cell effects from Tables II.2, II.3, and II.4. Statistics for amplitude and time to peak were computed on the actual values given in the tables, rather than on the transformed parameters.

A. Averages and standard deviations.

Amplitude (v_p) :	0.96 ± 0.25 mV	($\sigma/\mu = 0.26$)
Time to peak (t_p) :	81.48 ± 11.47 ms	($\sigma/\mu = 0.14$)
Relative width (w) :	0.226 ± 0.035	($\sigma/\mu = 0.15$)

B. Correlation coefficients.

	t_p	w
a	0.07	0.63*
t_p		0.27

*Significant at the $p < 0.05$ level.

Table II.6.

Correlation coefficients of intrinsic variability of bump parameters, computed by means of Eq. II.2.

A. Transformed parameters with normal distributions.

	$1/t_p$	s
$\ln(v_p)$	0.05*	0.18**
$1/t_p$		0.49**

B. Parameters as in Howard (1983).

	Delay	Half-width
Amplitude	-0.14**	0.18**
Delay		-0.40**

*Significant at the $p < 0.05$ level **Significant at the $p < 0.01$ level

This is qualitatively the same pattern found by Howard (1983). In his analyses, Howard used different parameters for the time course of bumps: latency and half-amplitude width instead of time to peak and relative width. Since the latter two parameters might be expected to be correlated simply by the definition of relative width, we calculated correlations using Howard's parameters (and Eq. II.2) for purposes of comparison. Latency and half-width were calculated from the fitted values of time-to-peak and relative width, using Eq. II.1. Howard's criterion was used to calculate the latency, *i.e.* the intercept between the baseline and a linear extrapolation between the points at which the response reaches 25% and 75% of its full amplitude. The results are also shown in Table II.6. While the correlations between amplitude and either of the other parameters were similar to those found by Howard, the correlation between latency and half-width was much stronger in our experiments. The scattergram of Fig. II.6 shows the joint distributions of time to peak and relative width. It would seem that at least part of the correlation is caused by bumps in the upper left corner of the diagram, having a time to peak greater than average and a relative width smaller than average. By contrast, bumps with large relative width, at the rightmost end of the diagram, tended to have a time to peak only slightly smaller than average. A subjective impression that there was a relatively small, but noticeable, number of narrow bumps with a long delay was borne out by visual inspection of the bumps even before statistical analysis.

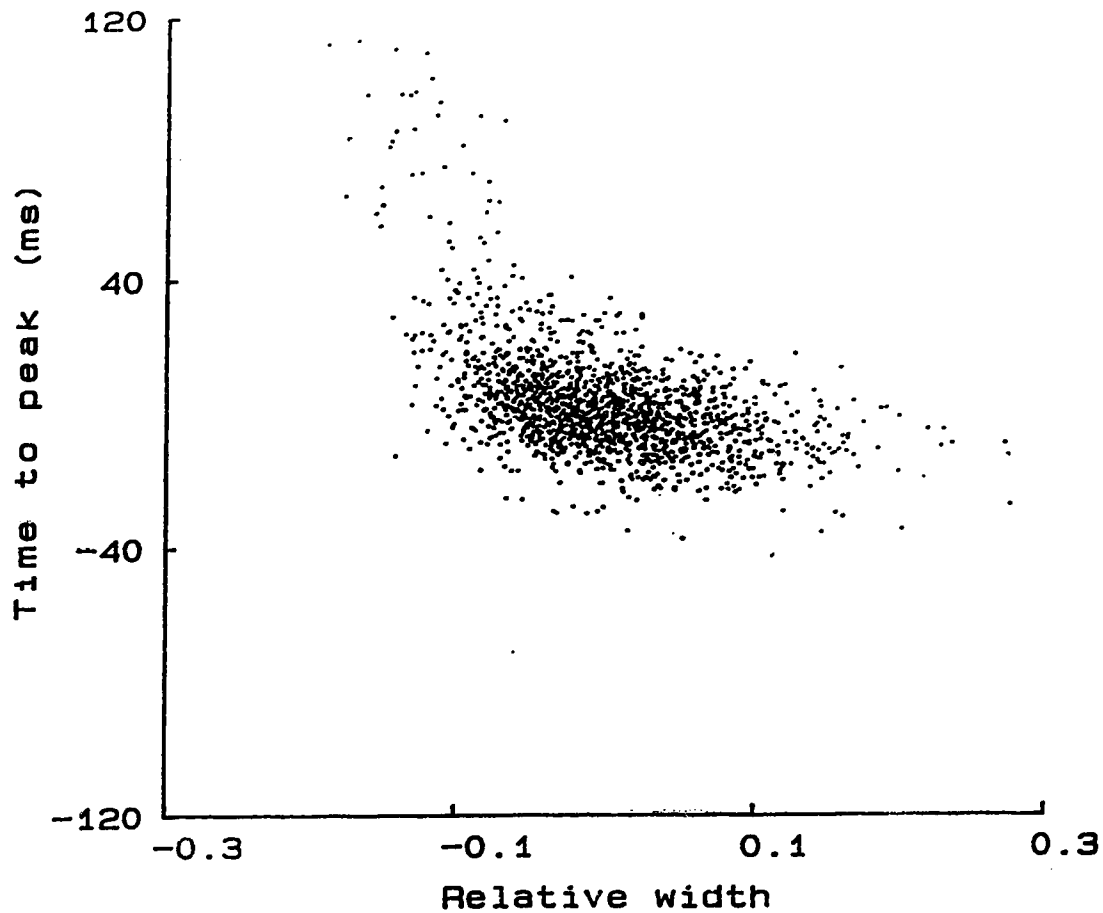


Fig. II.6. Scattergram including all the bumps which were analyzed. Each point represents a single bump and has coordinates equal to the relative width and time to peak of the bump, after subtraction of its subclass average. Therefore, half of the points lie to each side of the vertical axis corresponding to zero relative width, and half of the points lie to each side of the horizontal axis for zero time to peak.

II.4. Discussion

The wide difference in the fraction of photons transduced depending on the position of the stimulus indicates that scatter of light was limited. Scatter was probably similar in the longitudinal direction to that measured in the transverse direction, which had a 40 μm half-width. Bader *et al.* (1982) estimated light scatter along the long axis of the drone photoreceptor in a similar preparation but using a different method. Their results were similar to ours and no significant scatter was evident at large distances from the maximum. Note that even a fairly large amount of scatter would not qualitatively affect the results of the analysis of variance or our conclusions, as long as the light stimulus was partially localized. The cause of the lower frequency of photon transduction in the distal region of the photoreceptor was probably the local concentration of pigment granules (Wilson *et al.*, 1978), together with the fact that the cell being recorded from was usually not the first cell penetrated in the microelectrode track, so that pigment granules from overlaying cells would contribute to the screening of light.

For each cell, the noise amplitude was measured at various times during the experiment. The noise level set a lower limit to the size of the bumps which were recorded, so that many small bumps were not included in our statistics. As a consequence, the mean bump amplitude was overestimated and the frequency of bumps was underestimated. However, the highest recorded noise amplitude was used to set a threshold for bump discrimination at all locations for that particular cell, so

that the comparisons between the 3 sites of stimulation were not affected by differences in threshold. The range of times to peak that could be measured was limited by the duration of the recording after the flash, but very few bumps (less than one in 50 for most subclasses) had to be discarded because the recording was over before the falling phase of the bump, as can be inferred from the distributions in Fig. II.4.

The fact that the observed bump frequencies could be closely fitted by Poisson distributions (Table II.1), while some bumps were not detected because of their small amplitude, suggests that some of the responses that were analyzed contained multiple overlapping bumps. This problem is inevitably linked to the fact that locust bumps have an average width that is not negligible compared to the average latency. Howard (1983) estimated that about 10% of the responses that he analyzed as bumps were responses to more than one photon.

The significance of the interaction terms in the analysis of variance might suggest that different cells have different profiles of regional phototransduction properties. However, cells did not seem to cluster into well-defined classes on the basis of these profiles. Alternatively, the interaction terms might be due to slow changes in the average properties of bumps due to less than ideally stable recordings. These fluctuations would seem to be randomly different for each cell. Therefore, they should tend to cancel out when several cells are pooled together for fitting mean position effects.

The agreement of the bump time courses with the fits of the log-normal model

was very convenient for our analysis, but it is unlikely to indicate that the parameters of the model have a simple biophysical interpretation. The dynamics of the receptor potential is determined by rather complex mechanisms, as will be evident from the following Chapters.

Bump amplitudes

Lillywhite (1978) suggested that locust photoreceptors are electrically coupled to explain his observations of two different classes of bump sizes. Subsequently Howard (1983) could record bumps of the larger class only and suggested that smaller bumps arise because of artefactual coupling. In our preparation, bumps of a smaller class would not rise above the background noise and, if originating in neighbouring photoreceptors, would still be generated in the same region of the cell (proximal, central, or distal) as the larger bumps which we analyzed. Therefore, we do not think that this would be a potential problem in the interpretation of our results.

Average bump amplitudes were considerably smaller than reported for locust photoreceptors by Howard (1983). However, that investigation was concerned with the absolute values of the parameters, rather than with the comparison between different sites. Therefore, very stringent criteria were set for the cells to be included in the statistics, one of which was a high signal-to-noise ratio of the bumps. Only four cells out of more than 100 met those criteria. It might be possible to obtain larger bumps more consistently by optimizing the settings of a Brown-Flaming type microelectrode puller (Brown and Flaming, 1977; see also Smakman and Stavenga,

1987). The average delays and half-widths that we measured (about 53 ms and 44 ms respectively) were close to Howard's observations.

It has been shown that mean bump amplitude is independent of wavelength in locust photoreceptors (Lillywhite, 1978). Since different wavelengths have different absorption profiles along the photoreceptor axis, this provided indirect evidence that the absorption site does not affect bump amplitude to an extent which could be measured by that method. Our method allowed more control in the location of the stimulus so that small position effects could be detected.

These small differences in mean amplitudes are most likely to be due to cable attenuation between the stimulation site and the recording site. The voltage bump recorded by a microelectrode placed centrally will be the product of the underlying current bump, the input resistance of the cell at the site of bump generation, and the cable decrement from the site of generation to the site of recording. In our experiments, we tried to place the microelectrode within about 50 μm distally from the center of the ommatidia, but, since the extreme tip of the microelectrode was not visible, it was not possible to quantify the distances between recording and stimulating sites. Centrally-generated bumps should have been least attenuated by passive cable conduction to the recording site, and this was indeed the case. Distal bumps might be expected to be less attenuated than proximal bumps, because the photoreceptor has a larger cross-section (and therefore a larger length constant) in its distal part (Wilson *et al.*, 1978). However, a larger cross-section also implies a lower input resistance, and this might more than compensate for the smaller electrotonic distance

from the recording site.

In order to know what value of membrane length constant might account for the size of decrease that was measured, we assumed that the microelectrode was recording the membrane potential at the center of the cell and that the membrane time constant of the cell is negligible compared to the time course of a bump (Payne, 1982, estimated a membrane time constant of less than 15 ms for locust photoreceptors), so that steady-state cable equations could be used. We also assumed that all bumps arise exactly from where the stimulus was located (*i.e.* a very thin slit and no light scattering). The cell was approximated as a uniform cable, open-circuited at both ends (see *e.g.* Jack *et al.*, 1983). In such a system, the input resistance as a function of distance, d , from the closer end of the cell is the parallel combination of the input resistances of the two finite open-circuited half-cables of lengths d and $L-d$, where L is the length of the cell, and cable attenuation (ratio of voltage at site of recording to voltage at site of current injection) can be expressed by two independent equations for the two half-cables. Using Eq. 4.11 of Jack *et al.* (1983) for each of the half-cables, the input resistance is:

$$R(d) = \frac{\rho \lambda \coth[d/\lambda] \coth[(L-d)/\lambda]}{\coth[d/\lambda] + \coth[(L-d)/\lambda]} \quad (\text{II.3})$$

where ρ is the axial intracellular resistance per unit length and λ is the length constant. The attenuation factor for steady-state voltage is given by Eq. 4.10 of Jack *et al.* (1983), with appropriate modifications:

$$A(d) = \cosh[L/2\lambda] / \cosh[(L-d)/\lambda] \quad (\text{II.4})$$

Assuming that the average current generated by a single successful photon absorption is the same at any location in the cell, the ratio of voltage amplitudes recorded centrally for bumps generated at distance d to bumps generated at the center is:

$$\frac{R(d)A(d)}{R(L/2)} = \frac{2 \cosh[d/\lambda] \sinh[L/2\lambda]}{\sinh[(L-d)/\lambda] \{ \cosh[d/\lambda] + \cosh[(L-d)/\lambda] \}} \quad (\text{II.5})$$

The best fit of this function to the data was obtained with $\lambda = 450 \mu\text{m}$ (see Fig. II.3), which is fairly close to the value of $390 \mu\text{m}$ estimated by Payne (1982), on the basis of measurements of cell input resistance and geometrical parameters of the cell, together with a reasonable value of intracellular resistivity. The only assumption common to Payne's estimate and our own is that the cell can be approximated as a uniform cable open-circuited at both ends. Light scattering would decrease detected differences between different stimulus locations. Assuming that the measured differences between stimulus sites are only half of the real differences, the calculated length constant would become about $300 \mu\text{m}$.

The small variation of bump amplitude with position, and the fact that even this small variation can be explained by the expected cable decrement, provide evidence for the validity of our methods. In particular, they indicate that fluctuations of cell parameters were random and so tended to cancel out when data from several cells

were pooled together, and that the number of responses consisting of multiple bumps and erroneously interpreted as single bumps was either negligible or similar for each of the three stimulation sites.

Regional vs. intrinsic variability

The precise extent to which regional dishomogeneities contribute to the total variability of bump parameters cannot be estimated from our data alone. Knowledge of the exact distribution of bump parameters at all points in the cell and the fraction of bumps arising from each point would be required. However, it is possible to calculate the variability which would be due to a gradient of time to peak by making two simple assumptions: (1) naturally-occurring bumps are spread evenly over the length of the rhabdomere; (2) time to peak decreases linearly from the most proximal to the most distal part of the rhabdomere, as suggested by our measurements (Fig. II.2). Suppose that all bumps had a time to peak equal to the average for their location. In this case, the variability would be given by the formula:

$$\sigma^2 = [t_p(L) - t_p(0)]^2 / 12 \quad (\text{II.6})$$

which gives the variance of a rectangular distribution with a width equal to the difference between the average proximal time to peak $t_p(L)$ and the average distal time to peak $t_p(0)$ (Bendat and Piersol, 1986, page 51). Extrapolating linearly from our measurements, $t_p(0) = 75$ ms, $t_p(L) = 85$ ms, and $\sigma^2 = 8.4$ ms² ($\sigma = 2.9$ ms). The intrinsic variance that we measured was about 20 times larger than this value: The

error bars in Fig. II.2 show the size of the intrinsic standard deviation.

This estimate should be given with 2 qualifications, pointing in opposite directions. First, if the real differences between average times to peak were twice as large as the measured differences, due to light scattering, the above calculations would give $\sigma^2 = 33.3 \text{ ms}^2$, one fifth of the size of the intrinsic variance. Second, self-screening of the photopigment and screening by pigment granules reduce the relative frequency of bumps arising at more proximal locations with natural stimulation, so that the distribution of times to peak would be better approximated by an exponential or multiple exponential; however, the variance of a rectangular distribution is higher than the variance of a truncated exponential distribution with the same range, so the above values for the cases of no light scatter and limited light scatter are upper limits to the expected variability. Therefore we conclude that regional differences give a minor contribution to the normally-observed variance, even for this parameter which is the most sensitive to the location of the stimulus and the least intrinsically variable.

Temperature and light adaptation both affect the time to peak of photoreceptor responses, leaving the relative width apparently unchanged (Payne and Howard, 1981; Howard *et al.*, 1984). The time scale of the phototransduction mechanism of insects can therefore be changed in a continuous fashion by several factors, while the shape of the response remains unaffected. However, both temperature and light adaptation also affect the amplitude of the response, while it would seem that stimulation site does not by itself affect the amplitude of the transduction current in locust photoreceptors.

These results contrast with the finding in *Limulus* that amplitude but not latency is affected by stimulus position (Spiegler and Yeandle, 1974). It seems possible that several parameters can be independently affected by local differences in the transduction mechanism.

Interpretations of parameters correlations

The correlation between half-width and latency that we measured is much larger than the correlation found by Howard (1983). This is in part due to the fact that Howard could not factor out the correlation due to the site of generation of the bumps. We calculated the correlation between delay and half-amplitude width with Eq. II.2 in which α and β are parameters of individual bumps after the subtraction of their cell mean, instead of subclass mean, so that the correlation due to position was not factored out. The resulting correlation was -0.35, which is still greater than the correlations given by Howard, but somewhat closer. In *Limulus* ventral photoreceptors, Keiper *et al.* (1984) found no correlation between the delay and either the rise time or the decay time constant of bumps.

Howard suggested that the correlations he found were due to mis-scoring of overlapping multiple bumps as single bumps, since multiple bumps, compared to single bumps, would have a latency smaller than average (since it is the latency of the first bump) and a width and amplitude larger than average. This interpretation would imply that the number of mis-scoring was slightly higher in our analysis. The agreement between the expected and observed frequencies, shown in Table II.1,

could be accidental. However, from the scattergram of Fig. II.6 it would seem that it is not an excess of early, wide bumps that causes the correlation, but rather an excess of late, narrow bumps.

One hypothetical explanation for this finding might be that the initiation and termination of each bump are controlled by independent or partially independent processes. Bumps beginning relatively late after the flash would then be terminated relatively earlier because of the independent time course of the terminating mechanism. Correlations of amplitude with the above parameters would be in agreement with this hypothesis, since bumps with a smaller width and relatively earlier termination might not develop a full amplitude. In the following chapters, evidence for a feedback mechanism operating at very low response levels will be presented. The evidence for a distinct feedforward mechanism is limited to the above correlations between bump parameters, for which alternative explanations are possible.

II.5. References

- Bader CR, Baumann F, Bertrand D, Carreras J, Fuortes G (1982) Diffuse and local effects of light adaptation in photoreceptors of the honey bee drone. *Vision Res* 22:311-317.
- Bendat JS, Piersol AG (1986) Random data: Analysis and measurement procedures. Wiley, New York.
- Borsellino A, Fuortes MGF(1968) Responses to single photons in visual cells of *Limulus*. *J Physiol* 196:507-539.
- Brown JE, Coles JA (1979) Saturation of the response to light in *Limulus* ventral photoreceptor. *J Physiol* 296:373-392.
- Brown JE, Harary HH, Waggoner A (1979) Isopotentiality and an optical determination of series resistance in *Limulus* ventral photoreceptors. *J Physiol* 296:357-372.
- Brown KT, Flaming DG (1977) New microelectrode techniques for intracellular work in small cells. *Neurosci* 2:813-827.
- Fein A, Szuts EZ (1982) Photoreceptors: their role in vision. Cambridge University Press, Cambridge.
- French AS, Kuster JE (1985) Nonlinearities in locust photoreceptors during transduction of small numbers of photons. *J Comp Physiol A* 156:645-652.
- Howard J (1983) Variations in the voltage response to single quanta of light in the photoreceptors of *Locusta migratoria*. *Biophys Struct Mech* 9:341-348.

- Howard J, Dubs A, Payne R (1984) The dynamics of phototransduction in insects: A comparative study. *J Comp Physiol A* 154:707-718.
- Jack JJB, Noble D, Tsien RW (1983) Electric current flow in excitable cells. Oxford University Press, Oxford.
- Keiper W, Schnakenberg J, Stieve H (1984) Statistical analysis of quantum bump parameters in *Limulus* ventral photoreceptors. *Z Naturforsch* 39c:781-790.
- Lillywhite PG (1977) Single photon signals and transduction in an insect eye. *J Comp Physiol A* 122:189-200.
- Lillywhite PG (1978) Coupling between locust photoreceptors revealed by a study of quantum bumps. *J Comp Physiol A* 125:13-27.
- Payne R (1980) Voltage noise accompanying chemically induced depolarization of insect photoreceptors. *Biophys Struct Mech* 6:235-252.
- Payne R (1982) Chemical modifications to transduction in an insect eye. Ph.D. Thesis, Australian National University.
- Payne R, Howard J (1981) Response of an insect photoreceptor: a simple log-normal model. *Nature* 290:415-416.
- Searle SR (1971) Linear models. Wiley, New York.
- Smakman JGJ, Stavenga DG (1987) Angular sensitivity of blowfly photoreceptors: broadening by artificial electrical coupling. *J Comp Physiol A* 160:501-507.
- Spiegel MR (1975) Probability and Statistics. McGraw-Hill, New York.
- Spiegler JB, Yeandle S (1974) Independence of location of light absorption and discrete wave latency distribution in *Limulus* ventral nerve photoreceptors. *J Gen*

Physiol 64:494-502.

Stieve H (1986) Bumps, the elementary excitatory responses of invertebrates. In: The molecular mechanism of photoreception (H. Stieve, ed.) 199-230. Springer-Verlag, Berlin.

Wilson M, Garrard P, McGinness S (1978) The unit structure of the locust compound eye. *Cell Tiss Res* 195:205-226.

III. PHENOMENOLOGY OF GAIN CONTROL: A COMPARISON OF WHITE-NOISE AND IMPULSE RESPONSES²

III.1. Introduction

Early studies of insect photoreceptors employing white-noise stimuli demonstrated that the photoreceptor response is very linear, although a small second-order component is present (Eckert and Bishop, 1974; Gemperlein and McCann, 1974). Subsequently, the first-order Wiener kernel of the photoreceptor response has been shown to be affected by background light intensity (Kuster and French, 1985), an effect which can only be explained by nonlinear mechanisms. Since this nonlinear effect depends on background intensity, it is possible that it develops in a time scale substantially slower than that of the photoresponse.

By contrast, with flash stimuli clear nonlinearities have been demonstrated when as few as two photons are transduced at the same time (Lillywhite and Laughlin, 1982; French and Kuster, 1985). Grzywacz and Hillman (1985) argued on statistical grounds that even the response to a single photon is nonlinear in locust photoreceptors.

² A version of this chapter has been published. Pece AEC, French AS, Korenberg MJ, Kuster JE (1990) *Biophysical Journal* 57:733-743.

Predictions of cascade models

The responses of vertebrate photoreceptors to light have been shown to be mediated by a biochemical cascade between photon absorption by rhodopsin and the modulation of ion channels (for a review, see *e.g.* Lamb, 1986). There is reason to believe that the responses of invertebrate photoreceptors are mediated by similar mechanisms (Fein, 1986). Linear analysis of the response of *Limulus* photoreceptors to light provided evidence for such a cascade model of phototransduction before any chemical component of this system had been identified (Fuortes and Hodgkin, 1964). When the light intensity is low enough to prevent saturation at any stage, a simple cascade of first-order reactions would result in a linear relationship between light stimulus and photoreceptor response. If the voltage response of photoreceptors is recorded, instead of its current response under voltage clamp, then the membrane time constant phenomenologically appears as a further stage in the cascade.

While the response linearity observed with white-noise stimuli at a fixed background intensity is in agreement with such a model of phototransduction, other experimental observations, and particularly the sublinear summation of elementary responses to flashes (reviewed by Laughlin, 1981, pages 202 and following) cannot be explained by a linear model. Moreover, the frequency response of fly (French, 1980) and locust (Kuster and French, 1985) photoreceptors contains second-order poles, which, although linear, are not compatible with a simple cascade mechanism. However, all of these observations are still compatible with cascade models of slightly greater sophistication.

Organization of the chapter

In this chapter, the responses of locust photoreceptors to flashes and to white noise are compared to each other and to the predictions of some simple models, which include no specific biochemical reaction but which can be interpreted as models of biochemical cascades. In section III.3, the system kernels obtained with the two experimental methods are compared and shown to be similar. Furthermore, the response depression quantified by the second-order kernels is shown to be to a large extent reducible to the product of two functions, one being the linear component of the photoreceptor response as a function of time after the flash and the other the peak response depression as a function of inter-flash interval. Physically, this would mean that at all times the depression is a constant proportion of the response to the second flash.

This feature of the second-order kernel suggested some block-diagram models of the transduction and gain control processes. These models would have some implications for the biophysical mechanisms involved because they imply that the gain control lies at an early stage in the biochemical cascade of phototransduction. In section III.4, the predictive power of these models is tested by simulations of the experimental responses. The simulations did not provide conclusive evidence for or against any of the models, but demonstrated that the proposed mechanisms alone cannot account for the change of the photoreceptor gain observed when the photoreceptor is light-adapted to different levels of steady background light. One or more other mechanisms must act to reduce the gain of phototransduction depending

on the background light intensity averaged over a longer time scale.

The gain control process which is the main subject of this and the following chapters occurs within the time scale of the transduction process. We believe that this process underlies the sublinear summation of responses found in photoreceptors of several different species (Laughlin, 1981), on the basis of the similarities between response depressions obtained with flashes and with white noise. Other factors regulate the gain of phototransduction at time scales which are orders of magnitude slower (see for instance Claßen-Linke and Stieve, 1986). We will refer to these latter processes as adaptation and to the fast gain control process which we investigated simply as gain control for brevity. Furthermore, the term "response depression" will indicate the depression of membrane potential caused by the fast gain control mechanism, unless otherwise specified. As mentioned above, the effects of adaptation became evident when kernels obtained at different background levels were compared.

The research described in this chapter is speculative to different degrees. In section III.3, the Volterra and Wiener kernels were measured experimentally and the validity of the analysis is based on only one assumption, namely, that nonlinearities of order higher than the second were negligible; the separable kernels which were compared with the experimental kernels can be considered as tentative approximations to the experimental data. The separable models in section III.4 are somewhat more speculative: they are compatible with separable kernels but alternative models are possible. Finally, a biophysical interpretation is not implicit in the separable models, although one is certainly suggested by the knowledge that

phototransduction is mediated by a biochemical cascade.

III.2. Methods

Preparation

Locusts, *Locusta migratoria*, were from the same laboratory colony as in Chapter II. They were dark adapted for at least 1 hour before the experiment. The wings and legs were removed and the animal was immobilized with dental wax. Care was taken to avoid obstructing any of the respiratory spiracles. Experiments were performed at room temperature.

Stimulation

Light stimulation was provided by a high-intensity LED (light-emitting diode) with a peak emission wavelength of 565 nm (HPHLMP 3950; Hewlett-Packard Co., Palo Alto, CA) held by a Cardan arm at a distance of 5 cm from the eye.

The stimulation procedure used for the double-flash experiment was similar to that described previously by French and Kuster (1985). Single flashes and pairs of flashes with varying inter-flash intervals were delivered with the LED, each flash having a duration of 0.1 ms. One major difference with respect to the methods of French and Kuster was that the single flashes did not result in a single photon being transduced on average, but had an intensity of about 8 ep, estimated by comparison between the

amplitude of the single-photon response and of the single-flash response. Another modification of the methods was that flashes with a nominal inter-flash interval of 0 ms were not flashes of double intensity but pairs of flashes with an actual interval of 0.2 ms. The latter modification ensured that no artefact could arise from the nonlinearity of the LED.

For the white noise experiments, the stimulus was generated by a 33-bit shift register clocked at 1 KHz (Marmarelis and Marmarelis, 1978) to give a pseudo-random binary sequence, which was then filtered by a nine-pole active low-pass filter (corner frequency: 50 Hz) and a single-pole high-pass filter (corner frequency: 0.05 Hz). A DC component was then added to the signal. The DC level and power level of the signal were adjusted independently. The signal was used to drive the LED via a constant current circuit. For each DC level, the power level was set as high as possible while maintaining the LED forward-polarized. Conversion from LED current to LED light intensity was done off-line for each sample point by a program using a calibration curve obtained by means of a phototransistor (MRD 3050; Motorola Inc., Schaumburg, IL). Instantaneous light intensities could be converted to effective photons per second (ep/s, *i.e.* photons effectively transduced) by counting the frequency of single photon responses at a low steady level of illumination (producing 5-10 ep/s) and then extrapolating to higher light intensities. This calibration was only approximate because it was often difficult to distinguish single photon responses from random noise in the voltage trace on the oscilloscope. Of course, any error in the calibration would affect all background level

measurements by the same factor, leaving the relative levels unchanged.

Recordings

Glass microelectrodes filled with 3 M potassium acetate and having a resistance of 50-100 M Ω were used. They were lowered through a hole, made by means of a fragment of a razor blade in the cornea of the right eye, to penetrate reticular cells. The reference silver electrode was placed in the left eye. Intracellular voltage was measured by a conventional amplifier (Getting Inc., Los Altos, CA, model 5) and high-pass filtered at 0.05 Hz by a single-pole filter.

In the double-flash experiments, responses after the single flash, or after the second flash in a pair, were sampled at 2 ms intervals for a total of 200 ms and stored on-line in a digital computer. After the analysis, adjacent voltage samples were averaged together to produce kernels with an effective sampling interval of 4 ms.

In the white noise experiments, the response was further low-pass filtered at 100 Hz by a single-pole filter. The LED current and the intracellular voltage were sampled at 10 ms intervals and stored on-line in the computer. The photoreceptor response contains very little signal above a frequency of 50 Hz (the Nyquist frequency for a sampling interval of 10 ms). Low-pass filtering was used only to limit the random noise of the recordings.

Computational methods

Volterra kernels were computed from single- and double-flash responses by the

method first introduced by Schetzen (1965). The method can be briefly described as follows: If we assume that all higher-order nonlinearities are negligible at the stimulus intensities that were used, the response to a single flash will be:

$$v_1(\tau) = h_1(\tau) + h_2(\tau, \tau) \quad (\text{III.1})$$

where τ is the time after the flash, h_1 the first-order Volterra kernel, and h_2 the second-order Volterra kernel. An equivalent second-order kernel p_2 can be defined:

$$p_2(\tau, \delta) = 2 \cdot h_2(\tau_1, \tau_2) \quad (\text{III.2})$$

Where $\tau = \tau_2$ and $\delta = \tau_1 - \tau_2$. Eq. III.1 now becomes:

$$v_1(\tau) = h_1(\tau) + (1/2)p_2(\tau, 0) \quad (\text{III.3})$$

The response to a double flash will be:

$$\begin{aligned} v_2(\tau, \delta) &= h_1(\tau) + (1/2)p_2(\tau, 0) + h_1(\tau + \delta) + (1/2)p_2(\tau + \delta, 0) + p_2(\tau, \delta) \\ &= v_1(\tau) + v_1(\tau + \delta) + p_2(\tau, \delta) \end{aligned} \quad (\text{III.4})$$

δ is equal to the time interval between the first and the second flash, and τ is the

time after the second flash. $p_2(\tau, \delta)$ was calculated from $v_1(\tau)$ and $v_2(\tau, \delta)$, using Eq. III.4 . Then, $h_1(\tau)$ was calculated from $v_1(\tau)$ and $p_2(\tau, 0)$ using Eq. III.3. To calculate $p_2(\tau, \delta_1)$ over a square region with equal spacing between samples along both the τ and δ axes, one alternative is to record responses to pairs of flashes with inter-flash intervals varying between 0 and 200 ms in steps of 2 ms. However, we used responses obtained with inter-flash intervals of 0, 2, 5, 10, 20, and 40 ms. The missing intervals below 80 ms were obtained by Hermite interpolation and the values for intervals above 80 ms were set to zero.

Wiener kernels were computed from white-noise experiments using the fast orthogonal algorithm. This method was described previously by Korenberg (1988), and one of its first applications to a biological system by Korenberg *et al.* (1988). For our experiments, we found that reliable second-order kernels could only be extracted from records of at least 40,000 data pairs. Records of even greater length were required if extraneous noise (especially photon noise at low background levels) was present. The second-order kernels obtained with the fast orthogonal algorithm are symmetrical in τ_1 and τ_2 . They were converted to triangular format by eliminating all values above the diagonal and doubling all values below the diagonal. The kernels $p_2(\tau, \delta)$ could then be obtained by a simple coordinate transformation.

We were interested in reducing the second-order kernel $p_2(\tau, \delta)$, function of two time variables, to the product of two first-order kernels $k(\tau)$ and $f(\delta)$, according to the equations:

$$p_2(\tau, \delta) = -f(\delta)k(\tau) \quad (\text{III.5})$$

$$h_1(\tau) = k(\tau)$$

Each kernel p_2 was stored in computer memory as a square matrix; in order to extract the delta response $f(\delta)$ (which is a one-dimensional array) the 3 rows which correspond to the highest values of $h_1(\tau)$ were averaged, *i.e.* if the time to peak of $h_1(\tau)$ was t_p , we averaged $p_2(\delta, t_p-1)$, $p_2(\delta, t_p)$, and $p_2(\delta, t_p+1)$ to obtain $f(\delta)$. Once f was calculated, the 3 columns of p_2 corresponding to the highest values of f were averaged to obtain an estimate of k which we call k_p and which we expect to be identical to h_1 . If the second-order kernel is said to be separable, it is understood that it is separable in the sense of Eqs. III.5.

The variable δ in the above equations, being the difference between the 2 time variables τ_1 and τ_2 , is also known in the systems analysis literature as $\Delta\tau$. This notation is slightly more cumbersome but can be helpful to keep in mind the experimental meaning of the second-order kernel obtained in the double-flash experiments, in which $\Delta\tau$, *i.e.* δ , is the inter-flash interval.

Simulations of the models analyzed in section III.4 were done by explicitly computing the values of all the signals in the corresponding diagram of Fig. III.5 at 10 ms intervals. The outputs of the linear components were obtained by convolution and the output of the static nonlinear component by simple algebra. The estimate of k which we used in our simulations was h_1 because the first-order component of the

photoreceptor output is larger than the second-order component and therefore its estimate is likely to be more accurate. Unless otherwise specified, for our simulations k and f were scaled by finding scaling factors for each of them which would minimize the mean-square error between the experimental output and the simulated output over a record segment of 3000 data pairs. The scaling factors were found by an iterative procedure. Similar scaling factors were obtained for all models if the input to the simulated models was only the AC white-noise component of the experimental stimulus. The kernels shown in Figs. III.3 and III.4 were scaled under these conditions.

III.3. Experimental results

Flash experiments

The experiments described in this chapter differ from the flash experiments presented in the original publication (Pece *et al.*, 1990) in both stimulus intensity and inter-flash intervals. The flash intensity was estimated from the single-bump response amplitude of about 2 mV (observed with a dim steady background light) and the amplitude of the response to the single flash used in the experiments, which was 5.65 mV. Assuming a square-root relationship between flash intensity and response amplitude (see chapter V), the single-flash intensity was approximately 8 ep.

The response of a system to even a single impulse contains all the nonlinearities

of any order present in the system. However, for small stimuli, it is often possible to ignore nonlinearities above a certain order. In this case, we are interested in extracting first- and second-order Volterra kernels from single- and double-flash responses. In these experiments, the flash intensity was adjusted so that each flash resulted in about one photon being transduced on average. A total of 100 flash responses for each delay between flashes were averaged. The second-order kernel shown in Fig. III.2 contains the depression (thick contour lines) analyzed by French and Kuster (1985). The first-order kernel h_1 is shown in Fig. III.1 and is not very different from the system impulse response.

The question is whether the second-order kernel is separable. To answer this, the delta responses $f(\delta)$ and $k_p(\tau)$ were extracted as described in the previous section. The results of this procedure are shown in Fig. III.1, where $k_p(\tau)$ appears to be very similar to $h_1(\tau)$, as predicted.

French and Kuster also described a relatively small facilitation for τ smaller than t_p and δ close to zero. This facilitation is not resolved in Fig. III.2, but it can be seen in the kernel k_p in Fig. III.1 (arrow). As was discussed in the previous section, this kernel is a slice through the contour map of Fig. III.2. A more significant difference with the results of French and Kuster is that $f(\delta)$ has almost the same value for $\delta = 0$ ms as for $\delta = 5$ ms. This might be due to the different stimulus used in the present investigation (see section III.2): it is difficult to obtain a flash of exactly double intensity with the LED at low current levels, and if the effective intensity is

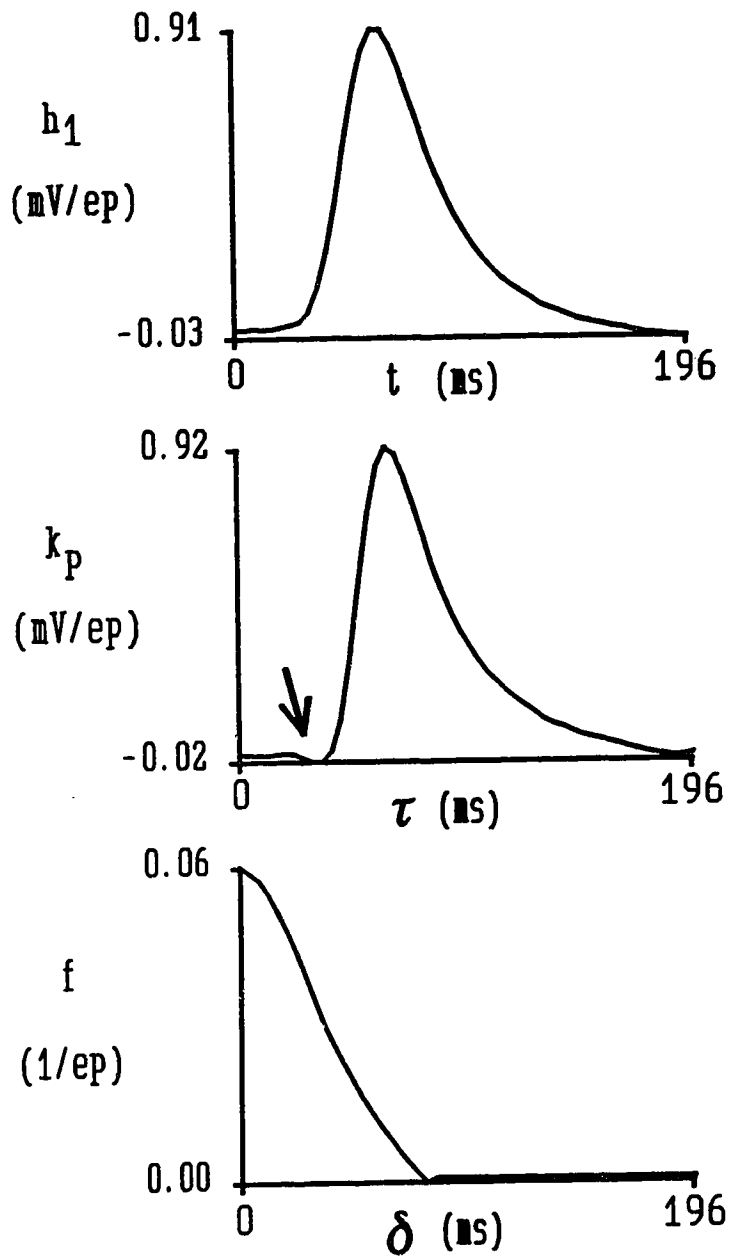


Fig. III.1. First-order Volterra kernel h_1 obtained from flash experiments and delta responses k_p and f extracted from the corresponding second-order kernel. Units of h_1 and k_p are given in mV/ep, while units of f are given in ep^{-1} . Arrow indicates facilitation (*i.e.* negative depression).

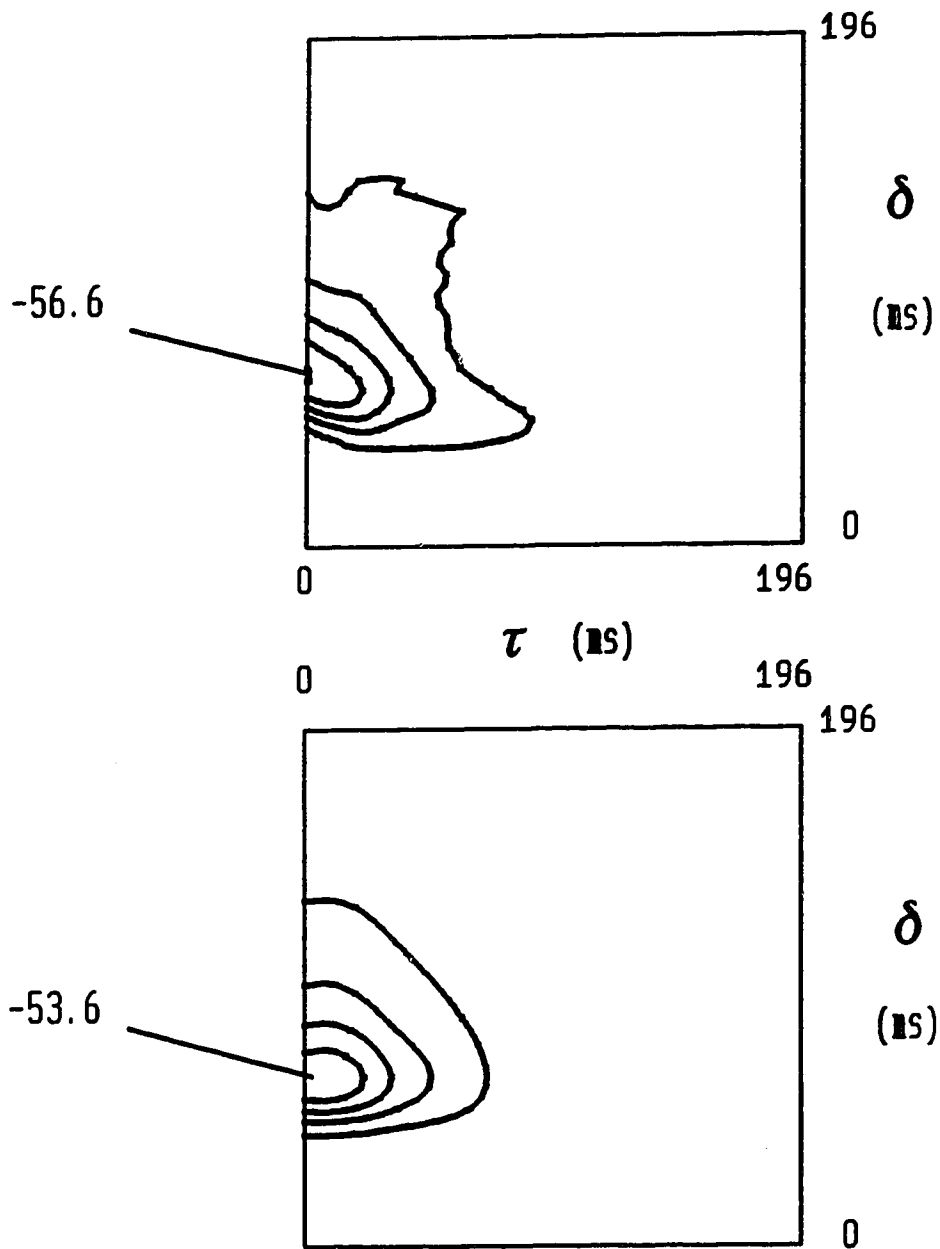


Fig. III.2. Upper: Second-order kernel p_2 as defined by Eq. III.2. Lower: Synthesized kernel $p_2(\tau, \delta)$ obtained by multiplication of the linear kernels $k_p(\tau)$ and $f(\delta)$ shown in Fig. III.1. For both kernels, τ is the time after the second flash and δ is the inter-flash interval. Units on both contour maps are given in $\mu\text{V}/\text{ep}^2$. Contour lines are separated from each other by $12.5 \mu\text{V}/\text{ep}^2$.

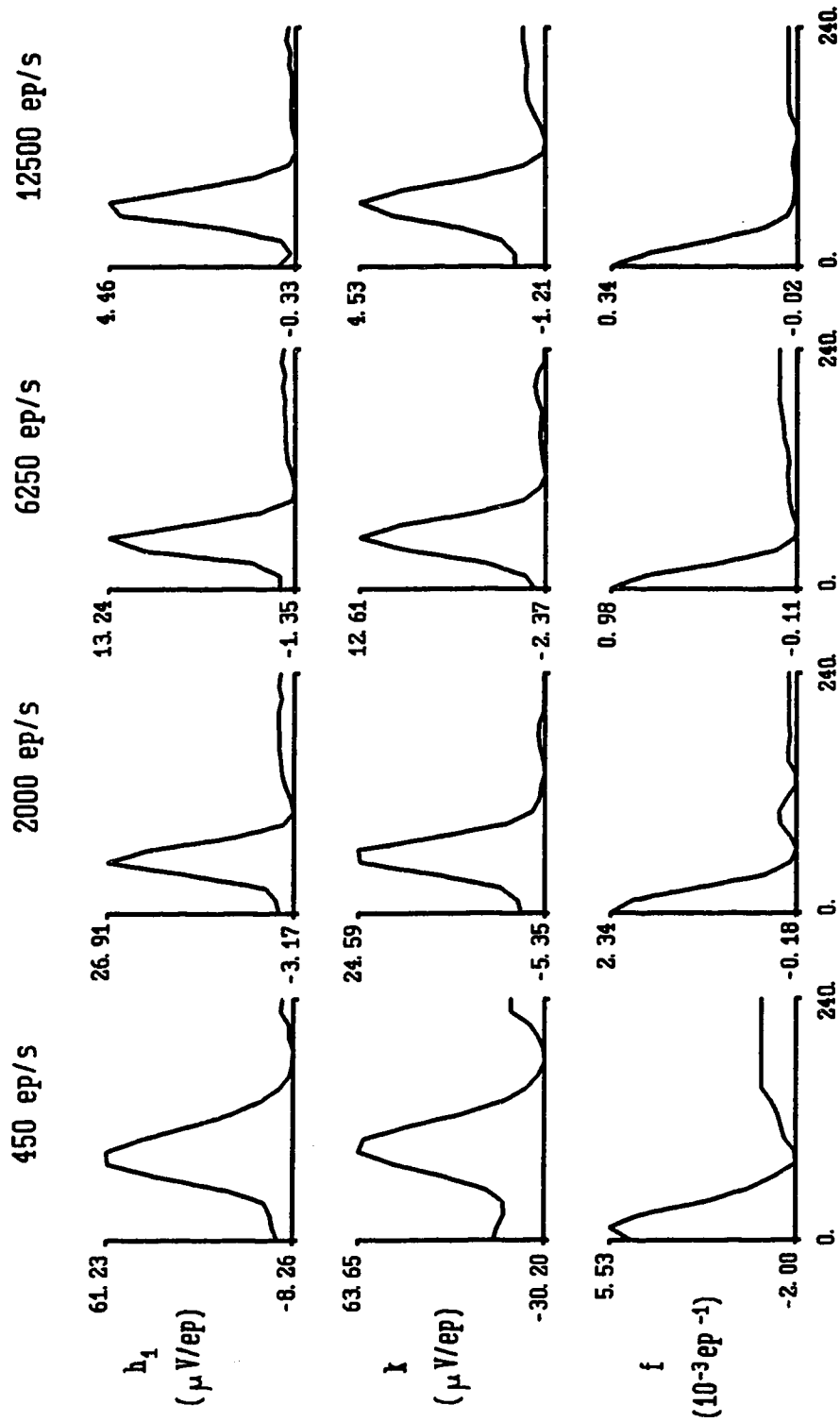
slightly more than double, then the depression will be partially compensated by the stronger stimulus. The results presented in chapter IV also indicate that the depression is about as strong for $\delta = 0$ ms as for any value of δ .

A further check for separability is the synthesis of $p_2(\tau, \delta)$ from the kernels $f(\delta)$ and $k_p(\tau)$. Fig. III.2 shows the experimental and synthesized p_2 kernels. The main difference between the two kernels was the skewness of the contour lines in the experimental kernel. This skewness indicates that the value of the time after the second flash τ for which p_2 is lowest decreases for increasing inter-flash interval δ , as shown already by French and Kuster (1985). This feature might be due to a distortion introduced by the early facilitation for low values of δ . An alternative interpretation is discussed in section III.5 .

White-noise experiments

First- and second-order Wiener kernels were measured at a range of background intensities from 500 to 15,000 ep/s. The noise power level of the input signal was always made as high as possible without clipping the LED output, so the ratio of mean background amplitude to noise power level was always approximately the same. As shown in Fig. III.3, the first-order kernel became faster when the background was increased from 500 to 2300 ep/s, but further increases only affected the gain and not the time course of the first-order kernel. The noise of the responses limited considerably the accuracy of the second-order kernels measured at less than 500 ep/s,

Fig. III.3. Linear kernels obtained from white-noise experiments at the background levels indicated along the top of the figure. Kernels are shown normalized to the same size for purposes of comparison. Absolute amplitudes were affected by the stability of the recordings, but the relative sizes of h_1 , k_p , and f were fairly constant, except at the lowest background level.



Time (ms)

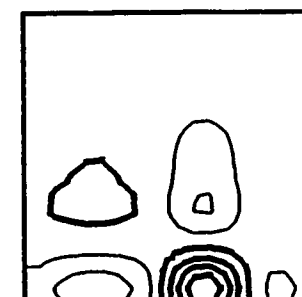
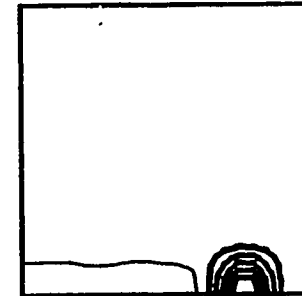
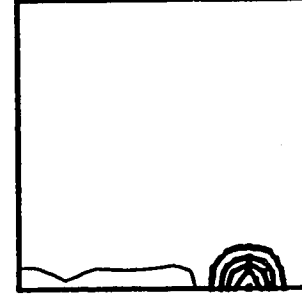
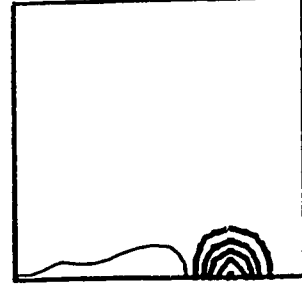
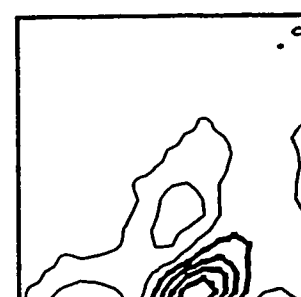
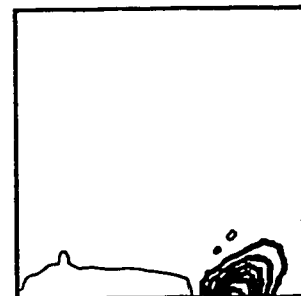
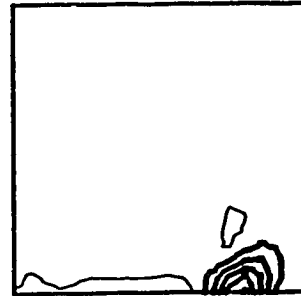
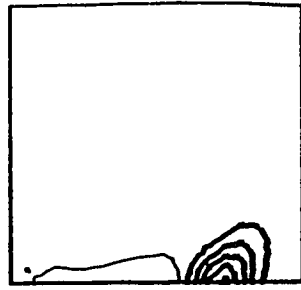
Fig. III.4. Second-order kernels p_2 obtained with white-noise stimulation at the background levels indicated along the top of the figure. Upper: from h_2 by coordinate transformation. Lower: synthesized from k_p and f . Contour lines are separated by 80 nV/ep² (500 ep/s), 10 nV/ep² (2300 ep/s), 2 nV/ep² (6800 ep/s), 0.3 nV/ep² (15000 ep/s).

15000 ep/s

6800 ep/s

2300 ep/s

500 ep/s



190

0

δ

(ms)

190

0

190

0

190

0

190

0

τ (ms)

but the first-order kernel appeared to become even slower at lower background levels.

All the kernels in Figs. III.3 and III.4 were obtained from the same cell. It can be seen that the $k_p(\tau)$ kernel extracted from $p_2(\tau, \delta)$ was very similar to the first-order Wiener kernel at every background level. Both $k_p(\tau)$ and $f(\delta)$ changed in amplitude with changing background and changed in time course only at the lowest background levels, in the same manner as the first-order kernel.

Fig. III.4 shows the experimental kernels $p_2(\tau, \delta)$ and the synthesized $p_2(\tau, \delta)$ from $k_p(\tau)$ and $f(\delta)$ for the same background levels as in Fig. III.3. The main features of the experimental kernels are a small facilitation low on the τ axis, resolved only at 500 ep/s, a slightly delayed inhibition further up on the τ axis, and a later (upper) facilitation, with the inhibition being much stronger than either facilitatory component, as in the double-flash experiments. When the background level was increased, the early facilitation became negligible. At all background levels, especially above 500 ep/s, the experimental $p_2(\tau, \delta)$ kernel could be synthesized fairly accurately from f and k_p , apart for the skewness of the inhibitory component already observed in the double-flash experiment.

III.4. Model simulations

Volterra and Wiener kernels obtained from a system with a single input are symmetrical by convention, *i.e.* $h_2(\tau_1, \tau_2) = h_2(\tau_2, \tau_1)$ for every τ_1 and τ_2 . However, for simplicity in this section we shall use triangular second-order kernels, *i.e.* kernels which are identically zero unless $0 \leq \tau_2 \leq \tau_1$. This convention is equivalent to defining τ_2 as the time after the second flash and τ_1 as the time after the first flash in the double-flash experiments.

Feedforward Gain Control

Four different models which are compatible with Eqs. III.5 were analyzed. Each of these models includes two distinct processes, a linear transduction process **K** and a linear gain control process **F**, and these two processes interact nonlinearly. The four models differ in structure (feedforward or feedback) and in the nature of the nonlinear interaction between the processes, as explained in detail below. A simple feedforward gain control scheme is shown in Fig. III.5a. The rectangular boxes are dynamic linear filters with delta responses $f(\delta)$ and $k(\tau)$, while the static nonlinear element **N** performs the operation:

$$z(t) = x(t)\{1-y(t)\} \quad \text{(III.6)}$$

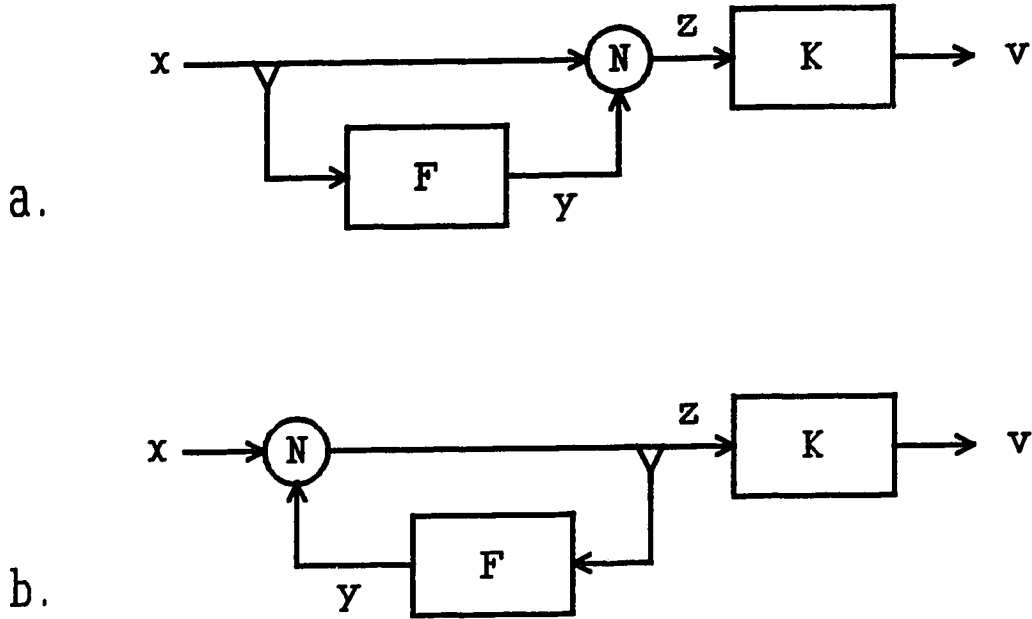


Fig. III.5. Minimum separable models of gain control. **a:** feedforward model; **b:** feedback model. The elements **F** and **K** are dynamic linear, while the element **N** is static nonlinear. The operation performed by this latter element can be a multiplication as in Eq. III.6 or a division as in Eq. III.14. The upturned triangles highlight the branching point of the gain control process from the transduction process.

where t is time, $x(t)$ is the input signal, and the other signals are as labelled in Fig. III.5a. Eq. III.6 may be expanded as follows:

$$z(t) = x(t) - \int f(\delta)x(t)x(t-\delta)d\delta \quad (\text{III.7})$$

and therefore:

$$v(t) = \int k(\tau)x(t-\tau)d\tau - \iint k(\tau)f(\delta)x(t-\tau)x(t-\delta-\tau)d\delta d\tau \quad (\text{III.8})$$

Substituting $\tau_+ = \delta + \tau$, and assuming that $f(\delta) = 0$ for $\delta < 0$:

$$v(t) = \int k(\tau)x(t-\tau)d\tau - \iint k(\tau)f(\tau_+)x(t-\tau)x(t-\tau_+)d\tau_+ d\tau \quad (\text{III.9})$$

Approximating the system by a Volterra series, or functional expansion:

$$v(t) = h_0 + \int h_1(\tau_1)x(t-\tau_1)d\tau_1 + \iint h_2(\tau_1, \tau_2)x(t-\tau_1)x(t-\tau_2)d\tau_1 d\tau_2 + \dots \quad (\text{III.10})$$

Then by comparison of Eqs. III.9 and III.10 the Volterra kernels of the system are given by: $h_0 = 0$, $h_1(\tau_1) = k(\tau_1)$, $h_2(\tau_1, \tau_2) = -f(\tau_1 - \tau_2)k(\tau_2)$, and all higher-order kernels are identically zero. Here we have again followed the convention that the second-order kernel is triangular. With the usual convention, the symmetrical

second-order kernel would be $h_2(\tau_1, \tau_2) = - (1/2)f(\tau_+ - \tau)k(\tau)$, where $\tau_+ = \max(\tau_1, \tau_2)$ and $\tau = \min(\tau_1, \tau_2)$.

Feedback Gain Control

A simple feedback gain control system is shown in Fig. III.5b, with similar linear and nonlinear elements to those of Fig. III.5a. The nonlinear element again performs the operation given by Eq. III.6 so that its output, $z(t)$, may be expressed as follows:

$$z(t) = x(t) - \int f(\delta)x(t)z(t-\delta)d\delta \quad (\text{III.11})$$

Eq. III.11 is a Fredholm integral equation of the second kind (Davis, 1962) and can not be solved analytically. A series approximation to Eq. III.11 may be developed by successively expanding the term in $z(t)$ within the convolution integral, introducing new time variables where necessary, and assuming that the functions $f(\delta)$ and $k(\tau)$ are zero at negative times. After the first such expansion, Eq. III.12 becomes:

$$z(t) = x(t) - \int f(\delta)x(t)x(t-\delta)\{1 - \int f(\theta)z(t-\delta-\theta)d\theta\}d\delta \quad (\text{III.12})$$

The output of the system, $v(t)$, may then be obtained from convolution of $z(t)$ with the final linear element, $k(\tau)$:

$$v(t) = \int k(\tau)x(t-\tau)d\tau - \iint k(\tau)f(\delta)x(t-\tau)x(t-\delta-\tau)d\delta d\tau + \dots \quad (\text{III.13})$$

If the system output is again approximated by a Volterra series, as in Eq. III.10, then the Volterra kernels in triangular format become: $h_0 = 0$, $h_1(\tau_1) = k(\tau_1)$, $h_2(\tau_1, \tau_2) = -f(\tau_1 - \tau_2)k(\tau_2)$, $h_3(\tau_1, \tau_2, \tau_3) = f(\tau_1 - \tau_2)f(\tau_2 - \tau_3)k(\tau_3)$, etc. These kernels are identically zero unless $0 \leq \tau_3 \leq \tau_2 \leq \tau_1$.

Gain control by a ratio nonlinearity

If the equation describing the nonlinear elements N in Fig. III.5 is:

$$z(t) = x(t)/\{1+y(t)\} \quad (\text{III.14})$$

instead of Eq. III.6, we have a system which is more difficult to describe by Volterra kernels, but which might be biologically more realistic, as we will discuss in section III.5. With Eq. III.14 as the nonlinear operation, the output of the system in Fig. III.5a becomes:

$$v(t) = \int k(\tau)x(t-\tau)/\{1 + \int f(\delta)x(t-\tau-\delta)d\delta\} d\tau \quad (\text{III.15})$$

while the output of the system in Fig. III.5b becomes:

$$v(t) = \int k(\tau)x(t-\tau)/\{1 + \int f(\delta)z(t-\tau-\delta)d\delta\} d\tau \quad (\text{III.16})$$

By expanding the fraction in Eq. III.14 into a MacLaurin series, it can be shown that the first and second terms of the series are identical to the right-hand side of Eq. III.6. Therefore, the first- and second-order Volterra kernels will be identical for systems containing the product (Eq. III.6) or ratio (Eq. III.14) nonlinearities. This can also be shown by expanding Eqs. III.15 and III.16 into MacLaurin series: in this case, the first- and second-order terms of the series become identical to those in Eqs. III.8 and III.12. However, the four systems produce different outputs because they differ in their higher-order kernels.

Separability of the second-order kernel

Eqs. III.8 and III.13 both predict that the second-order Volterra kernel, $h_2(\tau_1, \tau_2)$ should be separable into two functions, $f(\delta)$ and $k(\tau)$, if it is first re-arranged to give a new second-order kernel as in Eq. III.2. However, Eq. III.8 predicts that a complete description of the system output can be obtained from $h_1(\tau)$ and $p_2(\tau, \delta)$, while Eq. III.13 indicates that even a simple feedback nonlinear system requires an infinite series to represent the system behavior. Both equations also predict that the first-order kernel, $h_1(\tau)$, should be identical to the delta response of the linear system K which is in series with the nonlinear component N .

From our analysis in the previous section it follows that Eqs. III.5 are still valid if

the nonlinearity is of the form of Eq. III.14. However, in this case even a feedforward system requires an infinite series of Volterra kernels. We will refer to the models of Fig. III.5 as separable models, irrespective of the kind of nonlinearity.

Simulation results

In order to test the predictive power of the different models described above, we tried to reproduce the responses of photoreceptors by computer programs that simulated such models. At low power levels, the first- and second-order Wiener kernels of any system can be approximated by their Volterra equivalents (the relationship between Volterra and Wiener kernels is given by Marmarelis and Marmarelis, 1978, page 150). This approximation depends on the assumption that higher-order nonlinearities are negligible. Under this assumption, two kinds of simulations were carried out. First, we tried to reproduce the photoreceptor output by simulating a first-order Volterra system with the first-order kernel h_1 or a second-order Volterra system with the kernels h_1 and h_2 . In the second kind of simulation, the kernels h_1 and f of Fig. III.3 were used as the delta responses of the linear components **K** and **F** of the models of Fig. III.5; the models were simulated with both kinds of nonlinear element (product, Eq. III.6 and ratio, Eq. III.14). The Volterra simulations and the model simulations are compared with the actual experimental output in Fig. III.6.

The mean-square error between the linear simulation and the experimental response was about 17% of the output power of the experimental response, *i.e.* the

first-order kernel accounted for about 83% of the response. The exact values of these percentages varied in different sections of the records. Linear simulations are, of course, unaffected (except for a DC offset) by any background superimposed on the white noise. Second-order Volterra simulations as well as simulations of any of the models could be done using either the actual input (background plus white noise) or its AC component (white noise only). The Wiener kernels were extracted from the AC component of the input after subtraction of the background level. The resulting Wiener kernels approximate Volterra kernels for negative or positive stimuli superimposed on this background level. For this reason, the simulations too were performed using the AC component of the input only. Significantly worse results were obtained in both the kernel extraction and/or the simulations when the background level was not subtracted from the input before either computation. The mean-square error of the model simulations was about 16% of the output power, *i.e.* the nonlinear component of the model responses accounted for an additional 1% of the response. The penultimate trace shows the response of the second-order Volterra system. The error of this simulation was about 15% of the output power. The significance of a nonlinear mechanism which apparently contributes so little to the photoreceptor response will be discussed in section III.5.

Simulations of responses obtained at a high background level were also attempted using kernels obtained at a lower background level. In this case, the DC component of the input was not completely subtracted, but adjusted relative to the level at which

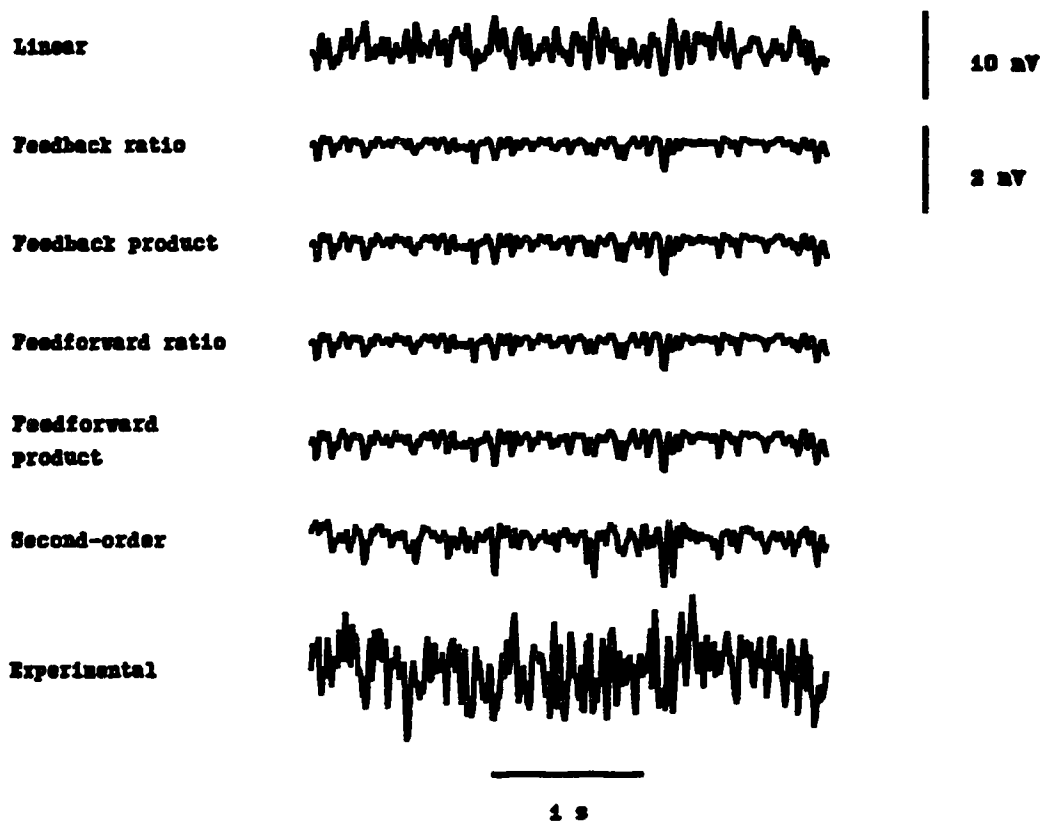


Fig. III.6. First trace: simulated linear component of the photoreceptor potential response to white-noise stimulation at a background level of 6800 ep/s. The other traces represent differences from this trace, at a different scale, of the simulations of the output produced using separable models (traces 2 to 5) or a Volterra second-order model (trace 6), or of the experimental trace (lowest trace), as indicated. The kernels used for the simulations were obtained from a larger record including the segment shown here. For these simulations, the background was subtracted from the input signal (not shown). The mean-square error of the linear model simulation was about 17 % of the output power; the mean-square errors of the separable model simulations were about 16 %; the mean-square error of the second-order model simulation was about 15%.

the kernels were obtained (e.g. if the kernels were obtained at a background level of 2300 ep/s, this latter value was subtracted from the real input being used in the experiment, leaving a smaller but considerable DC component). Most of these simulations produced responses which were either larger in amplitude than the experimental responses, or very different in shape, or even inverted in polarity. This discrepancy is likely to be due to an adaptation phenomenon at some point in the phototransduction pathway which decreases the signal amplitude in proportion to the background level. This adaptation process, rather than the intrinsic dependence of Wiener kernels on the input background level, would then be responsible for the differences between the kernels in Figs. III.3 and III.4. As can be seen from these figures, adaptation seems to affect the gain and time course of the kernels f and k in similar ways.

III.5. Discussion

Comparisons between the kernels obtained by the two methods

The main conclusion of this investigation was that the first- and second- order kernels obtained with both methods were very similar in time course. The differences of gain that were observed were most likely due to slow adaptation processes which could not be analyzed because both the Volterra and Wiener kernels were evaluated over 200 ms only.

When the components of the second-order Wiener kernels, k and f , were compared, the relative amplitudes of these components were seen to be unchanged by changes of background level. However, analysis of the second-order Volterra kernel produced relatively larger values for f compared to k . In fact, the second-order depression observed in the responses to double flashes was about 30% of the linear prediction (*i.e.* 60% of the response to a single flash), while the second-order component of the responses to white noise gave only a 2% improvement in the square error of the simulations. Gemperlein and McCann (1975) and Eckert and Bishop (1975), using white noise stimuli, obtained comparable results (improvements of 2.3% and of 0.3% respectively). With such a small nonlinear contribution, it would seem impossible to select any model by comparing simulated and experimental responses. Those earlier investigations reported mean square errors of 6.8% and 8.4% respectively for the linear simulations. This discrepancy might be due to the amplitude of the photon noise. In fly photoreceptors, Howard *et al.* (1987) found that the standard deviation of photon noise is maximal for background light intensities between 10^3 and 10^5 ep/s, while, for signals with constant contrast, the signal-to-noise ratio increases monotonically with background intensity. Unfortunately Gemperlein and McCann (1975) and Eckert and Bishop (1975) do not report the stimulus intensity that was used.

The above observations would seem to imply that the second-order component measured with white noise is of little, if any, biological relevance. Indeed, the underlying gain control mechanism probably evolved to regulate responses to

excursions of light intensity much larger than can be obtained in a white noise experiment. A flash stimulus provides such an excursion if the flash intensity is much larger than the background intensity, as was the case in our experiments. By contrast, white noise superimposed on a background \bar{x} is limited to fluctuations of intensity x in the range $0 < x < 2\bar{x}$.

The above ideas can be formulated somewhat more technically. When comparing responses at different background levels \bar{x} in a system capable of adaptation, what matters is not the RMS power level σ_x , but rather the ratio σ_x/\bar{x} , which constitutes the "effective" RMS power level. For equal \bar{x} , the value of σ_x of a symmetric binary stimulus is much higher than that of pseudo-random white noise (Larkin *et al.*, 1979). The double-flash stimulus is an asymmetric binary stimulus, in which \bar{x} is kept low by using a very short duty cycle and therefore σ_x/\bar{x} is even higher than for a symmetric binary stimulus. Since the nonlinear components of the response are relatively larger at higher σ_x/\bar{x} (the linear component is proportional to the RMS power level, while the second-order component is proportional to the square of the RMS power level), the double-flash experiments should produce relatively much larger nonlinear components of the response, as indeed was the case.

The Wiener kernels were affected only in amplitude, not in time course, at background levels above 2300 ep/s. This finding is in agreement with the results obtained by Howard (1981) with flashes superimposed on a background level. Howard found that the flash responses became faster with increasing background

levels up to about 1000 ep/s, while there was little change of time course above this level.

The Wiener kernels obtained by Larkin *et al.* (1979) from human ERG (electroretinographic) responses are similar in some respects to those we obtained because the ERG kernels also seem to be separable, except for the skewness of the response. Furthermore, the response time courses become faster with increased background levels both in the human ERG and in the locust receptor potential. We were motivated to investigate separable models primarily by S. Klein's analyses of the ERG responses (in preparation for publication).

An important question is whether these models only describe the input-output relationship of the system or whether they contain important features of the underlying biophysical mechanisms. Whatever the nature of this mechanism, it probably underlies both the noticeable nonlinearities observed with flash stimuli and the barely detectable nonlinearities in the responses to white noise.

Separability of the second-order kernel

There are two issues relating to the separability of the second-order kernel. One is how well two linear kernels f and k can approximate p_2 as in Eqs. III.5 . The other is whether there is a relationship between first- and second-order kernels in the sense that h_1 is approximately equal to k_p . The first question is whether all the information contained in the second-order kernel can be recovered from two perpendicular slices through it, so that the matrix of voltage measurements of size n^2 can be reduced to

two vectors of size n ; the second question is whether we really need to calculate only one of these vectors from p_2 , since k is identical to h_1 . Physically, this would imply that in the double-flash experiments the response to the second flash is decreased at all times by a constant factor, this factor being a function of the inter-flash interval δ . As a consequence, a separable second-order kernel predicts a change of amplitude, and not of time course in the double flash responses.

In both respects, Eqs. III.5 provided a good approximation to the measured kernels. The main discrepancies between the separable and the experimental kernels were the early facilitation and the skewness of the negative contours in Figs. III.2 and III.4, both implying a change of the response time course. The early facilitation is very difficult to investigate, since it is not only small, but also variable between cells. French and Kuster (1985) already pointed out that the facilitation is small compared to the depression, and they might have overestimated it because of the problems related to the nonlinearity of the LED current-to-light relationship. A facilitation during the rising phase of the response is also observed in *Limulus* ventral eye photoreceptors (Fein and Charlton, 1977; Payne and Fein, 1986; Grzywacz *et al.*, 1988), but not at very low light intensities.

There might be a partial overlap between facilitation and depression, leading to a partial cancellation of the two effects. In this case, the skewness observed in the contour maps might be a distortion arising from this partial overlap. Since the facilitation and the depression presumably are caused by separate mechanisms, the second-order kernel would be composed of a large separable negative component

(the depression) and a smaller positive component (the facilitation), which is not separable and is responsible for any change in the response time course.

An alternative interpretation for the skewness is based on the dynamics of the gain control process. More specifically, if the depression is due to a shunting conductance, as suggested by the results discussed in chapter IV, then it will take some time for this conductance to be activated after the response to the first flash depolarizes the membrane. After the activation, there will be a further delay due to the membrane time constant before the shunting conductance results in a depression of the membrane voltage. Therefore, the more the first flash response precedes the second, the sooner the depression will be observed relative to the second response. According to this second interpretation, although p_2 can be approximated as a separable kernel, the small changes of response time course that were observed are an essential result of the gain control mechanism.

Validity of the separable models

While the separability of p_2 would not imply the validity of the separable models of Fig. III.5, the reverse is not true, *i.e.* separable models imply a separable second-order kernel. As we discussed in the previous paragraph, the experimental kernels are open to different interpretations. The model simulations were not conclusive either, due to the linearity of the response, as discussed above. Therefore, separable models are neither excluded nor strongly supported by the experimental findings.

The biochemical equivalent of a separable model is a cascade with a control point

for the gain placed before any of the rate-limiting steps. If this nonlinear gain control is accomplished by inhibition of an enzyme, Eq. III.14 might be a reasonable mathematical approximation of the nonlinear element (Grzywacz and Hillman, 1988). This equation arises from the assumption that the gain at stage N is proportional to the fraction of enzyme which is not bound to its inhibitor. We point out that, although a feedback mechanism is generally less stable than a feedforward mechanism, a ratio nonlinearity increases the stability of the system as compared to a multiplicative nonlinearity, since dividing the input by some positive factor never changes the input's polarity.

In Chapter IV, more direct evidence will be presented in favour of a different model which will be analyzed in some detail in Chapter V. In this new model the gain control point is not located before the time-limiting steps of phototransduction, but after all of them except for the membrane time constant. Furthermore, the mechanism that reduces the gain should also decrease this time constant by decreasing the total membrane resistance, and therefore it cannot be reduced to a block diagram with only a static nonlinearity. However, if the effect on the time constant can be neglected (as it might happen if the time constant becomes much smaller than the time course of phototransduction), then the nonlinearity of the new model will be seen to be a ratio between the input signal and the feedback signal, although this nonlinearity is due to a biophysical mechanism different from enzyme inhibition.

III.6. References

- Claßen-Linke I, Stieve H (1986) The sensitivity of the ventral nerve photoreceptor of *Limulus* recovers after light adaptation in two phases of dark adaptation. *Z Naturforsch* 41c:657-667.
- Davis HT (1962) Introduction to nonlinear differential and integral equations. Dover Publications, New York.
- Eckert H, Bishop LG (1975) Nonlinear dynamic transfer characteristics of cells in the peripheral visual pathway of flies. Part I: The retinula cells. *Biol Cybern* 17:1-6.
- Fein A (1986) Excitation and adaptation of *Limulus* photoreceptors by light and inositol 1,4,5-trisphosphate. *Trends Neurosci* 9:110-114.
- Fein A, Charlton JS (1977) Enhancement and phototransduction in the ventral eye of *Limulus*. *J Gen Physiol* 69:553-569.
- French AS, Kuster JE (1985) Nonlinearities in locust photoreceptors during transduction of small numbers of photons. *J Comp Physiol A* 156:645-652.
- Fuortes MGF, Hodgkin AL (1964) Changes in time scale and sensitivity in the ommatidia of *Limulus*. *J Physiol* 172:239-263.
- Gemperlein R, McCann GD (1975) A study of the response properties of retinula cells of flies using nonlinear identification theory. *Biol Cybern* 19:147-158.
- Grzywacz NM, Hillman P (1985) Statistical test of linearity of photoreceptor transduction process: *Limulus* passes, others fail. *Proc Nat Acad Sci USA* 82:232-235.

- Grzywacz NM, Hillman P (1988) Biophysical evidence that light adaptation in *Limulus* photoreceptors is due to a negative feedback. *Biophys J* 53:337-348.
- Grzywacz NM, Hillman P, Knight BW (1988) The quantal source of area supralinearity of flash responses in *Limulus* photoreceptors. *J Gen Physiol* 91:659-684.
- Howard J (1981) Temporal resolving power of the photoreceptors of *Locusta migratoria*. *J Comp Physiol* 144:61-66.
- Howard J (1983) Variations in the voltage response to single quanta of light in the photoreceptors of *Locusta migratoria*. *Biophys Struct Mech* 9:341-348.
- Howard J, Blakeslee B, Laughlin SB (1987) The intracellular pupil mechanism and photoreceptor signal:noise ratios in the fly *Lucilia cuprina*. *Proc R Soc B* 231:415-435.
- Korenberg MJ (1988) Identifying nonlinear difference equation and functional expansion representations: the fast orthogonal algorithm. *Ann Biomed Eng* 16:123-142.
- Korenberg MJ, French AS, Voo SKL (1988) White-noise analysis of nonlinear behavior in an insect sensory neuron: kernel and cascade approaches. *Biol Cybern* 58:313-320.
- Kuster JE, French AS (1985) Changes in the dynamic properties of locust photoreceptors at three levels of light adaptation. *Biol Cybern* 52:333-337.
- Lamb TD (1986) Transduction in vertebrate photoreceptors: the roles of cyclic GMP and calcium. *Trends Neurosci* 9:224-228.

- Larkin RM, Klein S, Ogden TE, Fender DH (1979) Nonlinear kernels of the human ERG. *Biol Cybern* 35:145-160.
- Laughlin SB (1981) Neural principles in the visual system. In: Handbook of Sensory Physiology, VII/6B (H. Autrum, ed.) 133-280. Springer-Verlag, Berlin.
- Marmarelis PZ, Marmarelis VZ (1978) Analysis of physiological systems. The white-noise approach. Plenum Press, New York.
- Payne R, Fein A (1986) The initial response of *Limulus* ventral photoreceptors to bright flashes. Released calcium as a synergist to excitation. *J Gen Physiol* 87:243-269.
- Pece AEC, French AS, Korenberg MJ, Kuster JE (1990) Nonlinear mechanisms for gain adaptation in locust photoreceptors. *Biophys J* 57:733-743.
- Pugh E, Altman J (1988) A role for calcium in adaptation. *Nature* 334:16-17.
- Schetzen M (1965) Measurement of the kernels of a nonlinear system of finite order. *Int J Control* 1:251-263.

IV. PHYSIOLOGICAL DISSECTION OF THE GAIN CONTROL MECHANISM³

IV.1. Introduction

Gain control in photoreceptors has been shown to take place in time courses varying from milliseconds to several hours (see *e.g.* Autrum, 1981; Fein and Szuts, 1982; Claßen-Linke and Stieve, 1986), the term adaptation being generally reserved for processes taking place with time courses substantially slower than the time course of the photoresponse itself. In this study, we concentrate on a process taking place in the same time scale as the photoresponse. This gain control process can be described as an inhibition or depression of the light response resulting in a sub-linear relationship between light stimulus and response. The time scale of this process can be measured by stimulating the photoreceptor with pairs of flashes and measuring how the inter-flash interval affects the inhibitory effect of the first flash on the response to the second (French and Kuster, 1985). Such a fast process has only been demonstrated in insect photoreceptors (review: Laughlin, 1981).

In *Limulus*, crayfish, and vertebrate photoreceptors, the amplitude of a flash response is a simple function of the flash intensity, being described by Eq. I.3. This relationship between stimulus and response is predicted by the self-shunting of the

³ A version of this chapter has been submitted for publication. Pece AEC, French AS, *Biophysical Journal*.

photocurrent through the light-activated (or inactivated) membrane conductance. In locust photoreceptors, with the reversal potential for the light-activated current about 50 mV above the resting potential (Payne, 1982), self-shunting would predict a response amplitude of about 5.66 mV when a flash producing a peak response $v = 3$ mV is doubled in amplitude (see Chapter V). This corresponds to a response depression $\Delta v = 0.34$ mV with respect to the linear prediction, or a normalized depression of $\Delta v/v = 0.11$, which is much less than the normalized depressions of about 0.6 which are described below. Furthermore, the normalized depression induced by self-shunting should be very sensitive to the response amplitude, while the measurements presented in this paper show that $\Delta v/v$ is about 0.6 for a range of v of at least 1.5 mV to 4 mV. It has been found that the amplitude of flash responses of insect photoreceptors can be phenomenologically described by a modified self-shunting equation in which stimulus intensity is reduced by a fractional power (Eq. I.4; see also Laughlin, 1981). However, this equation leaves open the question of which biophysical mechanism might reduce the effective stimulus intensity. It should be pointed out here that a similar fractional power transformation is observed in vertebrate photoreceptors when the stimulus lasts for a few seconds, which is long enough to start adaptation processes (Normann and Werblin, 1974).

Broadly, we can distinguish 3 levels at which the gain could be regulated: before photon absorption, by regulating the amount of light available to the rhodopsin or the amount of rhodopsin ready to be isomerized; between photon absorption and channel opening, by regulating the gain of the biochemical cascade which links these two

events; or after channel opening, by shunting the photocurrent generated by channel opening. It should be kept in mind that the gain of one stage could also be regulated by the level of activation of another stage. For instance, the gain of the vertebrate phototransduction cascade is regulated by the level of intracellular calcium (Pugh and Altman, 1988), which is affected by calcium influx through the light-dependent channels. In principle, it is fairly straightforward to determine at which level the gain is regulated: a change of the gain involving membrane shunting would not be observed under voltage-clamp, and a change in the number of rhodopsin molecules being isomerized is the only mechanism which would affect the frequency but not the amplitude of single-photon responses (quantum bumps).

It has been proposed that the fast gain control process observed in insect photoreceptors is operating mostly at the level of the biochemical phototransduction cascade (French and Kuster, 1985). A reduction in the number of rhodopsin isomerizations was ruled out by the fast time scale and the small number of isomerizations required for the process, while a shunting conductance mechanism was thought to be unlikely because the process is manifest at very low levels of light-induced depolarization. Insect photoreceptors have not been voltage-clamped until very recently, and even now only in darkness or at very low light levels (Weckström *et al.*, 1990). Preliminary experiments under current-clamp suggested that depolarization due to current injection was not affected by depolarization due to phototransduction, and *vice versa* (French and Kuster, 1985).

On the strength of these earlier investigations, we showed in a previous publication

(Pece *et al.*, 1990; see also Chapter III) that the gain control process measured under flash and white noise stimulation is compatible with a mechanism in which the site of gain control is located at an early stage of the biochemical cascade, soon after rhodopsin isomerization and removed from ion channel opening by several rate-limiting steps. However, that investigation could not exclude the possibility of alternative mechanisms.

This chapter presents the results of new experiments which suggest that the biochemical inhibition hypothesis should be replaced by a model in which gain control is mediated by voltage-activated membrane conductances. First, we show that a localized optical stimulus produces a homogeneous reduction of gain within the photoreceptor without any detectable delay, which can be explained by the cable properties of the cell but not by realistic estimates of the diffusion speed of a biochemical inhibitor. Second, a more accurate measurement of the interaction between current injection and light responses produced results very different from earlier observations. We found that a flash stimulus and an electrical stimulus interacted in the same way as pairs of flashes. This suggests that the inhibitory effect is caused by membrane depolarization, irrespective of its source, and does not reduce the gain of the transduction cascade but rather shunts light-induced as well as artificially induced membrane currents.

Weckström *et al.* (1990) have recently described 2 potassium conductances in fly photoreceptors that could account for the phenomena under investigation. However, we show that the gain control mechanism that we investigated is not as sensitive to

intracellular tetraethylammonium (TEA) as the conductances found in fly photoreceptors.

Throughout this paper, we shall refer to the first in time of two stimuli as the adapting stimulus and the second as the test stimulus, even though in most experiments the effect of the first stimulus is not adaptation, but rather the fast gain control process.

IV.2. Methods

Locusts, *Locusta migratoria*, were from the same laboratory colony as in Chapters II and III. They were used at least 1 week after their imaginal moult and dark adapted for at least 1 hour before the experiment. Experiments were performed at room temperature. Intracellular voltage was measured with glass microelectrodes having a resistance of about 80 M Ω when filled with 3 M potassium acetate. In some experiments 0.5 M tetraethylammonium chloride (TEA) in 2.5 M potassium acetate was used instead of 3 M potassium acetate. Intracellular voltage was measured by a conventional amplifier (Getting Inc., Los Altos, CA, model 5) and high-pass filtered at 0.05 Hz by a single-pole filter. The intracellular voltage was sampled at 2 ms intervals by a 12-bit analog-to-digital converter and stored on-line in a digital computer. In the step response experiments, the responses were not high-pass filtered, but instead low-pass filtered at a cut-off frequency of 1 KHz and sampled at

4 ms intervals. The photoreceptor response contains very little signal above a frequency of 50 Hz (the Nyquist frequency for a sampling interval of 10 ms). Average responses were stored instead of individual responses, except for the local adaptation and step response experiments. No attempt was made to determine the average number of photons being transduced for each flash, but that number must have been small for 2 reasons: (1) the average amplitudes of the single-flash responses were smaller than 5 mV in all data files and the cells were dark-adapted; (2) the individual responses were variable in amplitude and occasionally a flash resulted in no detectable response. In most TEA injection experiments, measurements of interactions between two flashes (Fig. IV.7) followed measurements of the step response to light (Fig. IV.8) and therefore the photoreceptor was not completely dark-adapted.

In vitro experiments

For the *in vitro* experiments, we used the technique developed by Payne (1980, 1982) and described in Chapter II. Briefly, the head was isolated, then the lower part of the head was cut off and the upper part was split with a sharp razor blade across both eyes, so that in each eye an array of photoreceptors were exposed across their length. The frontal segment of the head was superfused with oxygenated saline, flowing at a rate of about 4.5 ml/min in a 1.5 ml chamber. The light sources were 2 Xenon strobe lamps or, in the local adaptation experiments, a Lucida 150 light guide source. The light was transmitted through light guides to the image plane of the

phototube of a Wild dissection microscope. The ends of the light guides were masked so that only a slit of light was focused by the microscope onto the photoreceptors in the object plane. The slits were 30 μm wide in the object plane. The strobe lights were triggered under computer control. The light energy of the flash at the level of the preparation, as measured by the phototransistor, was about $5 \cdot 10^{-4} \text{ J/cm}^2$. The irradiance of the steady light used for localized adaptation was about 2000 W/cm^2 . The actual values at the level of the photoreceptor being recorded from must have been much lower, since the cells which were used in the experiments were not located at the surface of the preparation, but at a variable depth. Overlaying cells therefore provided an unknown and variable amount of screening.

In vivo experiments

The methods used for the experiments employing current injection and TEA iontophoresis were similar to those described in Chapter III. The wings and legs were removed and the animal, particularly its mandibles and antennae, was immobilized with dental wax. Usually the ventral nerve chord was cut at the level of the neck or, more effectively, the thoracic ganglia were destroyed, to minimize movements of the animal. The microelectrodes were lowered through a hole in the cornea of the right eye to penetrate reticular cells. The reference silver electrode was placed in the left eye. High-vacuum silicone grease was used to seal all cuts in the eyes and in the thorax or neck. No attempt was made to determine for how long the preparation remained suitable for experiments, but in our experience it remained stable for at

least 24 hours when the neck was cut and 12 hours when the thoracic ganglia were destroyed.

Light stimulation was provided by the green LED held by a Cardan arm at a distance of 5 cm from the eye. The stimulus was placed at the angular position which gave the strongest intracellular response from the photoreceptor. The LED was controlled by the digital computer via a constant current circuit. The LED light intensity was kept constant for each flash within each experiment, so that any nonlinear relationship between LED current and light intensity could not affect our results. Pairs of flashes with a nominal inter-flash interval of 0 ms had an actual separation of 0.2 ms. The light energy of the flashes, as measured with the phototransistor, was about $7 \cdot 10^{-8}$ J/cm² but was adjusted to produce responses of amplitude between 2.5 mV and 4 mV. In the step response experiments, the irradiance during the stepwise illumination was $1.5 \cdot 10^{-3}$ W/cm².

Current clamping

Current was injected by conventional bridge-balancing techniques; care was taken to ensure that the electrode resistance was not changed at the end of the experiment. Slow, rhythmic changes of both electrode and cell resistance, probably due to respiratory movements of the animal, were sometimes observed when the thoracic ganglia were not destroyed; measurements were not done in these cases unless a slight change in the position of the electrode stabilized the observed resistances. The current injection was also controlled by the digital computer via a 12-bit digital-to-

analog converter.

The electrode time constant was about 0.8 ms (0.1 ms for each 10 M Ω of electrode resistance) and could be reduced to 0.1 ms by capacitance compensation. However, after capacitance compensation a slower component was observed in the electrode voltage relaxation following a step change in applied current. This component decayed to half its peak value in about 1 ms and accounted for about 20 M Ω of the 80 M Ω of total electrode resistance. Experiments were only performed in cells in which the membrane time constant was larger than 5 ms. Even under these conditions, it was not possible to distinguish by eye between the slow component of electrode voltage relaxation and the membrane voltage relaxation during stepwise stimulation with current. With this qualification, the measured membrane resistance was about 30 M Ω and the membrane time constant about 10 ms, but both were very variable. Since the uncompensated component of the electrode resistance was probably somewhat less than 20 M Ω (depending on how well the electrode voltage relaxation could be distinguished from the voltage relaxation of the cell membrane), the voltage responses were probably about half their measured values. After the resistance cancellation was set, the capacitance compensation was slightly reduced to lower the voltage noise resulting from the positive feedback through the compensation circuit.

IV.3. Results

Interactions between localized stimuli

Pairs of flashes with different inter-flash intervals were delivered to the photoreceptors in the slice preparation, each flash being localized to a 30 μm slit perpendicular to the photoreceptor main axis, as shown in Fig. IV.1. The 2 flashes in each pair were delivered through 2 different slits and the distances between the slits was set to either 0 or 120 μm . In each data file stored on the computer, the responses to the individual flashes and to pairs of flashes with different time intervals were recorded in a mixed sequence. However, the distance between the slits was constant within each data file, and not all cells yielded measurements for both slit separations.

The responses to single flashes were subtracted from the responses to pairs of flashes with the appropriate time shift, corresponding to the inter-flash interval. The difference trace obtained in this way always had a single minimum, as shown in Fig. IV.1 and in French and Kuster (1985) and in Chapter III. The peak depression was therefore taken as a measure of the interaction between the two stimuli, as in French and Kuster (1985). The difference between the time-to-peak of the depression and the time-to-peak of the test flash response was taken as a measure of the time course of the depression. A positive value for this time-to-peak difference indicates that the peak depression occurred later than the expected peak response to the test flash.

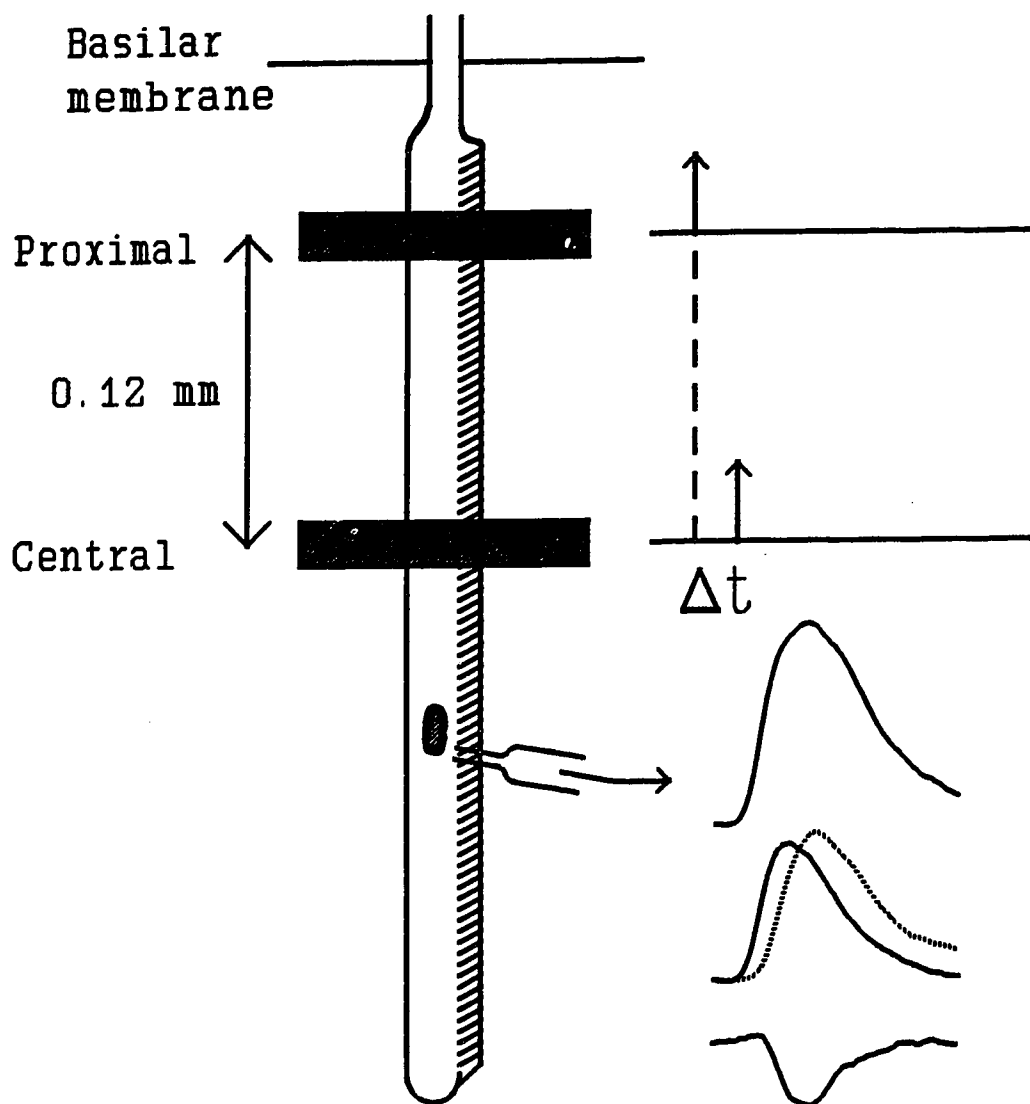


Fig. IV.1. Diagram of the experimental arrangement to measure the effect of stimulus distance on the interaction between stimuli. Transversal bars indicate the sites of light stimulation, $30 \mu\text{m}$ wide. Stimuli were separated in time as well as distance, by a variable inter-flash interval Δt . The responses to the single flashes were subtracted from the response to the combination of two flashes, resulting in the difference trace shown at the bottom right.

The measured depression must be normalized by taking into account the size of the stimuli. Empirically, we found that, when the single-flash response amplitudes were between 1.5 and 5 mV, the value of the normalized depression was independent of stimulus intensity if the normalization factor was the geometric average of the peak responses to the two stimuli (the square root of the product of the two peak responses). Although we can offer only an empirical justification for this procedure, its effectiveness is consistent with the square-root relationship between flash intensity and depolarization described by Laughlin and Lillywhite (1982) and with a model of the nonlinear depression which will be discussed in Chapter V. In Chapter III, the responses were normalized by dividing them by the peak amplitude of the response to a single flash. The two interacting stimuli were always of the same size in those experiments, so that there was no need for geometric averaging. The units for the normalized depression used in Chapter III were inverse effective photons (ep^{-1}), obtained by dividing the depression in mV/ep^2 by the single-flash response in mV/ep . Since the results presented here indicate that the depression is related primarily to depolarization and only indirectly to flash intensity, we shall simply divide the depression in mV by the single-flash response in mV, resulting in a normalized depression which is dimensionless.

As can be seen from Figs. IV.2 and IV.3, the observed interaction between the flashes was apparently unaffected in either amplitude or time course by the distance between the slits. For every inter-flash interval, the average normalized depressions observed with the two different slit distances were within 2 standard deviations of

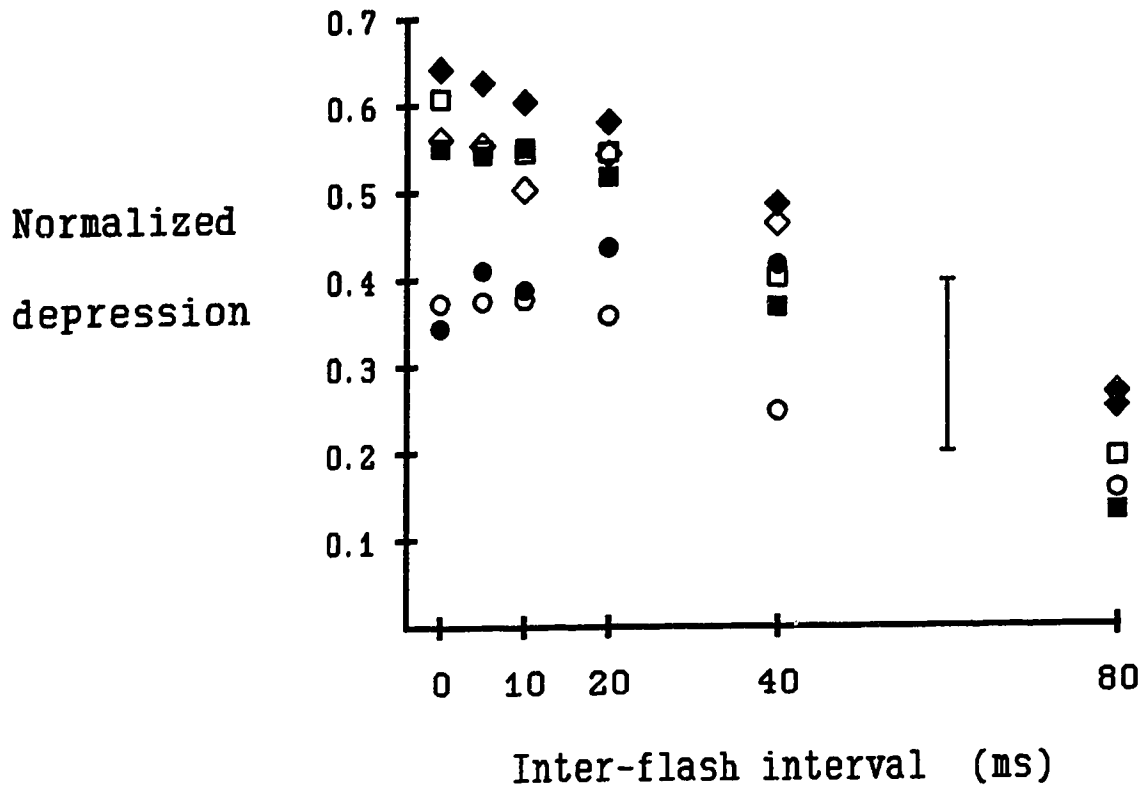


Fig. IV.2. Normalized depressions caused by interactions between flashes separated by different distances, for different response amplitudes. Empty symbols: overlapping slits; full symbols: slits separated by $120 \mu\text{m}$. Squares: responses between 3.59 and 2.49 mV; Diamonds: responses between 2.40 and 1.76 mV; Circles: responses between 1.51 and 0.94 mV. Each symbol represents 4 or 5 measurements including between 137 and 210 responses from between 2 and 5 cells. For each inter-flash interval, all the symbols represent a total of 508 responses from 8 cells for overlapping slits and 450 responses from 8 cells for slits separated by $120 \mu\text{m}$. The error bar is twice the (average) standard deviation of the measurements.

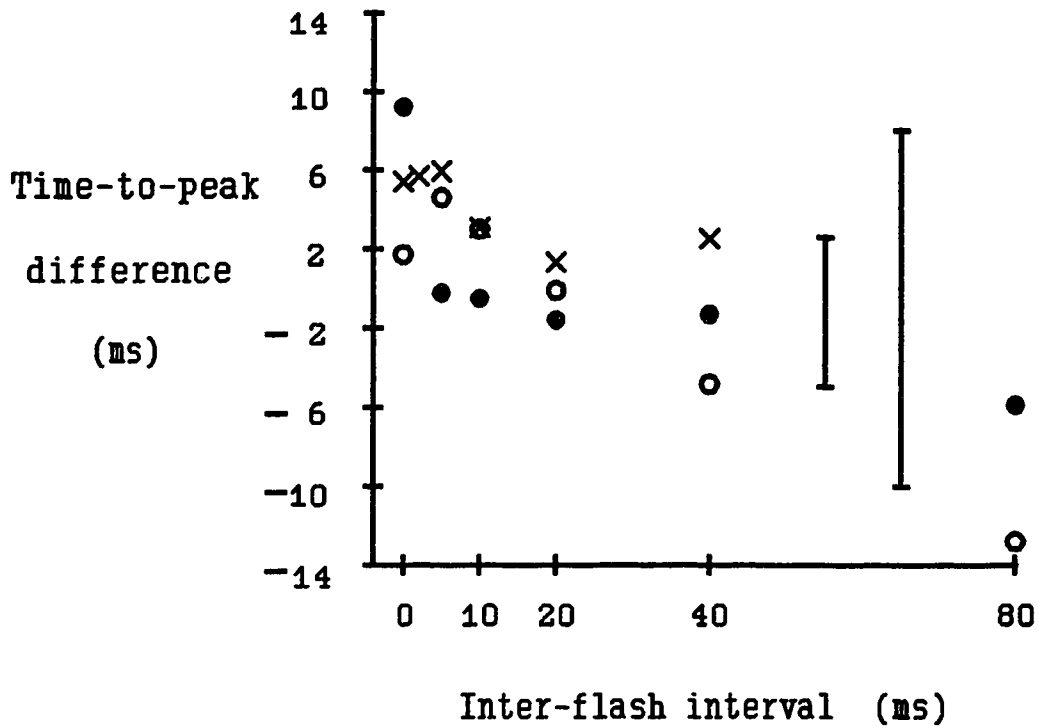


Fig. IV.3. Difference between the time-to-peak of the depression and the time-to-peak of the test flash when the latter is presented in isolation. Empty circles: overlapping slits (508 responses from 8 cells); full circles: slits separated by $120 \mu\text{m}$ (450 responses from 8 cells); crosses: *in vivo* measurements after TEA injection (239 responses from 3 cells). The standard deviation of the latter measurements is about 3 times smaller, most likely because of larger average response amplitudes and a larger number of responses averaged in each measurement.

each other. The normalized depression was equal to the average value of about 0.6 measured by French and Kuster (1985) if the single-flash response amplitude was greater than 1.7 mV. This value of 0.6 is suggestive of a certain class of feedback mechanisms, as will be discussed in Chapter V. If the response amplitudes were less than 1.5 mV, the relative depression was smaller, but even then it was not significantly affected by the distance between the stimuli.

The principal observation from this experiment is that there is a significant interaction between two stimuli even when they are separated by a distance of more than 100 μm and a time interval of less than 100 ms (the smallest interval between the adapting flash and the peak response to the test flash). If this interaction were mediated by an intracellular messenger with a realistic diffusion coefficient of 1 $\mu\text{m}^2/\text{ms}$ (see *e.g.* Hille, 1984, page 157), then after 100 ms the transmitter would have diffused within about 10 μm . At a distance of 120 μm , its concentration would be much lower than at the site of the adapting stimulus and would still be increasing for several seconds (unless it were rapidly inactivated).

Localized adaptation

One possible explanation of the results shown in Figs. IV.2 and IV.3 is that the stimuli were not localized because light scattering made the effective stimuli uniform in intensity over the length of the photoreceptor. Several pieces of evidence presented in Chapter II indicated that the stimulus was localized in the *in vivo* preparation. However, since light scattering could seriously compromise the validity

of the above experiment, we tried to obtain more evidence of stimulus localization. Our control experiment was similar to previous experiments in squid (Hagins *et al.*, 1962), *Limulus* (Fein and Charlton, 1975), frog (Jagger, 1979), toad (McNaughton *et al.*, 1980), drone bee (Bader *et al.*, 1983), and fly (Minke and Payne, 1990). After measuring average responses to test flashes at two sites separated by 120 μm , one of these sites (the central site, closer to the recording electrode, as in Fig. IV.1) was light-adapted by shining an intense steady light for 30 s through the same optical system as used for the test flashes. Five seconds after termination of the adapting stimulus, test flashes were resumed with 1 s inter-flash intervals, alternating stimulation at the two sites, so that each site was stimulated every 2 s. Responses after adaptation were averaged in groups of 5 and the amplitude of this average was obtained by fitting the log-normal model (Eq. II.1). The relative response amplitude was calculated as $\{a_0(t)/A_0\} / \{a_{120}(t)/A_{120}\}$, where A_d is the response before adaptation at distance d from the adapting light stimulus and $a_d(t)$ is the response at distance d at time t after adaptation.

Fig. IV.4 shows that responses from both sites were reduced in amplitude immediately after termination of the adapting stimulus. However, at the site of the adapting stimulus the response was reduced much more. Furthermore, while the distal site recovered very quickly (within 10-20 s in most experiments - not shown), the sensitivity of the stimulation site remained depressed for over 1 minute. The post-stimulus histogram shows that at all times after the adapting stimulus the proximal site was more adapted than the distal site.

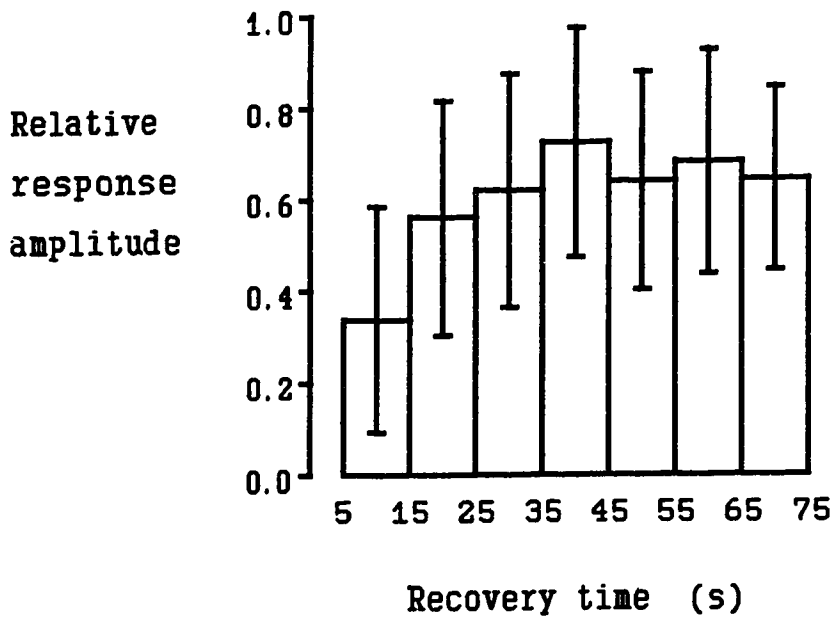
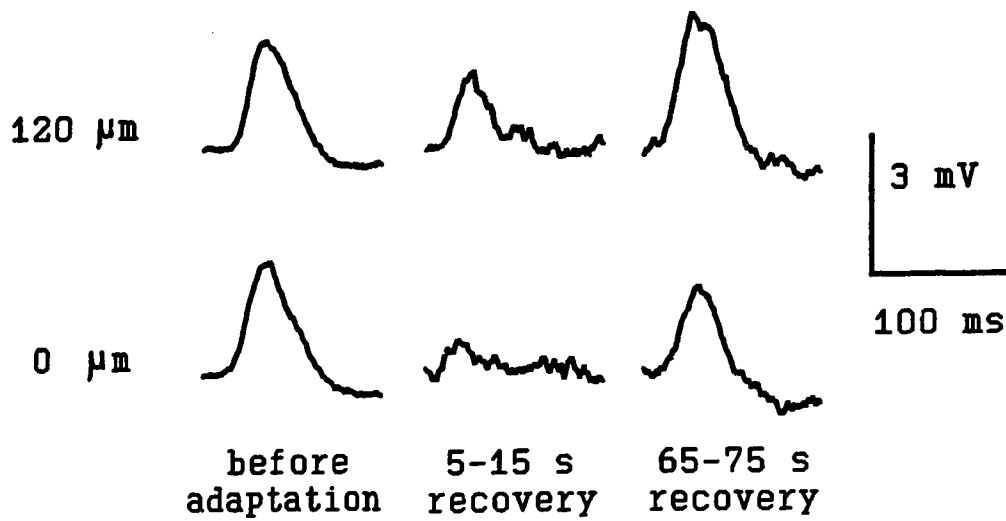


Fig. IV.4. Different levels of adaptation at the site of localized stimulation and at a distance of $120\ \mu\text{m}$. Top, a representative cell. Bottom, histogram of relative adaptation levels in 13 cells (mean \pm s.d.). For each cell, 5 responses from each site were averaged for each bin of the histogram. The relative response amplitude is defined as the ratio of response amplitudes at the two sites divided by the same ratio measured before localized adaptation.

This experiment indicates that steady prolonged illumination induces a depression of the response which is different not only in time course, but also in biophysical mechanism, from the interaction between two dim flashes described above. Notice that, in this experiment, there is sufficient time for a transmitter to diffuse from the proximal to the distal site, assuming that there are no restrictions to diffusion. Also, part of the adaptation, especially the earlier part, could be due to a membrane mechanism such as the opening of calcium-activated potassium channels. Even excluding these two possible explanations for the partial adaptation of the distal site, this experiment still indicates that most of the adapting light was absorbed locally, and therefore that light scattering is not sufficient to produce uniform light absorption within the photoreceptor in our system.

Interaction between current injection and light

It has been pointed out that a chemical transmitter cannot diffuse sufficiently fast to account for the results of Figs. IV.2 and IV.3 . By contrast, membrane depolarization spreads very fast, since the cell length constant is about 400 μm (Payne, 1982; see also Chapter II, section II.4) and its time constant about 10 ms. Depolarization could mediate the observed depression in several different ways. The light-activated conductance itself produces some self-shunting, but this is not sufficient to account for the observed depression, as was pointed out in section IV.1. However, other conductances with reversal potentials close to the resting potential could be activated either directly by the phototransduction cascade or by the light-induced

depolarization. In either case, the membrane resistance would be decreased and a superimposed depolarization induced by current injection would be reduced in size in the same way as a second flash response. Alternatively, the light-activated conductance might be inactivated by depolarization, in which case current injection would produce a reduction of the flash response.

The results of an experiment on the interaction between light and current injection are shown in Fig. IV.5 . This and all subsequent experiments were performed on the *in vivo* preparation, as described in the Methods. The top three traces are responses of a photoreceptor to a flash, to current injection, and to a combination of the two stimuli. The waveform of the injected current was the same as that of the average flash response, so that the voltage response to current injection mimicked the flash response in time course, except for the cable properties of the cell and the possible effect of voltage-activated conductances. An approximate coincidence between the peak response to the flash and the peak response to current injection was obtained by delaying the flash appropriately (16 ms in this experiment). The current intensity was adjusted to yield approximately the same depolarization as the flash response. The bottom trace is the difference obtained from the responses to individual and combined stimuli in the same way as in the double-flash experiments. An interaction between the two stimuli is evident. The relative depression, measured in the same way as in Fig. IV.2, is only 0.31 in this experiment. However, a quantitative comparison of the relative depressions obtained in the two experiments cannot be meaningful because of the problems encountered with the resistance cancellation.

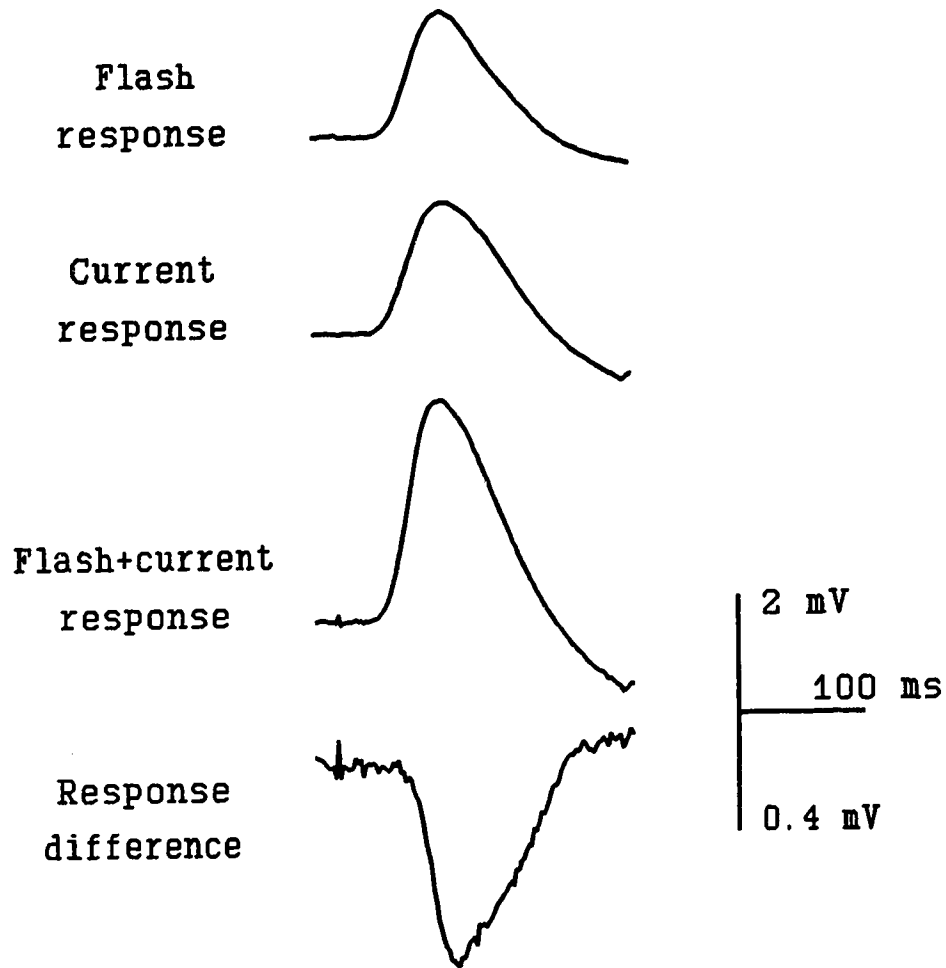
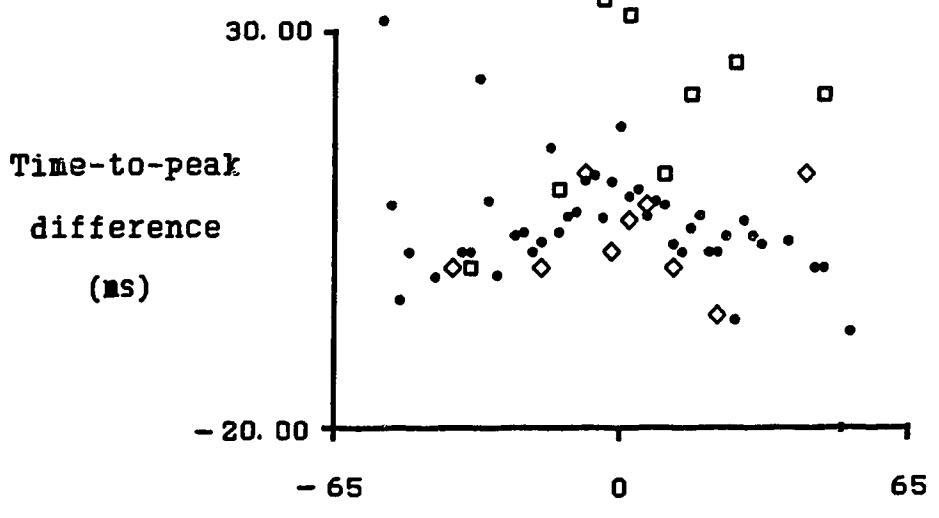
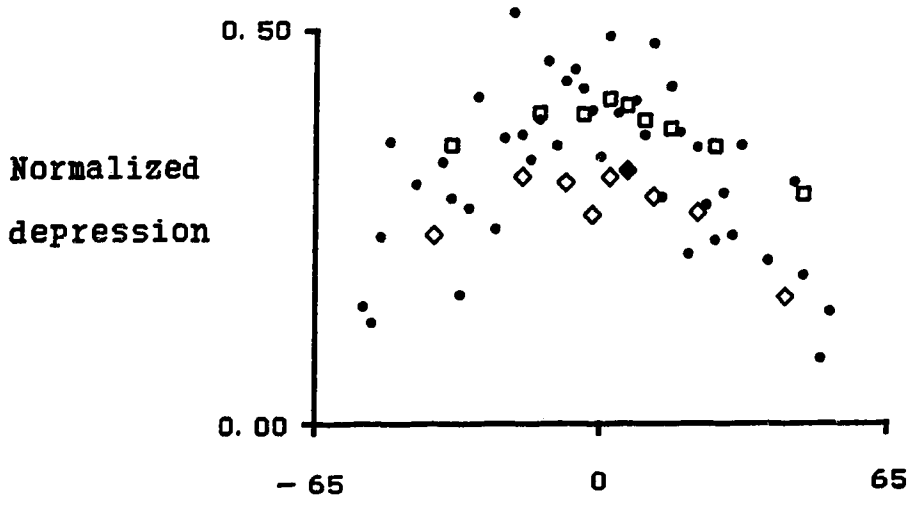


Fig. IV.5. Sub-linear summation of responses to light and to current injection. Note how the depression (bottom trace, expanded scale) follows the time course of the responses but with different polarity. All traces are averages of 100 responses from a single cell, the same cell represented by the squares in Fig. IV.6.

This experiment cannot exclude contributions from other mechanisms, but it constitutes good evidence for the involvement of membrane depolarization in the interactions that we observed.

A simple modification of this experiment can address the question of whether it is the flash that produces shunting of the response to the current, the current-induced depolarization that inactivates the flash response, or whether both stimuli produce a depression in each other's response. This modification consists of varying the timing of the two stimuli so that the peak current response does not always coincide with the peak flash response. The normalized depressions obtained with this method from three cells are shown in Fig. IV.6 . The scattering of the points along the horizontal axis is due to the fact that the values of the time to peak for the responses to the two stimuli could not be predicted exactly when the delays between the stimuli were set, so that the values of the differences between the times to peak had to be measured for each data file after the experiment (each data file included average responses to the two stimuli alone and with nine inter-stimulus intervals). The peak depressions and time-to-peak differences were the same within the error of the measurements for equal inter-stimulus intervals, irrespective of which stimulus was delivered first, suggesting that the influence of each stimulus on the response to the other was equal. A perfect symmetry in the measurements of Fig. IV.6 cannot be expected because the limited accuracy of the resistance cancellation implies that the amplitude of the response to current injection was probably substantially smaller than the amplitude of the flash response. However, the response depression was still detectable with

Fig. IV.6. Upper, normalized depressions of the voltage responses to a combination of a flash plus current injection, as a function of time interval between the peak response to a flash and the peak response to current injection. Lower, difference between the time-to-peak of the depression and the time-to-peak of the response to the test stimulus. Negative values of the abscissa indicate that the peak response to the flash occurred later and therefore the flash was defined as the test stimulus. Data from 3 cells: dots, 58.5 responses on average (each dot representing between 10 and 132 responses) with mean response amplitudes of 3.56 mV (to current) and 3.71 mV (to light); squares, 100 responses (mean response amplitudes: 2.22 mV to current and 2.15 mV to light); diamonds, 20 responses (mean response amplitudes: 3.11 mV to current and 2.47 mV to light).



Separation between peak responses
to flash and to current injection (ms)

intervals between the peak responses larger than 40 ms, whatever stimulus was delivered first. Besides, the peak depression occurred statistically at about the same time as the peak response to the test stimulus, whether the test stimulus was a flash or current injection.

Effects of intracellular TEA

Most shunting conductances are mediated by potassium permeant channels, and most of these can be blocked by TEA applied on either side of the membrane, although the required concentration of TEA varies by orders of magnitude between the two sides of the membrane and from one channel to another. Potassium conductances have recently been found in fly photoreceptors which could account for the response depressions which we observed (Weckström *et al.*, 1990). Since the fly photoreceptor conductances are very sensitive to intracellular TEA, the depression should be reduced or abolished by TEA injection if it is mediated by the same channel types. The following experiments were performed on intact animals to allow direct comparison with the results of Weckström *et al.* (1990) and of Tsukahara (1980).

As shown in Fig. IV.7, no reduction of the normalized depression was observed after iontophoresis of TEA for at least 3 s with a current of 2 nA. The relative time-to-peak of the depression was also unaffected, as shown in Fig. IV.3 (crosses). Using Hittorf's law (Purves, 1981, page 93), the total TEA efflux can be calculated as $1.8 \cdot 10^{-13}$ mol. With a cell volume of approximately 10^{-11} l (Payne, 1982), the final

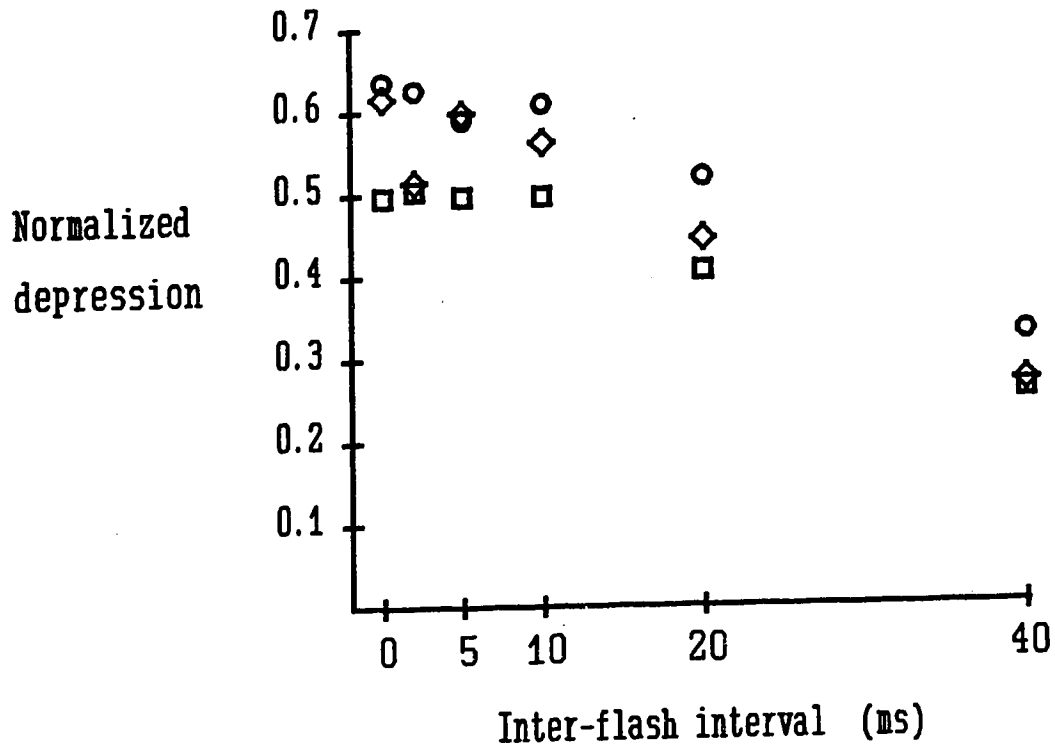


Fig. IV.7. Normalized depressions observed in 3 cells after intracellular injection of TEA for at least 3 min at 2 nA. Circles represent averages of 100 responses from cell 1 (average single-flash response: 3.9 mV). Squares represent 79 responses from cell 2 (average single-flash response: 2.4 mV). Diamonds represent 60 responses from cell 3 (average single-flash response: 4.3 mV).

intracellular TEA concentration should be about 18 mM. This figure was calculated assuming that the contribution of TEA to the current through the pipette tip is equal to its contribution to the current through the pipette shank, which can be calculated from the electric mobilities of potassium, acetate, TEA, and chloride ions (Hille, 1984, page 157) and their concentrations inside the pipette (see Methods). It is probably an underestimate, since chloride and acetate are removed from the electrode tip when current is flowing out of the tip.

TEA had some evident effects on the electrical properties of the photoreceptors. The main effect was an increase in the measured cell input resistance from 28 ± 17 M Ω (mean \pm s.d., 13 cells) to 49 ± 22 M Ω (6 cells). The above values include the contribution from the uncompensated electrode resistance, so that the actual increase was more likely to be from about 15 to 35 M Ω . The membrane time constant seemed to change from about 10 to 20 ms, but these measurements too must have been affected by the partially uncompensated electrode resistance. No clear effect of TEA on the resting membrane potential could be detected, since the potential could only be measured reliably after withdrawal of the microelectrode.

TEA had a drastic effect on the response to a square-wave light stimulus, as shown in Fig. IV.8. The response to this stimulus showed a typical decline from a transient to a steady-state value before TEA injection. This feature almost disappeared after injection. We routinely used a 500 ms light-500 ms dark stimulus for testing the effectiveness of TEA injection and the figure shows the steady-state response to this stimulus. Larger transients could usually be seen in the response to the first pulse of

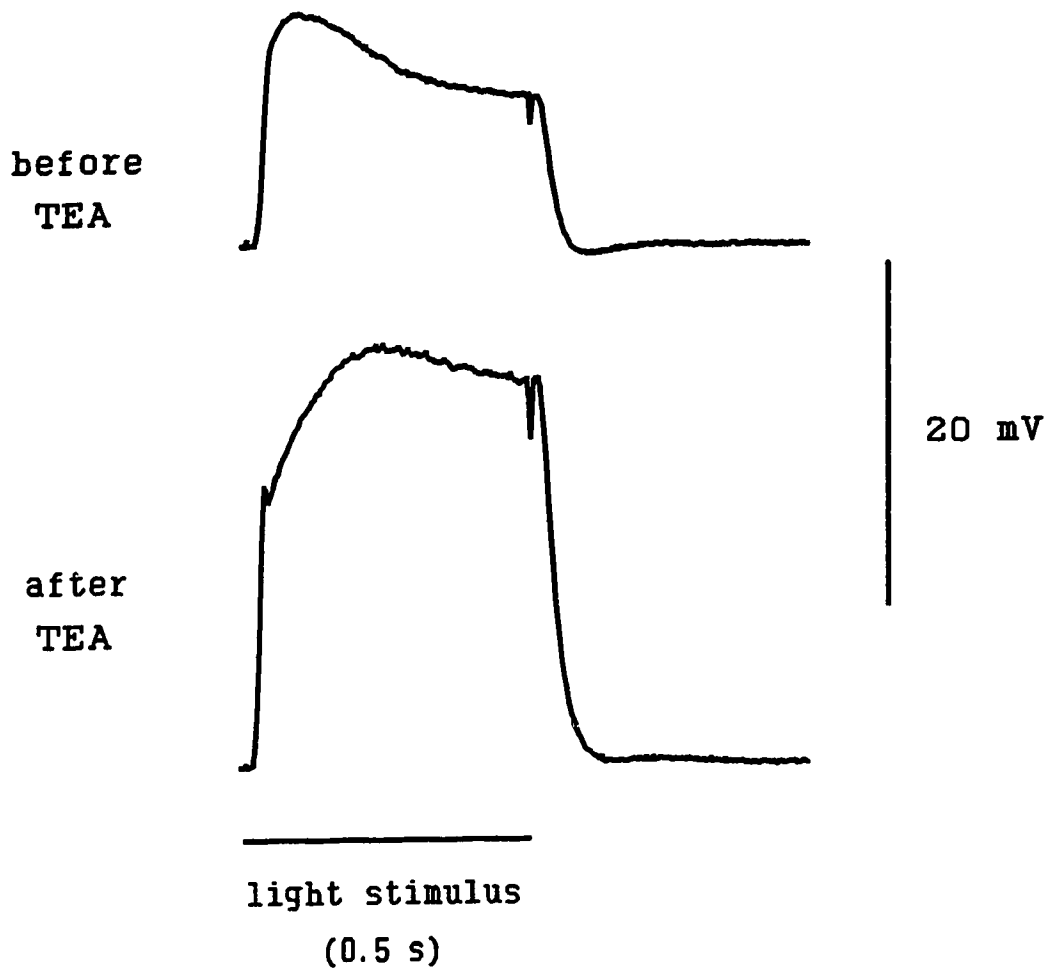


Fig. IV.8. Effect of TEA injection (3 min, 2 nA) on a photoreceptor's step response to light. Responses were from cell 1 (circles) of Fig. IV.7. Traces are averages of 10 responses. The stimulus had a 50% duty cycle.

light, both before and after TEA injection. However, the size of these transients was dependent on the duration of the previous dark-adaptation and could not be used as a measure of the effects of TEA injection.

IV.4. Discussion

The results described above suggest that deviations from linearity in light responses at very low intensities are due to a voltage-activated shunting conductance. French and Kuster (1985) previously presented indirect evidence that interactions between pairs of dim flashes occur when the two sites of photon absorption are statistically too far from each other for chemical diffusion to occur between the sites. The experiments of Figs. IV.2 and IV.3 provide direct evidence for the fast spread of interaction between two flashes. Given the long electrotonic length constant of a locust photoreceptor (about 400 μm , according to Payne, 1982, and to the calculations in Chapter II, section II.4), light-induced depolarization is almost uniform (within 5% between the two sites that were stimulated - see Chapter II) and therefore voltage-activated conductances are activated uniformly within the cell. Even if these conductances were to be activated locally, the long length constant would again ensure that they would provide an effective shunt for light responses occurring anywhere within the photoreceptor.

The earlier investigation mentioned above (French and Kuster, 1985) seemed to

rule out a shunting mechanism for the observed depression on the basis of current-injection experiments similar to those reported here. The contrast between those earlier findings and our own is puzzling. However, it should be kept in mind that a nonlinear effect can almost disappear if the electrode resistance is not cancelled accurately, because what appears to be a membrane depolarization might then be mostly a voltage drop across the electrode resistance, which is several times larger than the membrane resistance. Such a voltage drop would not activate any shunting conductance. On the other hand, it is difficult to see how an error in the bridge balance could produce an artefactual depression, since any additional voltage drop would simply add linearly to the actual trans-membrane voltage. Even the absolute value of the depression should remain unaffected by an error in the balance. Only its relative value could be affected, since the size of the current-induced depolarization might be under- or over-estimated. It should also be pointed out that it is easier to underestimate than to overestimate the electrode resistance in our preparation, since when the cancellation is excessive the recorded current response becomes biphasic, due to the delay between current and depolarization caused by the membrane time constant. Any small hyperpolarization preceding the depolarization is a sign that the electrode resistance has been over-cancelled.

Two other factors could, in principle, flaw a comparison between a double-flash response and a response to a flash plus current injection: (1) in the flash plus current experiments the current always has the same amplitude, while in the double-flash experiments both stimuli are variable in size, due to the random character of photon

absorption and to the variability of single-photon responses; (2) in the double-flash experiments, both stimuli activate the light-activated conductance, while in the flash plus current experiments the current only acts on voltage-sensitive conductances. However, as will be discussed in Chapter V, both of these factors are likely to give only very small contributions to the normalized depression if the single flash results in at least 6 photons being transduced on average and depolarize the cell by not much more than 3 mV. The randomness of the flash responses should actually decrease the normalized depression observed with a double flash relatively to that observed with flash plus current stimulation, in which one of the two stimuli has a fixed intensity.

In Chapter III we suggested that the nonlinear depression observed with a pseudo-random stimulus has the same mechanism as the depression observed with pairs of flashes. Models for this mechanism, in which the depression is due to enzyme inhibition within the phototransduction cascade, were analyzed. On the basis of the findings reported above, we believe that those models should be rejected, while the first hypothesis remains valid. Indeed, if the depression observed with white noise is due to a shunting conductance, that would explain why the changes in amplitude and time course of the depression follow so closely the analogous changes in the voltage responses of the photoreceptor at different levels of adaptation: the smaller and faster voltage response to each photon results in a smaller and faster shunting conductance activation (see also Chapter V, Eqs. V.12-V.15).

The shunting conductance responsible for the nonlinear response depression would

seem to differ from the conductances observed by Weckström *et al.* (1990) in having a lower sensitivity to intracellular TEA. However, as we shall discuss more fully in Chapter V, the value of about 0.6 for the normalized depression might not be very sensitive to a small reduction of the shunting conductance, especially when the resting membrane conductance is decreased to a small value. Of course, a total block would still be detected.

The mechanism responsible for the fast depression seems to be distinct from the slower calcium-activated potassium conductance which is thought to cause the decline in the step response to light from transient to steady-state (Muijser, 1979; Tsukahara, 1980). The same cells still showed a normal depression when the decline in the step response had been blocked by TEA. It was pointed out in Chapter III that the fast depression process must be distinguished from the slower adaptation, since the two processes alter the gain of phototransduction in very different time scales. We can now add that the slower changes of gain must be further distinguished into at least two components, one of which takes place in a time scale of 100 ms to 1 s and the other in a time scale of several seconds. The first can be blocked by TEA and, following Tsukahara (1980), we believe it is due to a calcium-activated potassium conductance. The second is at least partially localized in nature and can be demonstrated by the local adaptation experiment.

Bader *et al.* (1982) observed localized and unlocalized adaptation in drone bee photoreceptors. Since they only observed localized adaptation with a wavelength which is known to shift the balance between rhodopsin and metarhodopsin in drone

photoreceptors, they suggested that the localized process is due to local depletion of rhodopsin. A similar experiment cannot be repeated in our preparation at present, since the absorption curves of rhodopsin and metarhodopsin have not been determined in locust photoreceptors. However, it would seem likely that under different stimulus conditions a slow biochemical process of gain control could be shown to act together with the moderately fast TEA-inactivated shunting mechanism and the very fast shunting mechanism which is the main focus of this paper. Such slow processes are known to occur in *Limulus* photoreceptors (Payne *et al.*, 1990) and vertebrate photoreceptors (Pugh and Altman, 1988) and are caused by rhodopsin bleaching to only a small extent.

IV.5. References

- Autrum H (1981) Light and dark adaptation in invertebrates. In: Handbook of Sensory Physiology, VII/6C (H. Autrum, ed.) 1-91. Springer-Verlag, Berlin.
- Bader CR, Baumann F, Bertrand D, Carreras J, Fuortes G (1982) Diffuse and local effects of light adaptation in photoreceptors of the honey bee drone. *Vision Res* 22:311-317.
- Claßen-Linke I, Stieve H (1986) The sensitivity of the ventral nerve photoreceptor of *Limulus* recovers after light adaptation in two phases of dark adaptation. *Z Naturforsch* 41c:657-667.
- Fein A, Charlton JS (1975) Local adaptation in the ventral photoreceptors of *Limulus*. *J Gen Physiol* 66:823-836.
- Fein A, Szuts EZ (1982) Photoreceptors: their role in vision. Cambridge University Press.
- French AS, Kuster JE (1985) Nonlinearities in locust photoreceptors during transduction of small numbers of photons. *J Comp Physiol A* 156:645-652.
- Hagins WA, Zonana HV, Adams RG (1962) Local membrane currents in the outer segments of squid photoreceptors. *Nature* 194:844-847.
- Hille B (1984) Ionic channels of excitable membranes. Sinauer, Sunderland, MA.
- Jagger WS (1979) Local stimulation and local adaptation of single isolated frog rod outer segments. *Vision Res* 19:381-384.
- Laughlin SB (1981) Neural principles in the visual system. In: Handbook of Sensory

- Physiology, VII/6B (H. Autrum, ed.) 133-280. Springer-Verlag, Berlin.
- Laughlin SB, Lillywhite PG (1982) Intrinsic noise in locust photoreceptors. *J Physiol* 332:25-45.
- Minke B, Payne R (1990) Spatial restriction of desensitization in normal and mutant fly photoreceptors. *Biophys J* 57:369a.
- Muijser H (1979) The receptor potential of reticular cells of the blowfly *Calliphora*: The role of sodium, potassium and calcium ions. *J Comp Physiol A* 132:87-95.
- McNaughton PA, Yau KW, Lamb TD (1980) Spread of activation and desensitization in rod outer segments. *Nature* 283:85-87.
- Naka KI, Rushton WAH (1966) S-potentials from colour units in the retina of fish (Cyprinidae). *J Physiol* 185:536-555.
- Normann RA, Werblin FS (1974) Control of retinal sensitivity. I. Light and dark-adaptation of vertebrate rods and cones. *J Gen Physiol* 63:37-61.
- Payne R (1980) Voltage noise accompanying chemically induced depolarization of insect photoreceptors. *Biophys Struct Mech* 6:235-252.
- Payne R (1982) Chemical modifications to transduction in an insect eye. Ph.D. thesis, Australian National University.
- Payne R, Flores TM, Fein A (1990) Feedback inhibition by calcium limits the release of calcium by inositol trisphosphate in *Limulus* ventral photoreceptors. *Neuron* 4:547-555.
- Pece AEC, French AS, Korenberg MJ, Kuster JE (1990) Nonlinear mechanisms for gain adaptation in locust photoreceptors. *Biophys J* 57:733-743.

- Pugh E, Altman J (1988) A role for calcium in adaptation. *Nature* 334:16-17.
- Purves D (1981) Microelectrode methods for intracellular recording and iontophoresis. Academic Press, London.
- Tsukahara Y (1980) Effect of intracellular injection of EGTA and tetraethylammonium chloride on the receptor potential of locust photoreceptors. *Photochem and Photobiol* 32:509-514.
- Weckström M, Hardie RC, Laughlin SB (1990) The role of voltage-activated potassium channels in blowfly photoreceptors. Submitted for publication.

V. GENERAL DISCUSSION: GAIN CONTROL AT THE MEMBRANE LEVEL

This chapter is divided into three sections. Section V.1 will present a quantitative interpretation of the results presented in Chapter IV. Section V.2 will briefly review relevant research on voltage-activated conductances in photoreceptors. Section V.3 will summarize the conclusions of this dissertation and suggest future lines of research.

V.1. Modelling of the gain control process

The role of self-shunting

By making some simplifying assumptions, it is possible to demonstrate that the shunting conductance should have a relatively small role when the single-flash response has a peak amplitude $v_1 = 3$ mV. This demonstration is fairly general, but depends on the following assumptions: (1) the dynamics of the phototransduction process, membrane time constant, and activation or inactivation of conductances can be neglected; (2) all the voltage-activated conductances have a reversal potential equal to the resting potential; (3) the reversal potential of the light-activated conductance is 50 mV above resting potential; (4) the light-activated conductance is

linearly related to the number of photons being transduced. Since the time-to-peak of the response to a single flash is almost equal to the time-to-peak of the depression, assumption (1) should be a good approximation at the time-to-peak of the response. Assumption (3) is actually lower than the estimate of the reversal potential for the light-activated conductance given by Payne (1982); a higher estimate would lead to less self-shunting, but the exact value might change from one cell to the other depending on the damage to the cell membrane by the microelectrode, which might affect the resting potential. Assumption (4) is supported by the two-slit experiment described in Chapter IV, which indicates that any nonlinear interaction between two stimuli is mediated by membrane processes.

If the total light-insensitive membrane conductance $G(v)$ is a non-decreasing function of instantaneous membrane potential v , then the peak flash response will be:

$$v = \frac{axE_a}{G(v) + ax} \quad (\text{V.1})$$

where v is the depolarization above resting potential in mV, x is the number of photons being transduced or effective photons (ep), a is a gain factor relating photon absorption to the change in light-activated conductance in nS/ ep , E_a is the reversal potential of the light-activated conductance, which we assume is equal to 50 mV, and $G(v)$ is the total light-insensitive membrane conductance in nS, which is a function of depolarization. $G(v)$ must be non-decreasing for increasing v , otherwise the light response would increase superlinearly with increasing light intensity. On the right-

hand side, the numerator is the light-activated current and the denominator is the total membrane conductance. Eq. V.1 is equivalent to the Naka-Rushton curve (Eq. I.3). From Eq. V.1:

$$G(v) = ax(E_a - v) / v \quad (V.2)$$

So that if $v = 3$ mV, $G(v) = 15.67 ax$. Let us analyze three different sets of constraints:

(i) There are no voltage-activated conductances, i.e. $G(v) = G_r$ (a constant for all v). In this case, for $v_1 = 3$ mV, $G_r = 15.67 ax$. Doubling the flash intensity will result in a response:

$$v_2 = \frac{2axE_a}{(15.67+2)ax} = 5.66\text{mV} \quad (V.3)$$

The normalized depression would be equal to 0.11.

(ii) The normalized depression has the experimentally determined value of 0.6 . The response to a flash of intensity $2x$ will be $v_2 = 4.2$ mV and from Eq. V.2, $G(v_2) = 10.9a(2x) = 1.39 G(v_1)$. A 39% increase of the light-insensitive membrane conductance, caused by a depolarization of 1.2 mV (from $v_1 = 3$ mV to $v_2 = 4.2$ mV), would be necessary to cause the depression that was measured.

(iii) Current I is injected through the electrode and causes a depolarization $v_1 = 3$ mV. The current required would be $I = v_1 \cdot G(v_1)$. If the current is injected during the response to a flash producing an identical depolarization, then Eq. V.1 must be

modified:

$$v_* = \frac{axE_a + I}{G(v_*) + ax} \quad (V.4)$$

By approximating $G(v_*) \approx G(v_2)$ and setting the latter equal to 1.39 $G(v_1)$, as required for a normalized depression of 0.6, then $v_* = 4.26$ mV. Since this value is slightly larger than v_2 , it follows that $G(v_*) \geq G(v_2)$ and therefore $4.2 \leq v_* \leq 4.26$. In any case, the normalized depression would have decreased only from 0.6 to 0.58. This is significantly larger than the depression observed in the flash plus current experiments (section IV.3).

A quantitative model of the observed depression

The value $\Delta v/v \approx 0.6$ for the peak voltage depression Δv normalized by the voltage response v to the single flash, given in Chapter IV, can be expected for a general class of feedback gain control processes in a certain range of response amplitudes. To justify this statement, we shall derive an expression for the peak voltage response v for a cell in which depolarization linearly increases a shunting conductance with reversal potential E_b relative to the resting potential (E_b being close to zero, and in practice most likely negative). We shall maintain assumptions (1) and (4) above. Substituting $G(v)$ in Eq. V.1, we obtain:

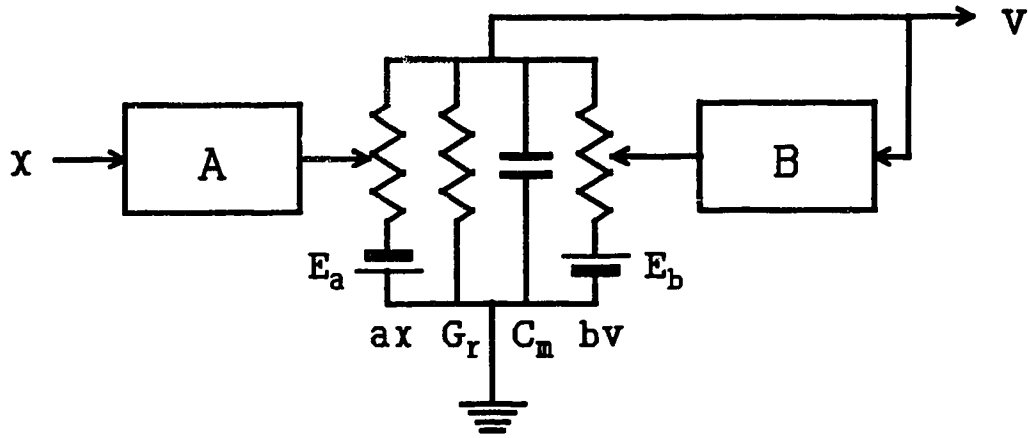


Fig. V.1. A schematic model of the photoreceptor light-to-voltage transduction mechanism. C_m is the membrane capacitance. For the other symbols, see text. Box **A** includes the biochemical transduction cascade and can be approximated as a chain of first-order reactions. Box **B** includes the kinetics of the voltage-activated shunting conductance, which we also assume to be linear. The nonlinear properties of the model are due to the interactions at the membrane level.

$$v = \frac{axE_a + bvE_b}{G_r + ax + bv} \quad (\text{V.5})$$

where G_r is the resting membrane conductance and b is a factor with the dimensions of nS/mV relating the voltage-activated conductance to the depolarization. Fig. V.1 is a schematic diagram representing the model cell which we shall analyze. A similar equation can be written for other feedback systems, including a stage of a biochemical cascade with feedback inhibition (Grzywacz and Hillman, 1988). Therefore the following demonstration does not support a specific hypothesis about the nature of the depression mechanism. However, for concreteness, we shall discuss only the case of a membrane shunting mechanism, on the basis of the evidence presented in Chapter IV.

Eq. V.5 can be rearranged:

$$bv^2 + (G_0 + ax)v - Hx = 0 \quad (\text{V.6})$$

where we substituted $H = a \cdot E_a$ and $G_0 = G_r - b \cdot E_b$. Solving the quadratic equation for v :

$$v = \frac{-(G_0 + ax) + \sqrt{(G_0 + ax)^2 + 4bHx}}{2b} \quad (\text{V.7})$$

Eq. V.7 can be simplified if there is a range of stimulus intensities for which the

shunting conductance is the largest component of total membrane conductance, so that $4bHx \gg (G_0+ax)^2$. In this range, we have:

$$v = \sqrt{Hx/b} \quad (\text{V.8})$$

so that the depolarization depends on light intensity raised to the power of 0.5, as experimentally measured by Matic and Laughlin (1981) and Laughlin and Lillywhite (1982) for small flash intensities. A stimulus of twice the intensity will generate a voltage response:

$$v_2 = \sqrt{H2x/b} \quad (\text{V.9})$$

and the measured depression will be $\Delta v = (\sqrt{2}-1)v_1$. Normalizing the response depression by the amplitude of the single flash response we obtain $\Delta v/v_1 = \sqrt{2}-1$, which is very close to the values given in Chapter IV and by French and Kuster (1985).

The assumptions that the shunting conductance is linearly proportional to the instantaneous depolarization when the flash response reaches its peak and that there is a range of stimulus intensities in which $4bAx \gg (G_0+ax)^2$ could be put to direct experimental test by means of voltage clamp methods.

Possible sources of error

The above analysis neglects the intrinsic variability of the responses and the asymmetry between the responses in the two-slit experiments and light plus current experiments. The responses to both the single flash and the double flash are not deterministic, but have a skewed distribution with a long tail of large responses and a minimum response amplitude of zero (see Chapter II). The large responses in the long tail are going to be "clipped" by the shunting conductance more than the small responses for both the single flash and the double flash. Let us approximate this variability as an equivalent input noise with a probability density function $p(x, \bar{x})$ for an input amplitude x when \bar{x} is the average flash intensity. If each individual response follows Eq. V.8, then the average flash response can be found by a weighted average of the response amplitudes:

$$\bar{v} = \sqrt{H/b} \int_0^{\infty} \sqrt{x} p(x, \bar{x}) dx \quad (\text{V.10})$$

Eq. V.10 can easily be integrated numerically by assuming that the probability density function $p(x, \bar{x})$ is a discrete Poisson distribution. This assumption would be strictly correct if all single-photon responses had the same amplitude and only the number of photons being absorbed were variable, which is not the case. However, the additional fluctuations in the responses to the individual photons will not extend the tail of the distribution, which already goes to infinity, but only smear the probability density function so that $p(x, \bar{x})$ is non-zero for non-integer values of x . Integration

shows that $\Delta\nu/\nu \approx 0.36$ for $\bar{x} = 1$. As \bar{x} is increased, $\Delta\nu/\nu$ becomes closer to $2-\sqrt{2}$. For $\bar{x} = 6$, $\Delta\nu/\nu$ is already 97% of $2-\sqrt{2}$.

With regard to the differences between the two single response amplitudes, assume the two intensities for the single flashes are x_0 and x_1 , with $x_0 > x_1$. Eq. V.8 must now be changed to a more complex formula:

$$\Delta\nu = \sqrt{H/b} \{ \sqrt{x_0+x_1} - (\sqrt{x_0} + \sqrt{x_1}) \} \quad (\text{V.11})$$

Normalizing the above equation by the geometric average of ν_0 and ν_1 would result in a value less than 3% lower than $2-\sqrt{2}$ as long as $x_0 \leq 2.25 x_1$ or equivalently $\nu_0 \leq 1.5 \nu_1$. This was always the case in the experiments presented in Chapter IV, except in the flash plus current experiments, where the exact current response could not be measured. In the non-deterministic case (Eq. V.10), $\Delta\nu/\nu$ would be at least 94% of $2-\sqrt{2}$ if $x \geq 6$ and $\nu_0 \leq 1.5 \nu_1$.

Laughlin and Lillywhite (1982) examined another effect of the randomness of responses to few photons: due to the variability of times to peak of bumps, individual responses containing two bumps have statistically smaller peak amplitudes than single-bump responses, because the peaks of the individual bumps do not coincide. However, this effect is negligible when the peak response amplitudes are measured from the averages of several traces, since in this case each average contains bumps with different times to peak. This was the procedure adopted in chapters III and IV.

Responses to white noise

At high light intensities the self-shunting of the light-activated conductance can contribute significantly to the relative depression which would then become greater than 0.58. In the limit, as the response saturates, $v(2x) = v(x)$ and $\Delta v/v = 1$.

By contrast, in conditions where the background membrane conductance G_0 is much greater than the light-activated or voltage-activated conductances, the relative depression becomes vanishingly small. When a background light is present, the effective background conductance includes not only the conductance in the dark, but also contributions from the light-activated, voltage-activated, and calcium-activated conductances. Matic and Laughlin (1981) found that the parameter n in Eq. I.4 gradually changes from about 0.5 to 1 with increasing background light intensity, which is in agreement with the prediction of the model in Fig. V.1. Under white-noise stimulation, a background light is present and self-shunting is negligible because of the small modulation depth. The dynamics of the elements A and B and of the membrane electrical analog in Fig. V.1 cannot be neglected under these conditions. However, for illustrative purposes, let us assume that Eq. V.7 still applies, in which case it can be approximated as:

$$v = \frac{-G_0 + \sqrt{G_0^2 + 4bHx}}{2b} \quad (\text{V.12})$$

since the self-shunting conductance ax is negligible compared to G_0 . Expanding Eq. V.12 into a MacLaurin series, we obtain:

$$v = (H/G_0)x - 2(H^2b/G_0^3)x^2 + \dots \quad (\text{V.13})$$

The first term on the right-hand side is the linear term in the relationship between light and depolarization and becomes predominant in the white-noise experiments. The second term gives a much smaller contribution to the response but can be detected by white-noise analysis (see chapter III and Eckert and Bishop, 1975; Gemperlein and McCann, 1975). Higher-order terms can be neglected. The depression of the response is dominated by the second-order negative response:

$$\Delta v = - (2H^2b/G_0^3)x^2 \quad (\text{V.14})$$

Since the response is dominated by its linear component, the depression is also approximately proportional to the square of the single-flash response:

$$\Delta v/v^2 = \frac{-(2H^2b/G_0^3)x^2}{(H^2/G_0^2)x^2} = -2b/G_0 \quad (\text{V.15})$$

As can be seen, at low modulation depths Δv is proportional to v_1^2 instead of v_1 and proportionality factor is not a mathematical constant as in Eq. V.8, but is related to the parameters of the model. These two qualitative conclusions would still apply if the dynamics of the model had not been neglected, since higher-order nonlinearities are negligible in the white-noise experiments, and therefore the depression can be approximated as a second-order nonlinearity. In Chapter III the value of $f(0)$, which

is approximately equivalent to $\Delta v/v$, was shown to be proportional to $h(t_p)$ over a 30-fold range of background light intensities, so that $\Delta v/v_1^2$ was approximately constant.

In conclusion, the model presented in Fig. V.1 is compatible with all the experimental findings, except the fact that the normalized depression is smaller in the flash plus current experiments than it is in the double-flash experiments. This discrepancy might be due to an additional contribution to the depression at the level of the transduction cascade. However, this hypothesis would be incompatible with the finding that there is no delay associated with the spread of the depression effect when the two stimuli are separated by a distance of 120 μm . Some additional experiments which would falsify the model of Fig. V.1 have been mentioned, *e.g.* voltage-clamp experiments could test whether the light-activated and voltage-activated conductances are linearly dependent on light and voltage respectively.

V.2. Voltage-activated conductances in photoreceptors

Apart from the light-activated conductance, all photoreceptors have at least one other conductance, *i.e.* a voltage-activated calcium conductance at the synaptic terminal which allows the visual signal to be transmitted to the nervous system. This section will review voltage-activated conductances responsible for the shaping of the response to light, rather than for the synaptic transmission of this response. This section will also concentrate on arthropod photoreceptors, although vertebrate

photoreceptors will be briefly discussed.

Flies

Muijser (1979) reported that the decline from peak to plateau responses in fly photoreceptors was accompanied by a change of reversal potential with respect to the plateau and an increase of membrane conductance. Furthermore, intracellular injection of EGTA could almost completely abolish this decline. He inferred the presence of a calcium-activated conductance, presumably a potassium conductance, which is activated with a delay of tens of milliseconds after the rising phase of the light response.

More recently, two voltage-activated potassium conductances with different kinetics have been extensively investigated in fly photoreceptors of the R1-6 class, which includes 6 of the 8 photoreceptors of each ommatidium (Weckström *et al.*, 1990). These conductances have been characterized by single-electrode voltage clamp. Patch-clamp recordings have revealed two classes of potassium channels, both having a single-channel conductance of 20 pS but differing in activation kinetics. Both channels seemed to activate and inactivate with a single exponential time constant, rather than with a sigmoidal time course. The time constant of the faster channel was found to be about 5 ms at resting potential, while that of the slower channel was substantially larger. Both channels were insensitive to calcium. They could be different states of the same type of channel.

Locusts

Tsukahara (1980) reported that the step response of locust (*Valanga irregularis*) photoreceptors to light changed shape after both EGTA and TEA injection. The change was similar to that illustrated in Fig. IV.8: The response became monophasic, losing the decline from peak to plateau. Tsukahara inferred that the decline to plateau is caused by a calcium-activated potassium conductance.

Payne (1980,1982) found two further pieces of evidence for shunting conductances in locust photoreceptors: a rectifying current-voltage relationship and a hyperpolarization which followed strong light responses and had a reversal potential below resting potential. Payne suggested that the hyperpolarization is caused by the same calcium-activated conductance which underlies the decline from transient to steady-state response (Tsukahara, 1980). The rectification was attributed to a different shunter conductance.

The current-voltage curve shows no evidence of rectification below -50 mV. From this curve, Payne calculated the effect that this conductance would have on responses to flashes of light. The curve predicts a somewhat more linear relationship between stimulus and response than that obtained experimentally by Lilywhite and Laughlin (1979), and an almost linear relationship for responses below 5-10 mV, which is contrary to the findings reported in Chapters III and IV as well as the previous findings by French and Kuster (1985). Since Payne's current-voltage curve was obtained with current steps lasting more than 20 ms, it is possible that the level of activation of the shunting conductance was different from that generated by a smooth

but transient depolarization, as in a flash response.

Voltage-activated potassium conductances in locust photoreceptors are now being investigated by Weckström (personal communication). Preliminary results indicate the presence of conductances similar to those found in fly photoreceptors, but with different kinetics.

Bees

Strong stimuli, either luminous or electrical, can trigger action potentials in drone bee and worker bee photoreceptors (Coles and Schneider-Picard, 1989). These action potentials are sodium-dependent and can be blocked by TTX (Baumann, 1974). An hyperpolarization after the action potential suggests that a potassium conductance is also present (Coles and Schneider-Picard, 1989). In natural conditions, it is unlikely that a spike would be triggered. The function of the TTX-sensitive current seems to be to enhance the amplitude of small fluctuations of membrane potential around the level of about -40 mV. This is the level reached with a background light intensity comparable to that of skylight. Therefore, the membrane properties would seem to be optimized to enhance small voltage fluctuations around the natural level of depolarization (Coles and Schneider-Picard, 1989).

Limulus

Ventral photoreceptors of *Limulus* have at least three voltage-sensitive conductances, all activated by depolarization (Fain and Lisman, 1981). An early

inward current is carried by sodium and potassium, while two outward potassium currents have properties similar to those of A-currents and delayed rectifier currents (Hille, 1984). The inward current can actually generate an action potential during the rising phase of a strong depolarization. All these currents require a rather large depolarization to be activated. The delayed rectifier current is slowly inactivated by light; during steady illumination, this slow process seems to counterbalance the effect of light adaptation, which reduces the light-activated conductance. The net effect is that the same depolarization is maintained with a lower metabolic expenditure, due to lower levels of membrane currents.

Barnacle

The response of barnacle photoreceptors to stepwise illumination shows an initial transient followed by a dip, which in turn is followed by a steady-state depolarization. This response is similar to that observed in insects. Hanani and Shaw (1977) presented various lines of evidence indicating that the dip is due to a calcium-activated potassium conductance. The dip appears with a latency of tens of milliseconds after the rising phase of the response. Subsequent research with voltage-clamp methods provided further evidence for a calcium-activated potassium conductance (Bolsover, 1981). A voltage-activated calcium conductance has also been investigated (Edgington and Stuart, 1979) and there is evidence for a voltage-activated potassium conductance (Ross and Stuart, 1978; Bolsover, 1981).

Lower vertebrates

Several conductances have been identified in salamander rods and cones by voltage clamping and pharmacological blocking (review: Attwell, 1986). The resulting currents can be divided into two classes: outward currents activated by depolarization (either directly or indirectly by calcium influx) and inward currents activated by hyperpolarization. Both types of currents counteract, with a delay, the change of membrane potential by which they were generated and therefore their effect can be described as high-pass filtering. However, since the two groups of currents are activated in different voltage ranges, the total membrane conductance changes less with voltage than it would if only one type of current were present. Therefore, the nonlinear shunting effect of the conductances would seem to be less important than the linear high-pass filtering effect.

Actually, the dynamics of the system is considerably more complex. To mention just two complications, the high-pass filtering properties of the membrane are more pronounced at lower membrane potentials, and electrical coupling between photoreceptors causes interactions between the spatial and temporal filtering properties of the photoreceptor network.

General principles

Although only a relatively small number of species have been investigated, at least one characteristic has been found in all photoreceptor membranes which have been investigated: negative feedback caused by the activation of currents which counteract

the light response. This negative feedback operates as a high-pass filter and gain control mechanism and therefore removes some of the redundancy of the visual signal (Barlow, 1961).

However, it is also clear that there is much diversity between species. *Limulus* and the drone bee have a positive feedback mechanism, which enhances low-intensity signals. This positive feedback is not necessarily in conflict with the negative feedback: since the sodium conductance is activated transiently, it enhances the response to high-frequency signals and therefore it contributes to the high-pass properties of the photoreceptor. Insects differ from both *Limulus* and vertebrates in having a clearly sublinear response to even the lowest intensity stimuli. If this mechanism has evolved with the purpose of expanding the operating range of the photoreceptor, it would seem that vertebrates might not need it: The electrical coupling of photoreceptors means that any single photoreceptor can hardly be saturated by any localized natural stimulus, since the photocurrent is spread over the rod network. *Limulus* might not need an extended operating range because of the relatively simple task that its visual system performs, namely, detecting potential mates (Barlow, 1990). For this species, maximum sensitivity might be more relevant than fine discrimination, so that a mechanism for depressing the response would be a disadvantage, at least for weak, transient stimuli.

V.3. Conclusions

Variability of responses

Chapter II presented evidence in support of the hypothesis that the variability of single photon responses is intrinsic to the transduction process. In terms of the scheme in Fig. V.1, this implies that the variability is generated within element A. Some variability could be generated by fluctuations in the number of channels opened at the output of E. However, with a single-channel conductance of 20 pS (Weckström *et al.*, 1990), about 1200 channels should be open to increase G_r by 40%, if $G_r = 1/(17 \text{ M}\Omega)$. Since this represents a small fraction of all available channels, the actual number of channels being open should follow a Poisson distribution. As a consequence, the variance should be equal to the mean and the standard deviation of the number of open channels should be $\sqrt{1200} \approx 35$. The number of open light-activated channels should be comparable to the number of open voltage-activated channels, but the variability of the former is larger, presumably because a much smaller number of molecules are active further upstream in the transduction cascade.

Validity of the separable models

Formally, the model in Fig. V.1 differs from those in Fig. III.5 in the location of the gain control point not before the time-limiting steps of phototransduction, but after all of them except for the membrane time constant. Furthermore, the mechanism that reduces the gain should also decrease this time constant by

decreasing the total membrane resistance. However, two conclusions from Chapter II should still be valid: (1) the nonlinearities observed in double-flash experiments and white-noise experiments are caused by the same mechanism; (2) other factors affect the gain of phototransduction in a slower time scale. The presence of one such factor, also a membrane conductance and only one or two orders of magnitude faster than the fast gain control, is demonstrated (by its block) in Fig. IV.7.

Location of the gain control point at the first stages of the cascade would be further useful because any stage located before the gain control point could be saturated by a high input level. However, abrupt changes of light intensity in a natural setting are generally limited to a small range, while large changes are associated with the daily rhythm and are slow. Presumably, abrupt changes in the locust visual environment are not sufficient to saturate the transduction mechanism.

On the other hand, some slower adaptation mechanisms are probably located further upstream and therefore prevent saturation of any biochemical stages, while also reducing the metabolic cost of transduction by reducing the number of molecules involved.

Although adaptation takes place with a slower time course and by different mechanisms, it appears to be formally similar to fast gain control as a feedback process. Fuortes and Hodgkin (1964) already found some evidence in favour of a feedback mechanism in *Limulus* photoreceptors. More recently, Grzywacz and Hillman (1988) have shown that only a negative feedback mechanism can account for the observed sublinear relationship between steady-state light intensity and

steady-state depolarization of *Limulus* ventral photoreceptors. Eq. III.8 of Grzywacz and Hillman is very similar to Eq. V.8 in this chapter. Payne *et al.* (1990) provided evidence for a feedback mechanism based on inhibition by extracellular calcium of additional calcium release. The current biochemical model of phototransduction in vertebrates also includes a feedback pathway for adaptation (for a short review, see Pugh and Altman, 1988).

The biophysical basis of gain control

The research described in Chapter IV aimed at understanding the biophysical mechanism of the gain control process. The project was started under the assumption that gain control takes place at the level of the intracellular transduction cascade. This hypothesis was suggested by the finding of French and Kuster (1985) that current does not have the same effect as a flash in producing a response depression, as well as by the quantitative estimate by Payne (1982) of the likely effect that the rectification properties which he measured. Subsequently, our working hypothesis was changed by the observation that distance between stimulation sites does not affect the depression of the responses, the measurement of a depression in the flash plus current experiments, and the communication by Weckström *et al.* (1990) of their findings of potassium channels activated by very small depolarizations from the resting potential. These results led to the formulation of the model in Fig. V.1.

The evidence is not yet conclusive that the model is a quantitatively accurate description of the gain control mechanism. In section V.1 we have begun an analysis

of the model. This analysis led to some testable predictions, *e.g.* that the voltage-activated conductance should increase approximately linearly with depolarization. Testing these predictions will entail overcoming the limitations of the current-injection methods described in section IV.2. In any case, the evidence indicates that a shunting conductance causes most if not all of the depression which is observed with small flash stimuli. The existence of a mechanism which generates this depression and is distinct from the transduction cascade suggests that the depression is not an epiphenomenon but plays an important role in encoding the voltage response of the photoreceptor.

The model of Fig. V.1 is simple enough to allow prediction of the photoreceptor output for arbitrary input signals, provided that the transfer functions of the elements A and B are determined. Such predictions are likely to be more accurate than those obtained with models which have no obvious biophysical interpretation, like the modified Naka-Rushton curve (Eq. I.4) or the log-normal model (Eq. II.1). Notice that the applications of these equations are more limited, since Eq. I.4 only predicts peak response amplitudes and Eq. II.1 only predicts responses in the linear range. The model of Fig. V.1 does not have these limitations.

The validity of other models in which the voltage response of the photoreceptor is assumed to reflect the dynamics of the phototransduction cascade (as in French, 1980, and in section III.4 of this dissertation) must also be questioned after the discovery of voltage-activated conductances sensitive to very small depolarizations.

V.4. References

- Attwell D (1986) Ion channels and signal processing in the outer retina. *Quart J Exp Physiol* 71:497-536.
- Barlow HB (1961) Possible principles underlying the transformations of sensory messages. In: *Sensory Communication* (W. Rosenblith, ed.) 217-234. MIT Press, Cambridge, MA.
- Barlow R (1990) What the brain tells the eye. *Sci Am* 262 (April 1990), 90-95.
- Baumann F (1974) Electrophysiological properties of the honeybee retina. In: *The compound eye and vision of insects* (G.A. Horridge, ed.) 53-74. Clarendon Press, Oxford.
- Bolsover SR (1981) Calcium-dependent potassium current in barnacle photoreceptor. *J Gen Physiol* 6:617-636.
- Coles JA, Schneider-Picard G (1989) Amplification of small signals by voltage-gated sodium channels in drone photoreceptors. *J Comp Physiol A* 165:109-118.
- Eckert H, Bishop LG (1975) Nonlinear dynamic transfer characteristics of cells in the peripheral visual pathway of flies. Part I: The retinula cells. *Biol Cybern* 17:1-6.
- Edgington DR, Stuart AE (1979) Calcium channels in the high resistivity axonal membrane of photoreceptors of the giant barnacle. *J Physiol* 294:433-445.
- Fain GL, Lisman JE (1981) Membrane conductances of photoreceptors. *Prog Biophys molec Biol* 37:91-147.
- French AS (1980) The linear dynamic properties of phototransduction in the fly

- compound eye. *J Physiol* 308:385-401.
- French AS, Kuster JE (1985) Nonlinearities in locust photoreceptors during transduction of small numbers of photons. *J Comp Physiol A* 156:645-652.
- Fuortes MGF, Hodgkin AL (1964) Changes in time scale and sensitivity in the ommatidia of *Limulus*. *J Physiol* 172:239-263.
- Gemperlein R, McCann GD (1975) A study of the response properties of retinula cells of flies using nonlinear identification theory. *Biol Cybern* 19:147-158.
- Grzywacz NM, Hillman P (1988) Biophysical evidence that light adaptation in *Limulus* photoreceptors is due to a negative feedback. *Biophys J* 53:337-348.
- Grzywacz NM, Hillman P, Knight BW (1988) The quantal source of area-supralinearity of flash responses in *Limulus* photoreceptors. *J Gen Physiol* 91:659-684.
- Hanani M, Shaw C (1977) A potassium contribution to the response of the barnacle photoreceptor. *J Physiol* 270:151-163.
- Hille B (1984) Ionic channels of excitable membranes. Sinauer Associates Inc.
- Laughlin SB (1981) Neural principles in the visual system. In *Handbook of Sensory Physiology VII/6B* (H. Autrum, ed.) 133-280. Springer-Verlag, Berlin.
- Laughlin SB, Lillywhite PG (1982) Intrinsic noise in locust photoreceptors. *J Physiol* 332:25-45.
- Lillywhite PG, Laughlin SB (1979) Transducer noise in a photoreceptor. *Nature* 277:569-572.
- Matic T, Laughlin SB (1981) Changes in the intensity-response function of an insect's

- photoreceptors due to light adaptation. *J Comp Physiol* 145:169-177.
- Muijser H (1979) The receptor potential of reticular cells of the blowfly *Calliphora*: The role of sodium, potassium and calcium ions. *J Comp Physiol A* 132:87-95.
- Payne R (1980) Voltage noise accompanying chemically induced depolarization of insect photoreceptors. *Biophys Struct Mech* 6:235-252.
- Payne R (1982) Chemical modifications to transduction in an insect eye. Ph.D. thesis, Australian National University.
- Payne R, Fein A (1986) The initial response of *Limulus* ventral photoreceptors to bright flashes. Released calcium as a synergist to excitation. *J Gen Physiol* 87:243-269.
- Payne R, Flores TM, Fein A (1990) Feedback inhibition by calcium limits the release of calcium by inositol trisphosphate in *Limulus* ventral photoreceptors. *Neuron* 4:547-555.
- Pugh E, Altman J (1988) A role for calcium in adaptation. *Nature* 334:16-17.
- Ross WN, Stuart AE (1978) Voltage sensitive calcium channels in the presynaptic terminals of a decrementally conducting photoreceptor. *J Physiol* 274:173-191.
- Tsukahara Y (1980) Effect of intracellular injection of EGTA and tetraethylammonium chloride on the receptor potential of locust photoreceptors. *Photochem and Photobiol* 32:509-514.
- Weckström M, Hardie RC, Laughlin SB (1990) The role of voltage-activated potassium channels in blowfly photoreceptors. Submitted for publication.